NASA CR-134887

TRW ER-7747F

COMPOSITE IMPACT STRENGTH IMPROVEMENT THROUGH A FIBER/MATRIX INTERPHASE

by

P. J. Cavano and W. E. Winters

TRW
EQUIPMENT

prepared for
NATIONAL AERONAUTICS AND SPACE ADMINISTRATION
NASA Lewis Research Center
Contract NAS 3-18902

Raymond F. Lark , Project Manager

TRW

January 15, 1976

Gentlemen:

Subject: NASA CR134887

Please find enclosed for your information and retention the subject technical report entitled "Composite Impact Strength Improvement Through a Fiber/Matrix Interphase." The report covers work conducted by Materials Technology of TRW Equipment, Cleveland, Ohio for the Materials and Structures Division of NASA-Lewis Research Center, Cleveland, Ohio under Contract NAS3-18902.

Any comments or suggestions you may have would be appreciated and should be directed to the undersigned.

Very truly yours,

TRW INC.

W. E. Winters, T/M 2164
Program Manager

WEW/cc
Encl.

DISCLAIMER NOTICE

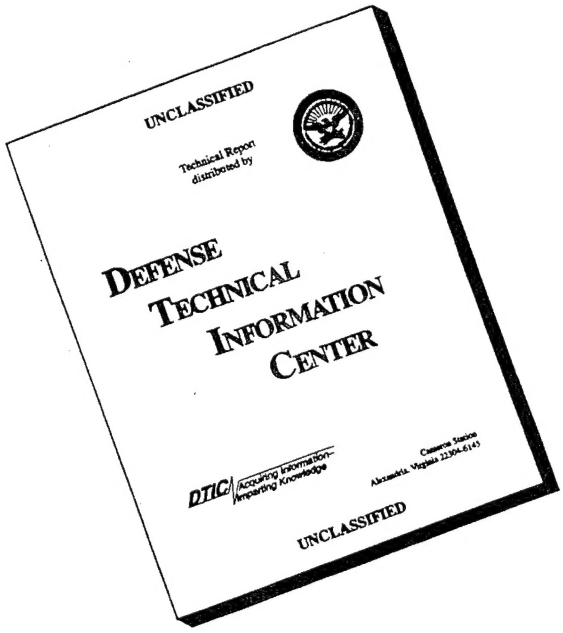

THIS DOCUMENT IS BEST QUALITY AVAILABLE. THE COPY FURNISHED TO DTIC CONTAINED A SIGNIFICANT NUMBER OF PAGES WHICH DO NOT REPRODUCE LEGIBLY.

1. Report No.	2. Government Accession No.	3. Recipient's Catalog No.
NASA CR-134887		

4. Title and Subtitle	5. Report Date
Composite Impact Strength Improvement Through a Fiber/Matrix Interphase	October 1975
	6. Performing Organization Code
7. Author(s)	8. Performing Organization Report No.
P. J. Cavano and W. E. Winters	TRW ER-7747F
	10. Work Unit No.
9. Performing Organization Name and Address	11. Contract or Grant No.
TRW Equipment 23555 Euclid Avenue Cleveland, Ohio 44117	NAS3-18902
	13. Type of Report and Period Covered
12. Sponsoring Agency Name and Address	Contractor Report - Final
National Aeronautics and Space Administration Washington, D.C. 20546	14. Sponsoring Agency Code

15. Supplementary Notes

Project Manager, R. F. Lark, Materials and Structures Division, NASA Lewis Research Center, 21000 Brookpark Road, Cleveland, Ohio 44135

16. Abstract

The objective of the program was to improve the impact strength and toughness of fiber/resin composites by means of a fiber coating interphase. Graphite fiber/epoxy resin composites were fabricated with four different fiber coating systems introduced in a matrix-fiber interphase. Two graphite fibers, a high strength and a high modulus type, were studied with the following coating systems: chemical vapor deposited boron, electroless nickel, a polyamide-imide resin and a thermoplastic polysulfone resin. Evaluation methods included the following tests: Izod, flexure, shear fracture toughness, longitudinal and transverse tensile, and transverse and longitudinal compression. No desirable changes could be effected with the high strength fiber, but significant improvements in impact performance were observed with the polyamide-imide resin coated high modulus fiber with no loss in composite modulus.

17. Key Words (Suggested by Author(s))	18. Distribution Statement
Graphite Fiber Composites Interface Modification Fracture Toughness Izod Impact Composite Toughness	Unclassified - unlimited

19. Security Classif. (of this report)	20. Security Classif. (of this page)	21. No. of Pages	22. Price*
Unclassified	Unclassified	97	

* For sale by the National Technical Information Service, Springfield, Virginia 22151

FOREWORD

This document represents the final report of the work accomplished between 25 June 1974 and 31 July 1975 by TRW Incorporated for the National Aeronautics and Space Administration, Lewis Research Center, Cleveland, Ohio under Contract NAS3-18902 on Composite Impact Strength Improvement Through a Fiber/Matrix Interphase. This work was carried out under two different Project Managers in the NASA-Lewis Materials and Structures Division. The program was initiated under Mr. Charles L. Younger, who served as Project Manager for the bulk of the program, and completed under the technical direction of Mr. Raymond F. Lark.

Work on the program was conducted at TRW Materials Technology of TRW Equipment, Cleveland, Ohio. Mr. W. E. Winters was the TRW Program Manager; the TRW Project Engineer was Mr. Paul J. Cavano.

COMPOSITE IMPACT STRENGTH IMPROVEMENT THROUGH A FIBER/MATRIX INTERPHASE

by

P. J. Cavano and W. E. Winters

SUMMARY

The major objective of the program was to improve the impact strength and toughness characteristics of graphite fiber/epoxy composites by means of a fiber coating interphase. It was anticipated that the coatings would function to alter fracture mode and modify interfacial bonding as a means of providing greater energy absorption in fracture. Four coating systems were investigated on both high strength and high modulus graphite fibers using a bisphenol-A epoxy resin as the primary composite matrix. The coating systems examined were as follows: Kerimid-500, a polyamide-imide resin, at three different thicknesses; electroless nickel at three coating thicknesses; boron, achieved by chemical vapor deposition, in one thickness; and a polysulfone resin, P-1700, in one thickness.

The various coating systems noted above were screened in the first phase by mechanical testing at room temperature. The tests conducted included un-notched Izod impact, determination of critical stress intensity factor, short beam shear, longitudinal tensile and three point flexural strength testing. The final examination consisted of an evaluation of the single selected system, Kerimid-500 coated high modulus graphite fiber, by subjecting specimens to longitudinal and transverse tensile, longitudinal and transverse compression and intralaminar shear tests. The latter test used was a new method employing an off-axis tensile specimen.

It was shown that it is clearly feasible to significantly alter the mechanical properties of graphite fiber composites by the introduction of a fiber/resin interphase. The single highest improvement over control values was a 117% increase in Izod impact strength with electroless nickel coated high modulus fiber. However, the system found to yield the best balance of improved properties for projected service use was the Kerimid-500 fiber on high modulus fiber. The K-500 system showed a 74% increase in impact strength at the highest coating thickness but with a drop in shear strength. The two thinner coating thicknesses displayed improved short beam shear strength. All thicknesses improved tensile strength with only minor loss (10%) in tensile modulus. Flexural strength with the K-500 coated HM-S composites was moderately reduced, but flexural modulus was improved. The worst coating performer with both fibers was the high modulus boron coating which showed a 66% decrease in impact strength on the high modulus fiber and an 82% loss in impact strength with the high strength fiber. None of the boron coatings served to consistently improve the performance of the high strength fiber system.

Because of the significant improvements noted, it is recommended that further work be performed to identify the mechanism by which the low modulus

high strain-to-failure Kerimid-500 coating effected the toughness improvement changes. Additionally, it is felt that further screening of other coatings and matrices should be done on high modulus graphite and boron fibers systems.

TABLE OF CONTENTS

TABLE OF CONTENTS (continued)

LIST OF TABLES

LIST OF FIGURES

LIST OF FIGURES (continued)

1.0 INTRODUCTION

This document constitutes the final report on NASA-Lewis Contract NAS3-18902, initiated 25 June 1974, and describes the work performed between that date and 31 July 1975. The major objective of the program was to improve the impact strength and toughness characteristics of graphite fiber/epoxy composites by means of a fiber coating interphase. It was anticipated that the coatings would function to favorably alter fracture mode and modify interfacial bonding as a means of providing greater energy absorption during fracture. Four coating systems were investigated on high strength and high modulus graphite fibers using a bisphenol-A type epoxy resin as the primary composite matrix.

The program was divided in two basic technical tasks as described below:

TASK I - Composite Design, Fabrication and Preliminary Evaluation

In this phase of the program, studies were conducted to establish the selection of fibers, primary resin matrix, and the candidate coatings to be investigated. An evaluation plan was prepared for methods of fiber coating, composite fabrication and evaluating composite mechanical performance. Composites were fabricated, tested and the results examined to permit the selection of the best fiber/coating/thickness combination for further characterization in the following phase.

TASK II - Final Evaluation

The best candidate system selected from the previous task was fabricated into additional composites and additional mechanical properties determined to further define design characteristics.

2.0 BACKGROUND

The development in recent years of high strength and stiffness graphite fibers has opened the door to a new generation of engineering materials which are of particular interest wherever structural requirements dictate minimum hardware weight. The substitution of graphite fiber/resin composites for more conventional materials of construction has been inhibited by, among other reasons, their brittle properties and inherently poor resistance to impact loading. For example, fan blades in aircraft gas turbine engines represent a prime example of an application where substantial engine weight savings and specific thrust performance improvements can and have been shown with the use of graphite/resin composite materials. Such applications have not come into general use primarily because of the susceptibility of composite fan blades to damage by ingestion of foreign material such as birds and ice balls.

Early in the development of graphite fiber/resin composites, difficulty was experienced in achieving a suitable adhesion of the matrix resin to the filament. Properties dependent upon a good bond, including transverse tensile, shear and compressive strengths were less than desired or needed for structural applications. Advances in technology through fiber treatments, fiber finishes and matrix resins provided improvements in fiber/resin adhesion to the point where composite shear and transverse tensile strengths were greatly enhanced.

The resultant improvement in static mechanical properties has been at the expense of dynamic characteristics. High shear-strength composites are also brittle, notch sensitive and sensitive to impact loading. Two important energy managing mechanisms in the fracture of low adhesion (fiber/resin) composites are delamination and fiber pullout. These factors are not available or are significantly reduced in high shear-strength systems; hence, composite materials offering maximum static performance often display inferior high strain-rate loading capability.

Thus, conflicting requirements in the properties of the interface arise from the dual requirements of the interface; on the one hand, the interface is required to bond the components together to transfer stress from one region to another but, on the other hand, the interface is required to deflect and/or modify crack propagation and to contribute to energy management by frictional losses through fiber pullout.

Many approaches have been taken to the solution of this dilemma. Some have been compromises while others have sought alternative approaches to graphite fiber/resin composite impact improvement, e.g., hybridization. One of the earliest efforts was made by Rolls Royce in attempting to upgrade graphite/epoxy fan blades to pass bird ingestion and other foreign object damage criteria on the RB-211 engine. In this case, composite shear strength was compromised by using a reduced level of an adhesion-promoting fiber treatment, less than that attainable for maximum shear properties, to achieve improved impact strength properties. Although incremental impact strength improvement could be achieved, the approach was not fully satisfactory.

A second approach was developed by Marston (1)* who considered an intermittent fiber/resin bond by treating discrete lengths of boron filaments with releast agent. Impressively, the concept demonstrated an effective means for the suppression of composite failures initiated by low strength boron filament failures. Not only did the intermittently bonded fiber composites have higher resistance to crack propagation, but unidirectional composites exhibited an improvement in tensile failure strain and an average ultimate filament stress greater than fully bonded boron fiber composits reported at that time.

Chamis et al (2) contributed substantially to the understanding of the mechanisms involved in composite impact processes through micro- and macro-mechanical analyses corroborating results with Izod impact strength tests using unidirectional composites. Chamis developed relationships among composite and constituent properties that allow prediction of the impact energy density of composite specimens of various types. Failure modes of cleavage, delamination and fiber pullout were used to define longitudinal, transverse and shear impact resistance. It was concluded that, for high performance composites, the parameters which enhance impact energy density (debonding and fiber pullout) are detrimental to composite structural integrity with respect to static strength and stiffness.

Perhaps the most unique approach to improved energy absorbing composites has been proposed by Professor Morley (3)(4)(5)(6)(7) at the Wolfson Institute of Interfacial Technology, Nottingham, England. Professor Morley concluded that the solution to the dilemma of a good fiber/resin bond needed for high shear, transverse tensile and compressive strengths and a poor bond needed for high failure strain, crack-stopping and good impact strength, was to provide two interfaces between the fiber and matrix. He suggests that this could be done by introducing a two-component fiber, an outer sheath giving a strong bond to the matrix, but with an inner core having only a weak bond to the outer sheath. Large amounts of energy could thus be released by fiber pullout; additionally, the duplex fiber concept provides fracture of the fibers at widely separated points rather than at a crack initiated in the matrix and progressing through the composite in a single plane (brittle fracture).

Pinchin and Woodhams (8) found that pyrolytic deposition of carbon, by chemical vapor deposition, on Thornel 50 graphite fiber (up to 30 w/o of the base fiber) enhanced interlaminar shear and flexure strength while Izod impact strengths were reduced. The amount of fiber pullout on the coated fiber specimens was significantly less than for uncoated fiber composites, accounting for, at least in part, lower impact values shown by coated fiber.

Still another approach of fiber coating suggested in the literature as a means of upgrading composite performance is the use of an organic coating. Kenyon and Duffy (9) observed, for example, that the ultimate elongation of cast, glass bead-filled epoxy composites can be increased by altering the nature of the resin in the vicinity of the interface with an excess of glycidoxy

---

* Numbers in parentheses refer to references listed in a separate section.

silane. Kenyon (10) went on to show that the toughness of such systems also can be increased by coating the beads with a thin layer of flexibilized epoxy prior to casting. More recently, Lavengood and co-workers (11) found that the transverse strength and fatigue properties of fiber reinforced composites could be increased through use of a ductile inner layer. Baer et al (12) demonstrated that polymers could be epitaxially crystallized from solutions and melts on heterogeneous surfaces to yield a layer of oriented crystallites. In reinforced thermoplastic composites, this approach presents the possibility of producing and interphase material modulus which is intermediate between that of the substrate and the bulk resin. Crystallinity in a polymer is normally attended by increases in both modulus and yield stress.

Using these references as background, Kardos et al (13) determined that graphite fiber/resin composites using a polycarbonate polymer could be significantly increased in tensile strength and modulus by molding at higher than normal temperature and annealing at temperatures 20-30°C below the T_g. Although the improvement could be explained in part by better fiber wetting, X-ray diffraction analysis revealed the formation, adjacent to the fiber surface, of a partially crystalline layer of resin on annealed specimens which was not present on untreated composites.

At TRW the organic inner layer concept had been previously investigated on a preliminary basis with encouraging results. The rationale used was to provide a ductile interface between the fiber and a brittle matrix (polyimide) as a means of blunting cracks in the matrix to limit initiation of fiber fracture. It was reasoned, as well, that the ductile interface might also better accommodate fabrication residual stresses resulting from mismatched thermal expansivity between fiber and matrix. The materials used for these experiments were Modmor I high modulus graphite fiber and P13N polyimide resin as the matrix. For the fiber coating, a thermoplastic polyamide-imide resin, Kerimid-500, was selected. This latter resin exhibits a strain-to-failure of 8 to 11%. Although Izod impact strength values for the K-500 coated composite were not nearly as impressive as those obtained on various hybrid systems, a comparison with MMI/4205 epoxy provided additional encouragement for the ductile coating system. Observation of the failure mode on the coated fiber composites indicated a significant increase in fiber pullout. In ballistic impact tests, it was noted that the coated fiber composite required over 50% greater energy input to achieve complete penetration than the uncoated fiber composite. Although only preliminary, the above results provided encouragement for considering the feasibility of studying the ductile organic coating concept for improving fiber translation efficiency and improved composite impact strength performance.

It is clear from a review of the discussion above that modification of the interface characteristics in a resin matrix fiber reinforced composite is considered to be one of the major approaches to achieving higher impact strength and reduced composite brittleness. For this reason, it was felt worthwhile to undertake a planned program aimed at introducing a number of materials, with varying properties, between the matrix resin and the fiber surface to observe any induced changes in the toughness of the systems when compared to control systems without the interphase coatings. Details of coating selections and experimental methods are described in the following sections.

3.0 FIBER COATINGS

3.1 Coating Criteria

A critical aspect of the program was the selection of candidate coatings to be applied to the graphite fibers. Analyses have indicated that coating performance involves not only the properties of the coating but its interrelationship with the reinforcement and matrix. For instance, one approach indicates that the coating should possess tensile and compressive moduli intermediate between matrix and fiber. Coatings having higher modulus and lower longitudinal strain-to-failure than the fiber could induce initial failure in the coating leaving the core fiber (assuming little or no coupling) to carry the major portion of the applied load. A coating of lower modulus and/or higher strain capability than the fiber might induce initial failure in the reinforcement. In either event, the coating was to provide a barrier layer between fiber and matrix to minimize or preclude an interaction between the two and prevent catastrophic in-plane failure.

Another coating performance characteristic that might theoretically contribute to composite performance was the adhesion between constituents. Once again, analyses have indicated a desired low-to-medium coating-to-fiber bond and a high coating-to-matrix bond. But the actual level of bonding obtained at these two interfaces depends upon other factors, such as the strength or load carrying ability of the coating material in the transverse direction, mismatches in thermal expansivity between constituents (fabrication residual stresses) and differential Poisson's effect between constituents. For instance, a coating of low strength coupled with little or no coating-to-fiber bond would produce low transverse strength in the composite.

A very real practical problem that limited selection was, of course, that of application method. All materials considered had to be suitable for state-of-the-art deposition on individual fibers in a large multi-filament tow without embarking on a major development program. As an example, certain plasma sprayed coatings were not suitable since coating interior fibers in a large bundle is not practical.

It can be seen, then, that many variables exist and the interactions of the variables made precise prediction of composite performance difficult. No single coating was expected to satisfy all of the requirements of a perfect composite. Therefore, compromises were expected in the optimum levels of all composite properties.

Coating candidates considered can be divided into two general categories, inorganic and organic. Two inorganic coatings were considered, boron and nickel. One organic coating, selected from a broad list of potential candidates, was a thermoplastic polyamide-imide resin system. The second organic coating selected was a thermoplastic polysulfone resin. Each of these are discussed below as to type of coating, application method and rationale for selection.

3.2 Boron Coating

Professor Morley has suggested[3] that core fibers consisting of high strength graphite fibers having an elastic modulus of 207 GN/m^2 (30 msi) and a strain-to-failure of 1.5% surrounded by a boron sheath of comparable cross-sectional area and having a modulus of 414 GN/m^2 (60 msi) and a strain-to-failure of 0.5% represent an example of a possible duplex fiber system that might potentially provide an improved energy absorbing composite. Another potentially desirable characteristic of the boron coating is an intermediate thermal expansion coefficient difference between fiber and matrix. The boron coating has a coefficient of about $4.2 \times 10^{-6}/^{o}C$ while the fiber coefficient is slightly negative or zero compared to the extremely high values observed with organic resins. For these reasons, it was felt that the boron coating was a suitable candidate representing one end of the modulus spectrum.

The technology for producing continuous filament by the chemical vapor deposition of boron onto a suitable substrate was well established. The substrate most frequently used onto which the boron is deposited is 0.012 mm diameter (1 mil) carbon monofilament. The coating of boron onto multi-filament graphite fiber tow had not been demonstrated. However, it was felt that the technology necessary to do this, with certain quality reservations, could be easily achieved. The two quality reservations were the anticipated thickness uniformity of deposit and the likelihood that some fibers in the center of the multi-filament tow might not be completely coated.

Recognizing these problems, a subcontract with AVCO was entered into. Two types of graphite fiber tow (HM-S and HT-S) were supplied to AVCO for application of three different boron coating thicknesses on each fiber type.

3.3 Electroless Nickel Coating

It was felt that a nickel-phosphorous (electroless nickel) coating offered another viable candidate for coated fiber composites. In processing, a nickel-phosphorous alloy is deposited from a solution of nickel salts, buffer and reducing agent to form hard, uniform coatings which deposit on any surface "seen" by the plating bath. Typical properties of the deposited material are shown below:

Phosphorous Content	6-10%
Tensile Strength	410-689 MN/m^2 (60-100 ksi)
Modulus	170 GN/m^2 (25 msi)
Elongation	2-6%
Thermal Expansion Coefficient	$13 \times 10^{-6}/^{o}C$ ($7.22 \times 10^{-6}/^{o}F$)
Specific Gravity	7.85

This system was chosen primarily because of its intermediate modulus and thermal expansion coefficient. Its major disadvantage is a high density; this might present a weight problem in the composite if significant thicknesses were to be used.

3.4 Polyamide-imide Coating

While it was recognized that the bulk of the literature suggests a coating material with properties intermediate between the fiber and matrix, there is some literature that proposes a "soft" interface. Additionally, previous TRW work with Modmor I graphite fiber and a polyimide primary matrix with the polyamide-imide system indicated a beneficial effect from the use of this system.

The system chosen was Kerimid-500, a polyimide-amide resin, from Rhodia Corporation. This material is a high temperature, high elongation (ca. 10%) liquid adhesive resin. No condensation volatiles are given off during thermal bonding treatment although the carrier solvent, 1-methyl-2-pyrrolidinone (NMP) has a high boiling point of 202°C (395°F) which, in certain cases, can present processing problems. While the material, as received in a 23 w/o solution, has a high viscosity, this was easily overcome by diluting to a 2 w/o solution for application to the fiber.

3.5 Polysulfone Resin Coating

Although originally only one organic coating was planned for evaluation, disappointing results with the boron material suggested that an alternate candidate be investigated. The system chosen was a polysulfone resin, Udel P-1700 from Union Carbide. Typical properties are shown below:

Typical Properties of P-1700 Polysulfone

Property		
Density	1.24 gm/cm^3	1.24/g/cm^3
Tensile Strength	10,000 psi	70 MN/m^2
Tensile Modulus	360,000 psi	2.5 GN/m^2
Tensile Elongation at Break	50-100%	50-100%
Flexural Strength	15,400 psi	106 MN/m^2
Flexural Modulus	390,000	2.7 GN/m^2
Coefficient of Linear Thermal Expansion	3.1 x $10^{-5}/°F$	5.6 x $15^{-5}/°C$

The P-1700 is an "engineering" thermoplastic and is widely used as an injection molding material (both filled and unfilled) for the manufacture of motor housings, aircraft cabin parts, battery cases, etc. In addition, both TRW and others in the industry had fabricated polysulfone composites with carbon fiber reinforcement that provided performance characteristics equivalent to epoxy matrix composites. A recent reference (14) concludes, "Hybrid polysulfone matrix composites incur much less impact damage than their epoxy matrix counterparts." It has a service temperature of 149°C-177°C (300-350°F). Based on the above information, it was felt that the P-1700 represented a suitable coating candidate for this program.

4.0 COMPOSITE CONSTITUENT SELECTION

4.1 Primary Resin Matrix

It was felt that the primary resin matrix for the coated fiber composites would also play an important role. Analysis of the requirements for such a material are not necessarily straightforward. For instance, Chamis (2) has demonstrated that the *in situ* strain-to-failure in the composite matrix, due to stress intensification between fibers, can be grossly different than that of the bulk resin. A most complex triple interaction thus exists between the properties of the matrix, coating and the core fiber.

The basic resin matrix finally selected for use throughout the program was Shell Chemical's Epon 828 epoxy resin. A hardener and an accelerator for this system were selected on the basis of work on failure mechanisms in advanced composites (15). The resin/hardener system was reported to have a total strain-to-failure of 2.7%; a value which would represent a reasonably brittle material. In this way, it was felt that interface improvements attempted during the course of this program would be more easily observed than if a high strain, tough matrix material were selected.

The system formulation is shown below:

Epon 828	100 parts by weight
HHPA (hexahydrophthalic anhydride)	78 " " "
BDMA (benzyldimethylamine)	1 " " "
MEK (methyl ethyl ketone)	As required

The MEK was used to reduce the viscosity of the resin so that the solution could be applied to the collimated graphite fibers.

4.2 Reinforcing Fibers

Graphite fibers selected for use on the proposed program were continuous American-made 10,000 filament tows from Hercules Incorporated, specifically, type HM, representing high-modulus, intermediate strength fiber and type A high-strength, intermediate modulus material. The following factors were taken into consideration in the selection:

- Both fibers are made from the same precursor differing only in processing methods and thus properties: a high strength, intermediate modulus fiber and a high modulus, intermediate strength filament.
- Both fibers are commercially available at relatively low cost.
- A wealth of experience is available with these fibers at TRW and throughout the industry from which generous amounts of baseline data were available.

- The untwisted tow form provides ease in spreading for ply thickness control and for ease of opening the fiber bundle to facilitate uniform coating by the candidates selected for this program.

- Hercules fiber has been shown to be of high quality, consistent and capable of producing composites of good properties and high fiber translation capability.

The A type fiber can be supplied with or without surface treatment (-S designation) for fiber/resin bond enhancement. Since one of the criteria for the coated fiber composite concept is moderate to low coating-to-fiber adhesion, it was expedient to procure both treated and untreated fiber for comparative purposes. However, the HM type fiber is available commercially only in the treated (-S) condition precluding a direct comparison of the effect of the adhesion enhancement process. Advertised vendor data on tensile strength, modulus and strain-to-failure are shown below for the three types of graphite fibers.

Vendor Graphite Fiber Property Data

	A-S	HT-S	HM-S
Tensile Strength			
MN/m^2	2827	2758	2344
ksi	410 min.	400 min.	340 min.
Modulus			
GN/m^2	207	234	345
msi	30 min.	34 min.	50 min.
Strain-to-Failure, %	1.4 Typ.	1.1 Typ.	0.6 Typ.

5.0 COMPOSITE PROCESSING

The following sections describe processing details on graphite fiber coating, resin impregnation, molding, postcuring and subsequent laminate inspection on the composites used in the program evaluation.

5.1 Fiber Coating

5.1.1 Electroless Nickel Coating

To obtain the nickel coating, a proprietary plating solution (bath) from Allied Research Products, Incorporated, Baltimore, Maryland, designated Niklad #792, was chosen. In order to initiate deposition of the nickel on the passive graphite fiber surfaces, a special activation system was required. For this purpose, Sensitizor #432 (stannous chloride solution) and Activator #440M (palladium chloride solution) from Enthone, Incorporated, New Haven, Connecticut were used. An electroless nickel plating line was set up using laboratory glassware; included were sensitizor, activator solutions, the nickel plating bath itself, and the necessary rinse, including an ultrasonic deionized water rinse.

Using the activator solutions and the nickel plating bath described above, no difficulty was experienced in achieving catalysis of the fiber surface and deposition proceeded rapidly and vigorously on short trial lengths of fiber immersed in the plating solution. Samples were potted in epoxy and metallurgically polished. Examination at 100 to 750X magnification revealed coating and encapsulation of nearly all of the filaments in the 10,000 fiber tow (see figure 1). Nickel thickness up to at least the diameter of the graphite filaments was achieved. The coating was reasonably uniform from the outside to the center of the fiber bundle and very little fiber agglomeration occurred. The violet gassing of the chemical reduction process was sufficient to create adequate solution flow through the dense fiber bundle to achieve uniform deposition and fiber separation.

A reel type fixture was fabricated on which graphite tows for program use could be wound and processed in batches through the various plating and rinse solutions. The fixture consisted of a steel plate into which four 3.2 mm (1/8 inch) steel rods approximately 20.3 cm (8 inches) long were threaded to form a 10.2 cm (4 inches) square spool arrangement. Three additional sets of four rods were located within the first set, providing four concentric layers of fiber. Using the fixture and a lead of four tows/inch, approximately 46 m (150 feet) of tow could thus be processed conveniently at one time. The fixture, with fiber in place, is shown in figure 2.

First attempts at using the four-layer reel resulted in violent reaction, and it was necessary to reduce the plating bath temperature in order to control the process. Using steel test coupons, the plating rate of the bath was established and it was found that at 77-78°C (171-173°F) the reaction was controllable and produced a deposition rate of 5 μm/hr. Coating thicknesses established for the composite studies were 0.5, 0.2 and 0.1 μm for each of the two fibers selected for the program.

After nickel plating the reel of fiber was rinsed several times in running water, ultrasonically cleaned in a final deionized water rinse, wound off the reel onto a plastic spool and oven dried. The fiber after plating exhibited a uniform metallic appearance and appeared reasonably uniform. Contact marks were observed where the fiber passed over the metal rods and, in some small areas of the length, some few fibers were not coated, presumably because a tight wind onto the reel precluded adequate solution migration through the fiber bundles. It was felt, however, that sufficient fiber has been coated to establish the feasibility of this coating concept in upgrading composite performance.

5.1.2 Polyamide-imide Coating

The procedure for applying the polyamide-imide coating to the fibers was essentially the same as used for applying the epoxy resin; this technique will be discussed in detail in the section "Matrix Impregnation." Briefly, the fiber was collimated onto a 30.5 cm (12 inch) diameter sleeve fitted over a winding drum, and a predetermined amount of coating was applied by means of a peristaltic pump to the rotating surface. After the coating process, the solvent, 1-methyl-2-pyrrolidinone (NMP), was removed by first drying with infra-red lamps on the winding machine and then removing the metal sleeve, with the fiber in place, for installation in an air circulating oven. The oven drying was programmed to remove all of the NMP over an eight-hour period to avoid blistering or disruption of the resin coating on the fiber. The final oven treatment was three hours at 300°C (572°F). After cooling the drum sleeve was replaced on the winding machine and the primary matrix (epoxy) solution applied.

The Kerimid-500 was applied in a 2 w/o solution in NMP in order that the viscosity be low enough to completely penetrate the fiber bundles and provide uniform coverage. Coating thicknesses of 0.05, 0.1 and 0.2 μm were selected and the amount of K-500 deposited in each case was calculated from known densities of fibers and resins.

Numerous attempts were made to observe the dried fiber coating microscopically, without success. Both finished molded laminates as well as discreet coated fibers were examined with various techniques including various mounting media, staining and ordinary as well as scanning electron microscopy. None of these techniques was successful.

5.1.3 Polysulfone Resin Coating

The P-1700 polysulfone resin was received as small pellets. These were dried and put into a 2 w/o solution in methylene chloride. After this the solution was applied to the fibers exactly as was the polyamide-imide, including the drying cycle. As was noted earlier, only one coating thickness was examined, 0.1 μm. Prepreg prepared with this coating system seemed to have less stiffness and slightly better integrity than the K-500 material.

5.1.4 Boron Coating

A process was devised by AVCO to coat both HM-S and A-U graphite tow with boron for subsequent composite studies. The technique developed is described below.

The standard fiber spool was mounted on a horizontal bearing support structure to serve as a payout assembly. A friction brake pulley was included on the shaft which turned with the supply package to apply a small tension to the graphite tow. A tension of the order of 50 grams was found sufficient to avoid slack in the tow feed line.

The tow was simultaneously heated and coated with boron in a small horizontal reactor assembly. The tow entered the reactor through a combined gas seal and electrode consisting of a mercury filled quartz tube. This liquid seal prevented leakage of the reactant gases from the reactor by maintaining the tow under the surface of the mercury pool. The mercury also served as an electrode to make electrical contact with the graphite for resistance heating of the fiber tows.

The gas mixture in the reactor was approximately 50% H_2 and 50% BCl_3. The reactor operating current was in the range 15 to 25 amperes, 60 Hz, during boron deposition creating a tow temperature in the range of 1200°C to 1450°C. The reactor length was about 35.6 cm (14 inches) and the tow operating speed was in the range 3 to 6 m/ft (10 to 20 ft/min).

Optical microscopic examination of the tow after boron deposition indicated that the boron deposition was nearly uniform. Some variation of boron thickness from the outer fibers (ca. 2 μm coating thickness) to the core of the bundle was noted with a slightly thicker deposit being near the core where the fibers were hottest.

5.2 Primary Matrix Impregnation

Epoxy impregnation of the fiber was carried out by dry wrapping the fiber onto Mylar sheet on a 30.5 cm (12 inch) diameter drum and then metering the resin solution onto the fiber surface with a peristaltic pump. The tow was brought off the spool under a slight tension created by an electrically operated spool brake. A roller and hoop arrangement on a lead screw spread the 10,000 filament tow so that an even fiber placement on the drum was achieved. The pump metering rate was correlated with the traverse speed of the head with the lead screw on the winder. In this way, the required, calculated amount of resin was deposited on the fiber surface. The first drying or devolatization process was carried out before the prepreg was removed from the drum. Six infrared lamps (250 watts each) on 17.8 cm (seven inch) centers were placed 15.2 cm (six inches) from the surface of the fiber. Volatiles driven off were removed through an overhead hood mounted over the winding area of the machine. Sufficient material was wrapped on the drum to provide sufficient prepreg for two 10 x 20 cm laminates having eight plies.

For calculation purposes, it was assumed that the same fiber fraction would be used for all composites and that the coating was to be treated as part of the matrix; i.e., epoxy resin content was adjusted so that a finished laminate with an interface phase would contain the same number of bare graphite fibers as a control laminate of equivalent thickness.

The epoxy resin and hardener formulation described in section 4.1 were dissolved in methyl ethyl ketone (MEK) at room temperature in a 50 w/o concentration. This concentration gave good wetting when applied to the fibers and inhibited any premature gelation due to the presence of the BDMA accelerator. MEK boils at 80°C (175°F) and thus presented no problem in subsequent staging or molding operations from the standpoint of residual solvent.

Prepreg was prepared with a nominal 51.5 v/o fiber volume to account for the flow that occurred in molding the epoxy system. This fiber volume corresponds to a w/o resin content of 38% for uncoated fiber. Prepreg thickness target was based on obtaining a finished molded ply thickness of 0.254 mm (0.010 inch). This was done by using the following formula during the wrapping of the bare fiber on the drum for subsequent resin coating:

$$N = \frac{T\ V_f\ \rho_f}{W}$$

where:

N = number of tows per inch

T = thickness per ply

V_f = fiber fraction

ρ_v = fiber density

W = fiber weight per unit length

5.3 Lamination and Molding Procedures

The prepreg, prepared as described above, was cut from the winding drum to form a sheet of unidirectionally oriented broadgoods approximately 900 x 400 mm (36 x 16 inches). Eight plies of the appropriate size were cut out with a template and stacked, one upon another, to make a preform. This was oven staged and then molded. Molding was accomplished in a close fitting matched metal mold in a thermostatically controlled, electrically heated platen press.

In early molding trials, processing problems were identified that required considerable experimentation. Even with the presence of the 1 w/o BDMA accelerator, the 828/HHPA epoxy system reacted very slowly in molding. The second problem was the extremely low viscosity developed by the resin as it was heated. This was so low that in the first molding attempts, the resin ran out the bottom of the molding tool, rather than coming out of the top in response to the application of molding pressure as is normally observed. The third problem identified after some experimentation, was the differing polymerization response rate of the resin with the various fiber and coating

surfaces. Another problem encountered was the effect of time on prepreg waiting to be molded. This was most clearly shown with the polysulfone material. The first A-U and HM-S laminates were molded the next day after the prepreg was prepared. In this condition, almost no flow was observed. A week later, a second set of laminates was prepared with the same prepreg and copious flow was observed with both the A-U and HM-S reinforcements. It was hypothesized that the MEK solvent used as a carrier for the epoxy resin was softening, over a period of time, the previously deposited layer of P-1700. This was confirmed by putting P-1700 resin beads into a small quantity of the epoxy resin solution; the discreet P-1700 beads turned into a gel in the solution.

These problems, all of which are related, affect the selected staging conditions and the rate of application of heat and pressure during the molding process for each of the different materials. A typical staging and molding cycle developed is shown in table I. The major modification required in handling the various fibers and surface coatings was that the 204°C staging time is reduced, in some cases to zero, for the different systems being fabricated.

While, ultimately, all the required laminates were prepared and accepted on the basis of ultrasonic inspection described below, a very high rejection rate was experienced. This specific system (828/HHPA) is felt to be inappropriate, from a manufacturing standpoint, for the fabrication process employed. A better system would have a higher melt viscosity and a shorter gelation period.

5.4 Postcure Procedures

The Shell Chemical Company recommends a postcure with the 828/HHPA/BDMA system. Additionally, even though the composites were to be tested at room temperature, the slow reaction times observed in molding made it clear that this was a requirement. First efforts were performed in an air circulating oven with a slow rise to 177°C (350°F). Ultrasonic inspection of a number of laminates before and after postcure revealed that several of the laminates were degraded by the oven postcure. In order to prevent the loss of ultrasonic quality, a pressure postcure in the molding tool was investigated and adopted as standard. The postcure used is shown below:

Temperature, °C	Pressure, MN/m^2	Time at Temperature
RT-77	Contact	15 min.
77-102	6.9	↓
102-127	↓	
127-151		
151-177		8 hours

5.5 Laminate Inspection

Laminate quality was monitored with the use of ultrasonic inspection. Each laminate was checked after postcure to assess void content and defect patterns. A through-transmission method with a C-scan recording was used. The tests were performed at 10 MHZ with a 2.38 mm (3/32 inch) diameter sending crystal of the SL type. The receiving crystal (SIZ) was 12.7 mm (1/2 inch)

in diameter. The ultrasonic unit was a Sperry UM-700 with an Automation Industries SR-194 C-scan recording unit; an HFN pulser was used. While the signal screen height was varied from 25 to 75%, it was found that the 50% level displayed good contrast between sound and flawed areas and was used as a general standard. In making repetitive setups, a 3.17 mm (1/8 inch) thick piece of titanium (6Al-4V) was used as a standard to set screen height at 30%.

Figure 3 displays a C-scan of an essentially void-free panel; the defect indications at each end represent expected edge effects. The C-scans also served the purpose of permitting the optimum location of test coupons for specimen machining. An example is shown in figure 4 where it can be seen that heavier defect areas were avoided by careful placement of the specimens within the panel configuration. The same ultrasonic inspection methods were employed in examining the off-axis 6.4 cm x 25.4 cm (2-1/2 x 10 inch) panels in Task II.

6.0 MECHANICAL PROPERTY TESTING

The following sections describe the properties selected for evaluation and the test methods used for both Task I (Preliminary Evaluation) and Task II (Final Evaluation).

6.1 Task I - Preliminary Evaluation Testing Approach

A first objective was, of course, to determine if any of the fiber coatings improved composite impact strength and toughness. Two tests were directed at obtaining this information. These included an un-notched Izod impact test and a determination of the critical stress intensity factor, K_c, with a fracture toughness specimen. It was also important to know if other properties, more commonly measured, were affected. For these determinations, three tests were selected; these were shear strength by the short beam method, a flexural strength test, and longitudinal tensile strength.

6.2 Task II - Final Evaluation Testing Approach

Once a material system was selected on the basis of Task I work, the plan was to further define the system by collecting data on other characteristics which would also be of potential interest to designers. The tests selected were as follows: longitudinal and transverse tensile, longitudinal and transverse compression, and intralaminar shear by a new test method proposed by NASA-Lewis. Test results from each of the methods were to be accompanied by stress-strain diagrams. The new intralaminar shear method proposed by NASA-Lewis personnel is described in Section 6.4.

6.3 Task I Test Methods

All of the test data on the program were generated using two basic pieces of equipment. These were the Instron Universal Testing Machine, Model TTC, with a 4448 Newton (10,000 pound) capacity, and the Tinnius-Olsen "Change-O-Matic" Impact Test Machine with a capacity of 23 N·m (200 inch-pounds). Strain measurements on fracture toughness and tensile specimens were conducted with Instron strain gage extensometers.

Three of the test specimens employed are industry standards and require little explanation. These were the short beam shear specimen, the flexure specimen and the 0° fiber orientation tensile specimen. These specimens are illustrated in figures 5, 6 and 7, respectively. The short beam shear test is essentially a three point loaded flexure specimen with a very small span-to-depth ratio (4.5 ±0.5 to 1). The flexure specimen used was a three point loading design with a span-to-depth ratio of 35 ±2 to 1. A tensile failure in the composite on the bottom side of the flexure specimen was sought. This failure mode has been observed to yield the highest values with a material, and it is felt best fulfills the classic definition of a flexure test. Each specimen was observed after test and the failure mode recorded. The tensile specimen shown in figure 11 was held with wedge grips in the Instron and the strain was measured with an extensometer.

The un-notched Izod impact specimen used is shown in figure 9. As can be seen, the specimens were built up by bonding cured laminate sections together with an epoxy adhesive. A nominal thickness of 6.1 mm (0.240 inches) was desired based on thickness of individual laminates. The bonded specimen is an accepted practice; however, the overall size of the specimen is not. Previous work at TRW has indicated that specimen size can have a large effect on the values obtained. Further, certain very thin specimens can be tested that eliminate or minimize the delamination effect, a major contributor to energy management. The selected size was chosen because of TRW's past experience with it and general knowledge of probably performance with various materials. Other workers have employed a similar specimen; Chamis et al (16) used a specimen 7.9 x 7.9 x 37.6 mm (0.311 x 0.311 x 1.5 inches). Since all data are comparative in the impact data gathered, it was felt that the specimen selected represented a suitable choice.

The fracture toughness specimen shown in figure 8 was based on work reported (17) by M. A. Wright and F. A. Iannuzzi. In this paper, one of the conclusions drawn is that "The principles of linear elastic fracture mechanics can be used to describe the failure of carbon reinforced epoxy specimens irrespective of whether the specimens fail by transverse crack propagation or longitudinal splitting." Additionally, their investigations established a width correction factor for specimen widths from 12.7 to 25.4 mm (0.5 to 1.5 inches). Since the correction factor for the 12.7 mm (0.5 inch) wide specimen is 1.00, this specimen width was selected for all evaluations.

Wright and Iannuzzi give the following equation for the critical stress intensity factor, K_c:

$$K_c = \frac{P_c\sqrt{a}}{wt}\left[1.98 + 0.36\left(\frac{2a}{w}\right) - 2.12\left(\frac{2a}{w}\right)^2 + 3.42\left(\frac{2a}{w}\right)^3\right]\left[\frac{1}{\beta}\right]^{\frac{1}{2}}$$

Where:

P_c = critical load
a^c = notch depth
w = specimen width
t = specimen thickness
β = correction factor for specimen width

Note that the numerical values reported are termed K_c, indicating a condition of plane stress in determining the critical stress intensity factor. The symbol K_{Ic} is commonly construed to represent the critical stress intensity factor under conditions of plane strain. The K_{Ic} value can only be determined by testing a large number of specimens of increasing thickness until the K values become asymptotic with thickness increases (18). This kind of test program was obviously beyond the scope of the program, and since no industry standards have been developed, the specimen geometry of Wright and Ianuzzi was chosen and the values obtained designated as K_c values.

Specimens were prepared on the subject program by bonding on the tab material with a room temperature curing epoxy adhesive and then cutting the laminate axially to provide individual specimens. The specimen edges were then ground and stacked together, with a back-up material between each specimen, and the notches put in with a grinding wheel with a 28 degree included angle and the tip dressed to as small a radius as possible. Optical comparitor measurements of each of the specimens indicated that the notch radius ranged from 0.038 mm to 0.050 mm (0.0015 inch to 0.002 inch). An examination under a microscope determined that the notches were clean and without ragged edges. The depth of notches did not vary by more than 0.050 mm from the desired 3.17 mm dimension (0.125 inch) shown in the specimen sketch.

In first trials of this specimen in test, it was planned to accept, as the critical load, that load which corresponded to first visual signs of cracking or splitting in the specimen. However, it was noted that visual splitting was proceeded by both audible indications of specimen damage and a disruption of the load-displacement curve being autographically recorded. Since these events indicated initiation of crack propagation, the first significant disruption of the load-deflection curve was finally chosen as representing the critical load and was used for calculating all values shown. Figure 10 shows two typical load deflection curves collected on fracture toughness test specimens. The upper curve clearly shows a large extension without accompanying increase in load; this point was selected as indicating the critical load (P_c) for this specimen. In the bottom curve of figure 10, an example is shown that is perhaps not quite so clear cut. However, judgments were made with each curve, and as can be seen from the data, concordant results were obtained.

6.4 Task II Test Methods

The longitudinal tensile specimen is described above. The transverse tensile specimen that was used is shown in figure 11. The significant feature of this design is the pin gripping. This provides two advantages; first, the application of uniaxial loads in testing without the occurrence of extraneous loads from improper alignment of the tabs in wedge grips, and second, ease of specimen installation in the Instron load yokes without having to torque wedge grips on the tabs, a practice which leads to a high specimen mortality rate.

The compression fixture used for both longitudinal and transverse loading is shown in figure 12; this is the Celanese type fixture. This method eliminates two serious problems commonly encountered in compression testing, namely, specimen end brooming and off-axis loading during test. TRW has used this method for several years with good success. The specimen design is shown in figure 13 and was used for both transverse and longitudinal tests.

The specimen for the new intralaminar shear test is shown in figure 14. In essence, it is an off-axis tensile coupon with a rosette strain gage in the center. The strain and stress values collected are transformed by the equations shown in figure 15. Figure 16(a) shows the equations required to reduce the strain values obtained from the strain gages on the specimen for use in

the governing transformation equations. Figure 16(b) shows the solution of the matrix algebra equations of figure 16(a). Strain outputs during test were recorded on a Honeywell Visicorder, a high speed light oscillograph type unit.

7.0 TEST RESULTS AND DISCUSSION

7.1 Task I Results

All of the property data collected in Task I are listed in tables II through VI. Since only two specimens were tested for each condition, it was felt that each value should be reported, rather than averages. Figures 17 through 23 present the most significant test data in graphic form with all values plotted. Table VII summarizes all the results in a single table by comparing the properties of coated fiber laminates with those of the uncoated fiber control laminates. The values in the body of the table are percent increases or decreases for each property (maximum values used) from the control laminate standards. Additionally the number of improved properties is shown at the bottom of the table.

As was noted previously, the 828/HHPA epoxy matrix system is a difficult one to work with and responded differently with each fiber and coating so that some difficulty was encountered in obtaining a narrow fiber fraction range. Resin flow values in laminating and laminate thickness were used as controls on fiber volume. Excessively thin laminates or those experiencing too much resin flow during laminating were rejected for use. It is estimated that the majority of laminates had a 55-60 v/o fiber content.

In each case, the fiber coating applied was considered as part of the matrix for calculation purposes. This latter fact has two consequences; first, all the composites were targeted to contain the same total number of carbon fibers to carry the load imposed during testing; i.e., each composite was calculated to have the same volume percent graphite fiber. Second, this technique materially reduced the amount of epoxy resin available in composites with heavier coatings for transferring the load from fiber to fiber. For example, the prepreg prepared for laminate 719-52, the HM-S control laminate with no fiber coating, had a resin weight percent of 39.6%. The prepreg prepared, using the calculations described above, for laminate 719-91, the HM-S fiber coated with 0.5 μm of nickel, had 25.7 w/o resin binder. Presuming some nominal flow in molding, it can be seen that laminate 719-91, in finished form, had considerably less resin available to transfer imposed test loads. It is not known what effect this variable had on each of the different properties.

Since the objective of the program was to identify a fiber-matrix interphase that provides improved toughness or impact characteristics, an important property to consider is that of Izod impact strength. Table II lists each value for all specimens tested. Since the specimens were of somewhat different thickness because of their bonded construction, the impact values are also recorded as impact energy per cross-sectional area. These latter values were used in plotting figure 17, and as can be seen, both the K-500 coating and the nickel improved the Izod impact strength of the HM-S laminates to a significant degree. Improvements as much as 117% are noted for the heaviest nickel coating (table VII). It is also apparent that each of the fiber coatings, with the exception of the P-1700, degraded the impact strength of A-U fiber laminates. The exact percentage change effected can be noted in table VII.

Figure 24 displays selected fractured Izod specimens. The brittle fracture of the bare HM-S vs. the A-U and A-S control specimens can easily be seen. A careful examination of the bare HM-S specimen fracture surface shows an interesting phenomenon. It is apparent that there are alternating layers of material that experienced repeated tensile and then compressive failure. A very dramatic comparison, illustrating the brittle nature of the boron coated A-U fiber specimens, is shown by observing the clean fracture of the boron coated A-U fiber specimen vs. the A-U control specimen.

The mechanism of contribution of the various coatings to the altered Izod impact strength is not clear. In order to gain information of this type, samples were subjected to scanning electron microscopy (SEM). It was hoped that an examination of the fractured faces under high magnification would provide the basis for a suitable hypothesis. Samples were selected to include all three control materials and representative samples of fiber/coating systems in multiple coating thicknesses. In each case, SEM's were taken at magnifications of 20, 200 and 2000. All specimens were ultrasonically cleaned and coated with approximately 2×10^{-8} m (200 angstroms) of gold prior to examination. In each case, the tensile failure side of the specimen was examined, i.e., the side of the specimen exhibiting fiber pullout.

Figures 25 through 31 show a limited number of SEM's at 200X and 2000X. A review of the SEM's was inconclusive. With the exception of the heavy nickel coating, which is easily discerned in Figure 30, little definitive evidence could be observed indicating the presence of fiber coatings. There was also little apparent reason for identifying any single specimen as exhibiting a failure mode that could be attached to a very high Izod value or a very low one. This portion of the work was disappointing since it was hoped that this kind of a microscopic examination of fractured surfaces would reveal important information about failure modes, mechanisms and fiber coating contributions.

A further examination of table VII shows that, with the method of testing used, the fracture toughness of the HM-S composites was decreased by the introduction of fiber coatings. The losses with the HM-S ranged from 6% to 22%. With the A-U fiber, the trends were inconclusive with the nickel coating at two thicknesses producing increases and the boron coating showing the greatest loss (22%). In addition to showing one of the largest numerical losses, the boron coated fibers, both HM-S and A-U, failed in a manner different from any other material tested.

As was noted earlier, the critical load was selected as that point in which a significant disruption of the load-displacement curve was observed. In the case of all materials tested, this first sign of specimen damage was followed by visually observable splitting along the fiber axis, originating from the point of the pre-machined notch. This failure mode can be seen in the upper specimen in figure 32. At this point, the specimen was still capable of sustaining load. In all cases with the boron coated fibers, complete specimen failure was observed shortly after the first disruption of the load-displacement curve; the failure locus is shown in the bottom specimen in figure 32. In testing laminate 722-23 (boron on HM-S), the first specimen showed curve disruption at a load of 4599 N (1034 lb) and complete failure at 4866 N (1094 lb).

The second specimen showed curve disruption at 3923 N (882 lb) and failure at 3932 N (884 lb). For comparison, consider the values for a trial specimen with uncoated HM-S fibers taken completely to failure. This specimen, tested early in the program as an evaluation of the test method, showed curve disruption at 3848 N (856 lb), visible splitting at 4599 N (1034 lb) and complete failure at 13,255 N (2980 lb). The boron coated A-U fiber laminate (722-42) behaved in the same manner as the boron coated HM-S specimens. Samples 1 and 2, respectively, showed catastrophic failure at loads of 4840 N (1088 lb) and 4537 N (1020 lb), with no observable initial occurrence of axial splitting. It seems obvious that the boron coating, on both HM-S and A-U fibers, induced an undesirable failure mode.

Changes in each of the other six characteristics measured, for all the fiber/coating combinations, can be observed in the same manner as followed above, i.e., by first reviewing the tabular data, then examining the bar charts, and finally, finding the percent change effected in table VII. A review of all the A-U fiber data indicates that the P-1700 polysulfone resin had the most postitive effect of any of the coatings on this fiber with large increases in modulus values and minimum changes in other characteristics. The nickel coating did show some improvements in fracture toughness behavior, but these increases were more than offset by the other losses experienced.

In considering the coatings on HM-S, it is obvious that the K-500 polyamide material provided the most consistent and the greatest number of property improvements. The P-1700 coating provided the next greatest number of improvements, with the largest being in tensile performance with a small improvement in impact strength and minimum losses in other areas. The nickel coating on the HM-S did show the largest improvement in Izod impact and modulus values. This latter fact is not surprising since a portion of the low modulus resin was replaced by the nickel coating which has an approximate modulus of twenty-five million pounds per square inch. However, the losses in other property values in addition to the cost and the added weight in low density composites made the nickel a less than desirable system for consideration.

On balance, then, the K-500 resin coating with the HM-S fiber appeared to provide a system with significant worth. Improvements were noted with each coating thickness in Izod impact, tensile strength, tensile elongation and flexural modulus. Consistent losses were shown with fracture toughness, tensile modulus and flexural strength. Short beam shear, surprisingly enough, showed improvements with 0.05 and 0.10 μm coating thicknesses but fell off sharply with the heaviest (0.2 μm) coating.

In comparing the performance of the three thicknesses of the K-500 coating on the HM-S fiber, it would appear that an intermediate thickness coating provided the best tradeoff of desirable properties. The 0.05 μm coating shows an improvement in five out of the eight properties investigated but shows only a 2% improvement in Izod impact. The 0.2 μm K-500 coating exhibits the largest improvement in impact, 75%, but produces a large loss in short beam shear strength. Additionally, the 0.20 μm coating shows the greatest loss in flexural strength and fracture toughness. For these reasons, the K-500 polyamide-imide coating material at a thickness level of 0.15 μm was chosen as

representing a useful, desirable material for further investigation in Task II, Final Evaluation, of the program.

7.2 Task II Results

The tabulated results of all data collected in Task II are shown in tables VIII through XII. The stress/strain curves for each of the five different characteristics investigated are shown in figures 33 through 37. Photographs of fractured specimens are displayed in figures 38 through 41.

The longitudinal tensile properties of the K-500 coated HM-S fiber/resin composites are shown in table VIII. Figure 33 displays the stress/strain curves of these specimens taken from extensometer readings. The failure mode of the tensile specimens, with extensive, widespread disruption, is illustrated in figure 38. This can be compared to boron coated fiber composite specimens tested in Task I work which displayed a brittle fracture confined to a single failure locus normal to the direction of the load. It is felt that the K-500 coating aids in transferring the tensile stress from fiber to fiber and thus leads to the type of failure shown in figure 38.

The transverse tensile data are shown in table IX and the stress/strain curves in figure 34. While the strain and modulus values are what might be expected, the strength values are about half of what might be anticipated. Considering that the 0.05 and 0.10 μm coating thicknesses had shown substantial improvements in shear strength in Task I, indicating an improved bonding compared to bare fiber, the low transverse tensile values were unexpected. On the other hand, the drastic drop in shear strength at the heaviest coating level (0.02 μm) might indicate a maximum or optimum coating thickness for this property. Four specimens from one laminate represent a limited base on which to draw conclusions, but this level of strength values indicates a need for further investigation.

Table X lists the longitudinal compression test results obtained. Figure 35 shows only one of the three stress/strain curves; difficulties were encountered with the strain gages on two of the specimens in the latter portions of the test so that complete curves were not possible. Moduli data were taken from the first sections of the curves before difficulty was encountered. The values shown represent fairly typical levels for an HM-S reinforced epoxy system. A failed specimen is shown in figure 39, demonstrating the location and type of failure experienced.

As can be seen from an examination of table XI, no strain data are shown for the transverse compression tests run. While figure 36 displays the three stress/strain curves obtained, the data are not deemed reliable. It is felt that this may be the result of the test method used for transverse compression. The Celanese type specimen used was strain gaged to record strain in the direction of loading only. It was observed, as shown in figure 40, that the specimen bulged under load so that the strains indicated by the strain gages may not have been representative of actual behavior. The modulus values shown were taken from the first portions of the curves before the knee in the curve

occurred. These modulus values compare well with typical numbers shown in the literature, but the ultimate strength average of 94 MN/m^2 (13.6 ksi) is lower than the expected typical figure of 138 MN/m^2 (20 ksi). It is obvious that further work in the area of transverse compression would be warranted.

The data from the last test series, on intralaminar shear, is given in table XII. Figure 41 shows the two failed test specimens with the failure mode clearly seen. The ultimate strength values for this material, by the 10^o off-axis tensile test, while relatively closely grouped, are about half of what the literature indicates for in-plane shear for typical HM-S epoxy laminates. Once again the optimum coating thickness may have been missed. The literature gives a typical shear modulus of 4.5 GN/m^2 (0.65 msi); this compares to the two values developed on this program of 31.7 and 14.5 GN/m^2 (4.6 and 2.1 msi). Figure 37 displays the two stress/strain curves plotted from the strain gage data. Instrumentation difficulty was encountered with the strain gages on the third specimen so no data are available. Further work in this area is required since it is difficult to define any potential problem as the test method used is new and the material represents a system that has not been examined before. To finally determine if the fiber coating approach is responsible for the erratic data obtained, a large number of repetitive tests would have to be run, preferably with various similar coatings and multiple matrices.

In summary, the test values for the K-500 coated HM-S fiber laminates that were developed on straightforward, recognized test methods such as longitudinal tensile and compression, compare well with published data for uncoated HM-S materials. The values from tests which are more difficult to run were less than anticipated. It can only be concluded that further work with multiple specimens and laminates would be required before final judgments were made.

8.0 CONCLUSIONS

1. It has been shown that it is feasible to significantly alter the properties of graphite fiber reinforced composites by introducing a fiber/resin interphase. For example, in one case an improvement of 117% in Izod impact strength was realized with an electroless nickel coating on high modulus graphite fiber. Boron coating, on the other hand, produced a 66% drop in Izod impact strength of composites with the same fiber.

2. Low modulus, high strain-to-failure coatings showed the best balance of property improvement and the most consistent performance. It was also shown that property performance is a function of coating thickness. While it is not possible to make a final judgment with the limited number of experimental iterations and thicknesses evaluated, it is probable that specific characteristics respond optimally to different coating thicknesses.

3. Specifically, the system providing the best combination of cost effectiveness, coating ease and property enhancement was that of high modulus graphite HM-S fiber coated with a Kerimid-500 polyamide-imide resin in the thickness range of 0.10 to 0.15 μm.

4. The high strength graphite type A fiber did not show significant improvement beyond bare fiber control values with any of the coatings investigated. It is concluded that further work with this type of reinforcement is not warranted.

5. Certain properties, specifically transverse tensile, transverse compression and intralaminar shear for coated fiber composites, were lower than literature values for uncoated fiber composites with the high modulus graphite reinforcement. It should be noted, however, that no direct back-to-back comparisons of these properties were run with control specimens on this program. Additional work with varying coating thicknesses would have to be performed to determine if the characteristics noted above respond to different optimal coating thicknesses. Further, it is suggested that alternate and/or additional test methods would have to be employed to fully evaluate the properties in question before a final conclusion could be reached on the behavior of the coated fiber composites in the loading modes mentioned above.

6. In summary then, it is felt that the program objective of demonstrating the feasibility of increasing the impact strength of composites by the introduction of a fiber/matrix interphase has been met.

9.0 RECOMMENDATIONS

Because of the established feasibility of inducing significant property improvements with a fiber coating on high modulus graphite fiber composites and, because of certain unanticipated anomalies identified during the course of the program, it is recommended that further work be pursued to further develop and refine the concept and characteristics of composites containing an intermediate coating between fiber and matrix. This work should include further survey work with similar coatings of the low modulus, high strain capability of the type identified in this program with other more suitable primary matrices; other high modulus fibers, e.g., the extremely high modulus graphite fibers as well as boron; and with the testing of additional characteristics such as ballistic impact, elevated temperature testing, and time dependent characteristics such as fatigue and creep. A careful study of test specimens and methods should be considered and perhaps changes made to standard approaches which, for the most part, were developed for more conventional composites. No less important would be an investigation of mechanisms operating to induce these property improvements. This type of investigation should include, for example, studies of failure of single fiber specimens, coating completeness and uniformity, and bonding characteristics of the fiber, interphase and matrix system. The SEM approach used on this program did not reveal the performance mechanisms involved as anticipated. Perhaps other techniques such as high speed motion pictures of specimens during fracture along with SEM would be instrumental in identifying the modes involved.

TABLE I

TYPICAL MOLD CYCLE FOR 828/HHPA/BDMA RESIN COMPOSITES

1. Stack prepreg.
2. Expose for 30 minutes at 121°C (250°F) (circulating air oven).
3. Expose for 30 minutes at 204°C (400°F) (circulating air oven).
4. Cool.
5. Preheat die in press to 213°C (415°F).
6. Install stack in die and apply contact pressure with preheated punch.
7. Wait 5 minutes.
8. Apply pressure as required (up to 1000 psi) to induce a small bead of resin flash on the end of the laminate.
9. Hold 1-1/2 hour.
10. Cool to room temperature under pressure.
11. Deflash, weigh, measure, etc.

TABLE II

TASK I - UN-NOTCHED IZOD IMPACT STRENGTH RESULTS

Fiber	Fiber Coating	Calculated Coating Thickness μm	Lam. No.	Izod Value Joules	Izod Value ÷ Area X 10^4 J/m^2	Izod Value in-lbs	Izod Value ÷ Area in-lbs/in^2
A-S	None	-	719-34	8.47 8.81	18.1 18.6	75 78	1037 1064
A-U	None	-	719-28	9.94 9.26	21.1 19.2	88 82	1209 1102
HM-S	None	-	719-52	2.93 4.06	5.5 7.8	26 36	319 448
HM-S	K-500	0.05	719-57	3.16 3.61	6.8 7.9	28 32	394 456
HM-S		0.1	719-58	5.08 2.93	10.2 5.9	45 26	588 342
HM-S		0.2	722-3	6.77 6.77	13.6 13.4	60 60	779 766
A-U		0.05	719-72	10.50 8.47	20.0 16.5	93 75	1144 945
A-U		0.1	722-14	7.68 9.71	13.6 17.1	68 86	777 977
A-U		0.2	719-73	7.79 7.34	14.5 13.5	69 65	830 773
HM-S	Ni	0.10	719-95	3.95 4.06	7.9 8.2	35 36	455 473
HM-S		0.20	722-1	4.74 4.97	11.3 11.6	42 44	649 665
HM-S		0.50	719-91	7.68 9.71	13.4 17.0	68 86	770 974
A-U		0.10	719-89	8.47 9.15	16.7 17.8	75 81	958 1017
A-U		0.20	719-79	7.11 7.90	15.6 16.9	63 70	897 967
A-U		0.50	719-77	6.10 8.47	13.0 17.5	54 75	743 1002
HM-S	Boron	0.20(a)	722-23	1.1 1.4	2.2 2.7	10 12	126 152
A-U	Boron	0.20(a)	722-42	1.4 1.2 1.6	3.2 2.9 3.8	12 11 14	182 167 215
A-U	P-1700	0.10	722-60	5.8 7.2 5.3	15.9 19.1 14.9	51 64 47	910 1093 850
HM-S	P-1700	0.10	722-59	3.8 3.7 4.1	8.1 8.1 8.9	34 33 36	464 463 508

(a) Estimated

TABLE III

TASK I - FRACTURE TOUGHNESS RESULTS

Fiber	Fiber Coating	Calculated Coating Thickness μm	Lam. No.	Critical Stress Intensity Factor, K_c $\frac{MN}{m^2\sqrt{m}}$	Critical Stress Intensity Factor, K_c $ksi\sqrt{in.}$
A-S	None	-	719-34	19.0 18.1	17.3 16.5
A-U	None	-	719-28	15.3 15.4	13.9 12.2
HM-S	None	-	719-52	20.8 20.3	18.9 18.5
HM-S	K-500	0.05	719-57	17.4 14.9	15.8 13.5
HM-S		0.10	719-58	16.3 17.2	14.8 15.6
HM-S		0.20	722.3	16.2 16.3	14.7 14.8
A-U		0.05	719-72	15.5 14.1	14.1 12.8
A-U		0.10	722-14	13.1 13.0	11.9 11.8
A-U		0.20	719-73	12.8 13.4	11.7 12.2
HM-S	Ni	0.1	719-95	15.4 17.2	14.0 16.7
HM-S		0.2	722-1	16.1 15.7	14.7 14.3
HM-S		0.5	719-91	12.5 16.4	11.4 14.9
A-U		0.1	719-89	13.9 11.0	12.6 10.0
A-U		0.2	719-80	16.8 17.7	15.2 16.1
A-U		0.5	719-78	15.8 15.6	14.4 14.2
HM-S	Boron	0.20[(a)]	722-23	18.3 15.4	16.7 14.0
A-U	Boron	0.20[(a)]	722-42	7.0 11.9	6.4 10.9
A-U	P-1700	0.10	722-60	15.2 15.3	13.8 13.9
HM-S	P-1700	0.10	722-59	19.6 18.9	17.8 17.2

(a) Estimated

TABLE IV

TASK I - SHORT BEAM SHEAR STRENGTHS

Fiber	Fiber Coating	Calculated Coating Thickness μm	Lam. No.	Strength MN/m^2	Strength ksi	
A-S	None	-	719-34	81.3	11.8	
				78.6	11.4	
				80.6	11.7	
				79.9	11.6	Avg
A-U	None	-	719-28	76.5	11.1	
				75.1	10.9	
				75.1	10.9	
				75.8	11.0	Avg
HM-S	None	-	719-52	69.6	10.1	
				66.8	9.7	
				66.8	9.7	
				67.5	9.8	Avg
HM-S	K-500	0.05	719-57	90.3	13.1	
				93.7	13.6	
				94.4	13.7	
				93.0	13.5	Avg
HM-S		0.10	719-58	83.4	12.1	
				86.1	12.5	
				77.9	11.3	
				82.7	12.0	Avg
HM-S		0.20	722-3	34.4	5.0	
				41.3	6.0	
				39.9	5.8	
				38.6	5.6	Avg
A-U		0.05	719-72	51.0	7.4	
				48.2	7.0	
				48.2	7.0	
				48.9	7.1	Avg
A-U		0.1	722-14	42.0	6.1	
				42.7	6.2	
				37.9	5.5	
				40.6	5.9	Avg
A-U		0.20	719-73	38.6	5.6	
				39.3	5.7	
				39.9	5.8	
				39.3	5.7	Avg

TABLE IV (continued)

TASK I - SHORT BEAM SHEAR STRENGTHS

Fiber	Fiber Coating	Calculated Coating Thickness μm	Lam. No.	Strength MN/m^2	Strength ksi	
A-U	K-500	0.10	719-69	45.5	6.6	
				52.4	7.6	
				51.0	7.4	
				48.2	7.0	Avg
HM-S	Ni	0.10	719-95	48.2	7.0	
				48.9	7.1	
				46.8	6.8	
				48.2	7.0	Avg
HM-S		0.20	722-1	39.9	5.8	
				41.3	6.0	
				27.5	4.0	
				36.5	5.3	Avg
HM-S		0.50	719-91	39.9	5.8	
				36.5	5.3	
				40.6	5.9	
				39.3	5.7	Avg
A-U		0.10	719-89	29.6	4.3	
				30.3	4.4	
				30.3	4.4	
				30.3	4.4	Avg
A-U		0.20	719-79	30.3	4.4	
				25.5	3.7	
				30.3	4.4	
				28.9	4.2	Avg
A-U		0.50	719-77	42.0	6.1	
				46.8	6.8	
				35.8	5.2	
				41.3	6.0	Avg
HM-S	Boron	0.20[a]	722-23	53.8	7.8	
				49.0	7.1	
				53.1	7.7	
				52.0	7.5	Avg
A-U	Boron	0.20[a]	722-42	61.4	8.9	
				60.0	8.7	
				59.2	8.6	
				62.1	9.0	
				60.7	8.8	Avg
A-U	P-1700	0.10	722-60	56.5	8.2	
				67.6	9.8	
				60.0	8.7	
				61.4	8.9	Avg.
HM-S	P-1700	0.10	722-59	50.3	7.3	
				54.5	7.9	
				52.4	7.6	
				52.4	7.6	Avg

(a) Estimated

TABLE V

TASK I - TENSILE STRENGTH TEST RESULTS

Fiber	Fiber Coating	Calculated Coating Thickness μm	Lam. No.	Strength MN/m^2	Modulus GN/m^2	Elongation %	Strength ksi	Modulus msi
A-S	None	-	719-34	1556 1407	126 106	1.1 1.2	225.7 204.2	18.4 15.5
A-U	None	-	719-28	1432 726	97 117	1.2 0.6	207.7 (a) 105.4	14.1 17.0
HM-S	None	-	719-52	1073 1065	189 164	0.6 0.6	155.7 154.5	27.5 23.9
HM-S	K-500	0.05	719-57	1210 1227	175 176	0.7 0.7	175.5 178.0	25.5 25.6
HM-S		0.10	719-58	1156 1055	168 171	0.6 0.6	167.7 153.1	24.4 24.9
HM-S		0.20	722-3	1148 1048	179 170	0.7 0.6	166.6 (a) 152.1	26.0 24.7
A-U		0.05	719-72	1154 1074	111 96	1.1 1.2	167.5 155.8	16.1 14.0
A-U		0.10	722-14	961 1174	90 99	1.0 1.1	139.5 170.3	13.1 14.4
A-U		0.20	719-73	1047 1098	95 101	1.2 1.0	151.9 159.3	13.9 14.7
HM-S	Ni	0.10	719-95	634 544	151 173	0.4 0.3	92.0 79.0	22.0 25.2
HM-S		0.20	722-1	661 682	177 197	0.4 0.4	95.9 99.0	25.7 28.6
HM-S		0.50	719-91	854 810	204 193	0.4 0.4	123.9 117.5	29.7 28.0
A-U		0.10	719-89	1130 1142	115 113	1.0 1.1	163.9 165.7	16.7 16.5
A-U		0.20	719-80	810 764	89 99	1.0 0.8	117.6 110.9	13.0 14.4
A-U		0.50	719-78	1062 1109	117 111	0.9 1.0	154.1 160.9	17.0 16.2
HM-S	Boron	0.20 (b)	722-23	336 343	168 165	0.2 0.3	48.8 49.8	24.3 23.9
A-U	Boron	0.20 (b)	722-42	274 324	112 139	- 0.8	39.8 47.0	16.3 20.2
A-U	P-1700	0.10	722-60	1280 1361	129 148	(c) (c)	185.6 197.4	18.7 21.4
HM-S	P-1700	0.10	722-59	1409 1375	172 177	0.8 0.7	204.3 199.4	24.9 25.6

(a) Tab slip during test.
(b) Estimated.
(c) Test difficulties encountered, values estimated to be 1%.

TABLE VI

TASK I - FLEXURAL STRENGTH TEST RESULTS

Fiber	Fiber Coating	Calculated Coating Thickness μm	Lam. No.	Strength MN/m^2	Modulus GN/m^2	Strength ksi	Modulus msi	Mode of Failure
A-S	None	-	719-34	1632	113	236.8	16.5	Complete
				1656	117	240.2	17.1	
A-U	None	-	719-28	1582	108	229.5	15.7	
				1575	112	228.5	16.3	
HM-S	None	-	719-52	1125	140	163.3	20.4	Complete
				998	124	144.8	18.1	Buckling & Delam.
HM-S	K-500	0.05	719-57	1068	150	155.0	21.9	Buckling & Tensile
				1039	152	150.7	22.1	Buckling & Tensile
HM-S		0.1	719-58	983	144	142.6	21.0	Buckling
				994	146	144.3	21.3	Complete
HM-S		0.2	722-3	841	172	122.0	25.0	Delamination
				865	140	125.5	20.4	Buckling
A-U		0.05	719-72	1150	99	166.9	14.5	Delamination
				1307	101	189.6	14.7	Delamination
A-U		0.1	722-14	1234	91	179.1	13.2	Buckling & Delam.
				1287	92	186.8	13.4	Buckling & Delam.
A-U		0.2	719-73	666	79	96.6	11.6	Buckling & Delam.
				1015	92	147.3	13.4	Buckling
HM-S	Ni	0.1	719-95	1149	155	166.7	22.6	Buckling & Tensile
				966	140	140.2	20.4	Buckling & Tensile
HM-S		0.2	722-1	1061	175	153.9	25.5	Delamination
				735	163	106.7	23.7	Irreg. Buckling

TABLE VI (continued)

TASK I - FLEXURAL STRENGTH TEST RESULTS

Fiber	Fiber Coating	Calculated Coating Thickness μm	Lam. No.	Strength MN/m^2	Modulus GN/m^2	Strength ksi	Modulus msi	Mode of Failure
HM-S	Ni	0.5	719-91	443	155	64.3	22.5	Delamination
				1214	175	176.2	25.4	Buckling
A-U		0.1	719-89	1060	107	153.8	15.6	Delam. & Buckling
				970	107	140.7	15.6	Delamination
A-U		0.2	719-79	1040	108	150.9	15.7	Buckling
				959	104	139.1	15.1	Buckling
A-U		0.5	719-77	1044	117	151.5	17.0	Delamination
				1506	122	218.5	17.7	Buckling & Tension
HM-S	Boron	0.2(a)	722-23	639	127	92.7	18.4	Tensile
				526	124	76.3	18.0	
A-U	Boron	0.2(a)	722-42	652	85	94.6	12.3	
				594	84	86.2	12.2	
A-U	P-1700	0.1	722-60	1660	132	240.8	19.2	
				1600	135	232.0	19.6	
HM-S	P-1700	0.1	722-59	1024	145	148.5	21.0	
				1098	153	159.3	22.2	

(a) Estimated

TABLE VII

CHANGE IN COMPOSITE PROPERTY VALUES WITH FIBER COATING SYSTEMS AS PERCENT OF CONTROL LAMINATE PROPERTIES

Fiber	HM-S								A-U							
Fiber Coating	K-500			Nickel			B	P-1700	K-500			Nickel			B	P-1700
Thickness, μm	0.05	0.10	0.2	0.1	0.2	0.5	0.20	0.10	0.05	0.1	0.2	0.1	0.2	0.5	0.20	0.10
Property	% Change								% Change							
Izod Impact	+ 2	+31	+74	+ 2	+48	+117	-66	+13	- 5	-19	-31	-16	-20	-17	-82	-10
Fracture Toughness	-16	-17	-22	-17	-22	- 21	-12	- 6	+ 2	-14	-16	- 9	+16	+ 3	-22	0
Short Beam Shear	+36	+24	-41	-30	-41	- 42	-23	-22	-33	-32	-48	-60	-60	-39	-19	-12
Tensile Strength	+14	+ 8	+ 7	-41	-36	- 20	-68	+31	-19	-18	-23	-20	-43	-23	-77	- 5
Tensile Modulus	- 7	- 9	- 5	- 8	+ 4	+ 8	-12	- 7	- 5	-15	-14	- 2	-15	0	+19	+26
Tensile Elongation	+17	0	+17	-33	-33	- 33	-50	+33	0	- 8	0	- 8	-17	-17	-33	-17
Flexural Strength	- 5	-12	-23	+ 2	- 6	+ 8	-43	- 2	-17	-19	-36	-33	-34	- 5	-59	+ 5
Flexural Modulus	+ 8	+ 4	+23	+11	+25	+ 25	-10	+ 9	-10	-18	-18	- 4	- 4	+ 9	-25	+20
Total No. of +'s or Unchanged	5	5	4	3	3	4	0	4	2	0	1	0	1	3	1	4
Total No. of -'s	3	3	4	5	5	4	8	4	6	8	7	8	7	5	7	4

NOTE: Percent change calculated from highest value in each case.

TABLE VIII

LONGITUDINAL TENSILE STRENGTH TEST RESULTS
0.15 μm K-500 on HM-S
(LAMINATE 722-39)

	Ultimate Strength		Modulus		Ultimate Strain
	MN/m^2	ksi	GN/m^2	msi	%
	1081	156.8	190	27.5	0.6
	1114	161.5	191	27.7	0.6
	1234	179.0	182	26.4	0.7
Avg.	1143	165.8	188	27.2	0.6

TABLE IX

TRANSVERSE TENSILE STRENGTH TEST RESULTS
0.15 μm K-500 on HM-S
(LAMINATE 722-85)

	Ultimate Strength		Modulus		Ultimate Strain
	MN/m^2	ksi	GN/m^2	msi	%
	18.6	2.7	8.3	1.2	0.2
	20.0	2.9	9.0	1.3	0.2
	20.0	2.9	9.0	1.3	0.3
	18.6	2.7	7.6	1.1	0.2
Avg.	19.3	2.8	8.5	1.2	0.2

TABLE X

LONGITUDINAL COMPRESSION STRENGTH TEST RESULTS
0.15 μm K-500 on HM-S
(LAMINATE 722-39)

	Ultimate Strength		Modulus		Ultimate Strain
	MN/m^2	ksi	GN/m^2	msi	%
	743	107.8	-	-	-
	776	112.5	175	25.4	0.5
	831	120.5	168	24.4	0.7
	645	93.5	190	27.5	0.8
Avg.	749	108.6	178	25.8	0.7

TABLE XI

TRANSVERSE COMPRESSION STRENGTH TEST RESULTS
0.15 μm K-500 on HM-S
(LAMINATE 722-85)

	Ultimate Strength		Modulus		Ultimate Strain
	MN/m^2	ksi	GN/m^2	msi	%
	97.2	14.1	-	-	-
	80.0	11.6	9.0	1.3	-
	99.3	14.4	11.0	1.6	-
	99.3	14.4	10.3	1.5	-
Avg.	94.0	13.6	10.1	1.5	-

TABLE XII

INTRALAMINAR SHEAR STRENGTH TEST RESULTS
0.15 μm K-500 on HM-S

Ultimate Strength $\sigma_{\ell 12}$		Modulus G		Ultimate Strain $\varepsilon_{\ell 12}$
MN/m^2	psi	GN/m^2	msi	μm/m
28.1	4070	31.7	4.6	1474
36.7	5320	-	-	-
32.6	4727	14.5	2.1	2890

NICKEL COATING

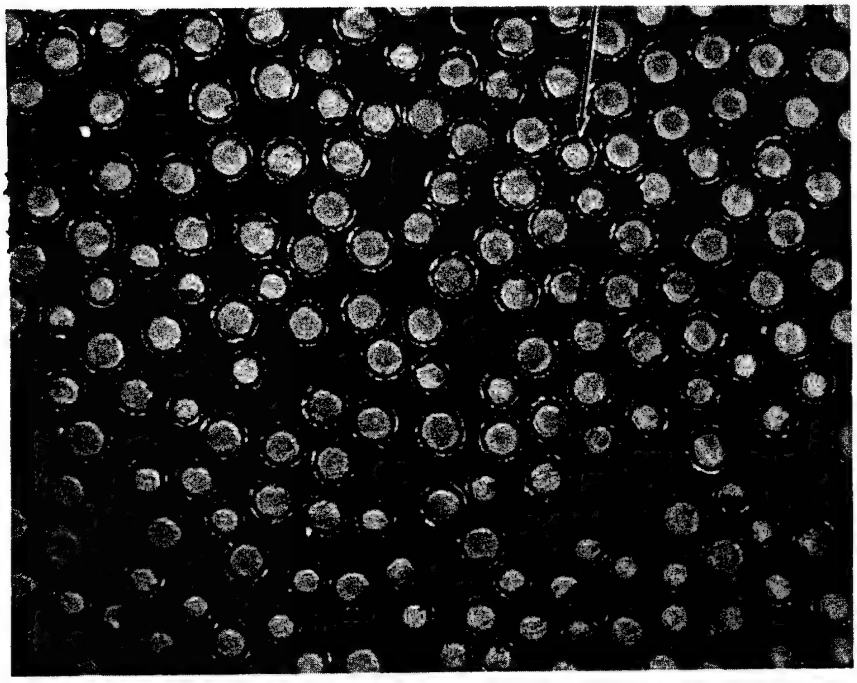

500X

FIGURE 1 ELECTROLESS NICKEL COATING ON HT-S FIBERS

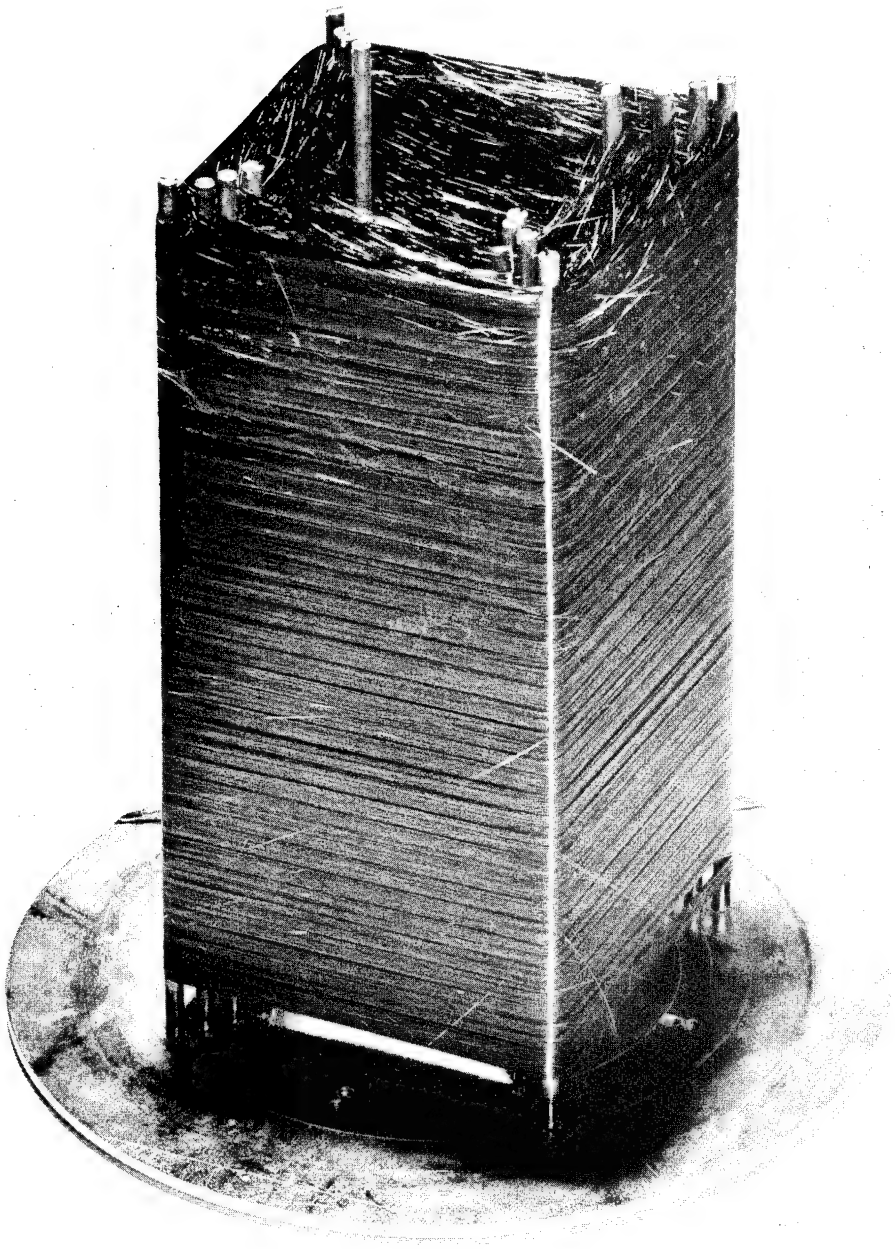

FIGURE 2 REEL FIXTURE USED IN ELECTROLESS NICKEL COATING OF FIBERS

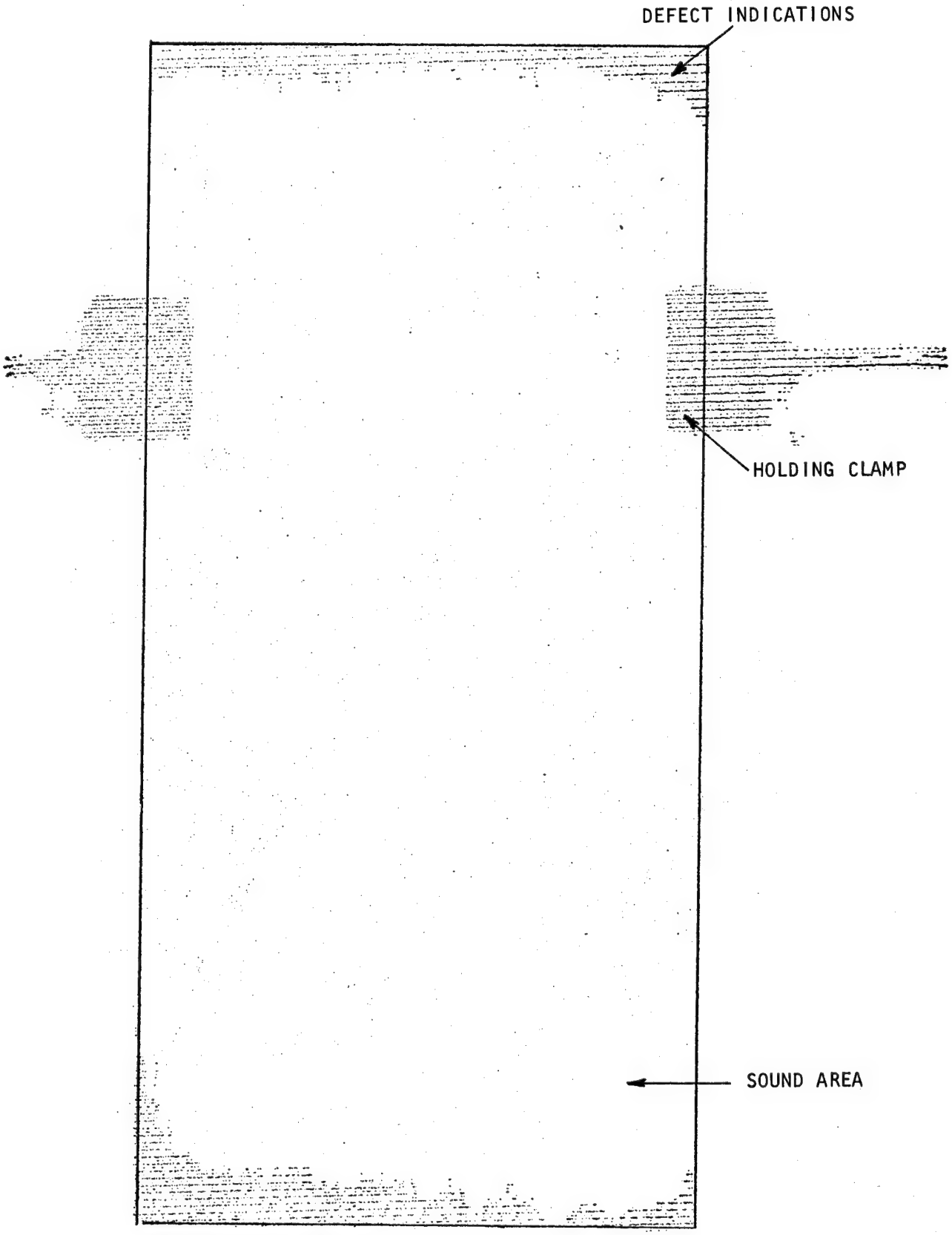

FIGURE 3 ULTRASONIC C-SCAN SHOWING SOUND AND DEFECT AREAS

7405-C

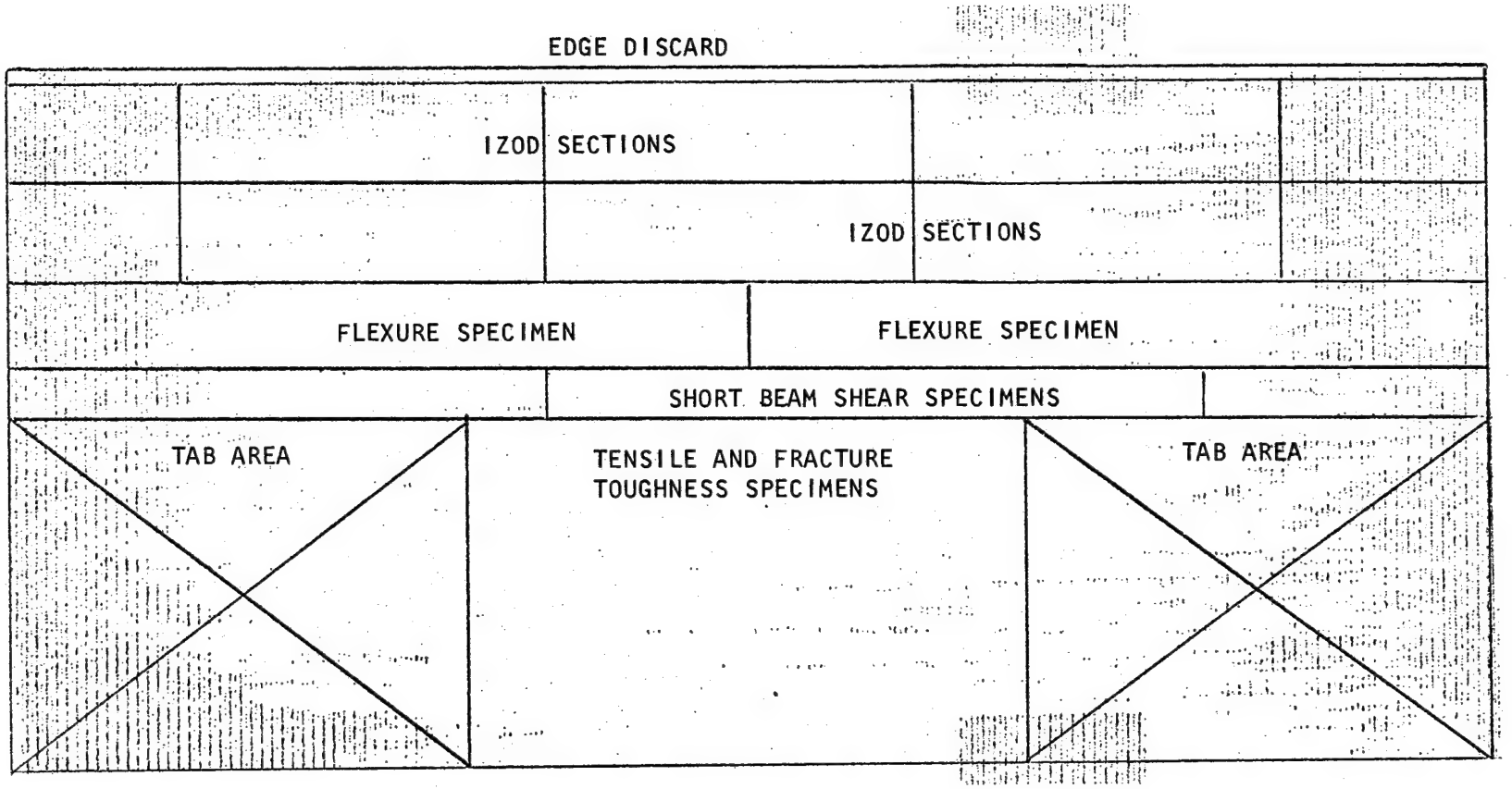

FIGURE 4 ULTRASONIC C-SCAN SHOWING USE AS SPECIMEN MACHINING MAP

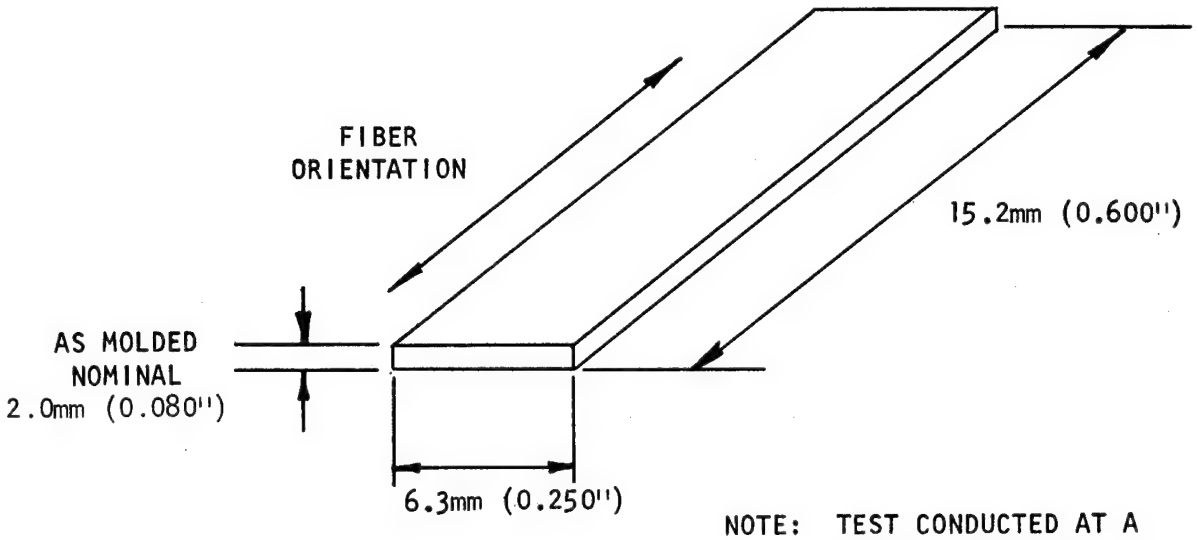

FIGURE 5 SHORT BEAM SHEAR STRENGTH SPECIMEN

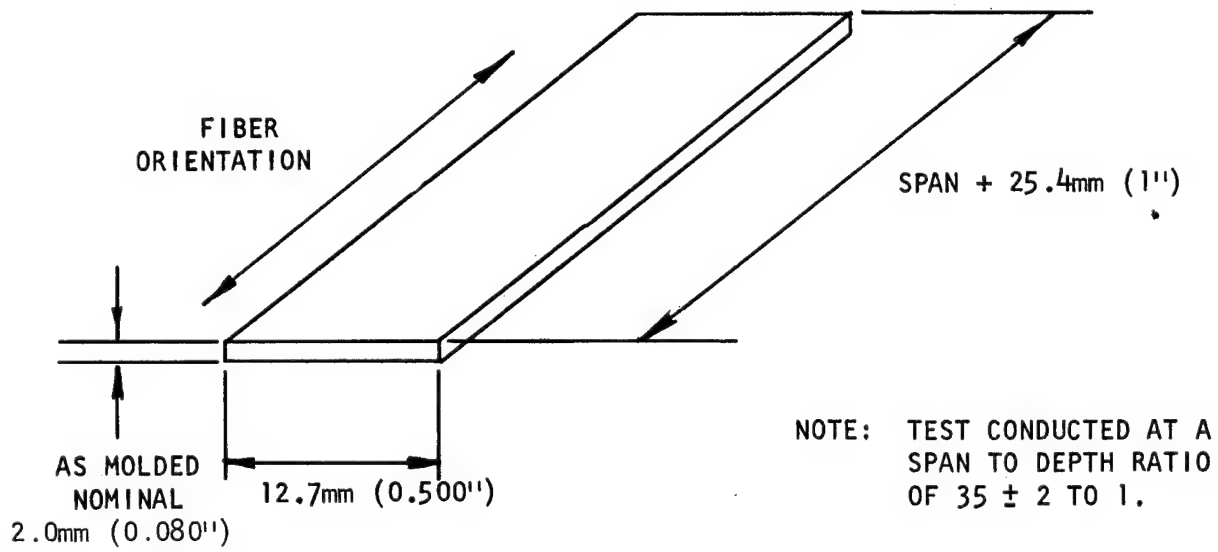

FIGURE 6 FLEXURAL STRENGTH SPECIMEN (THREE POINT)

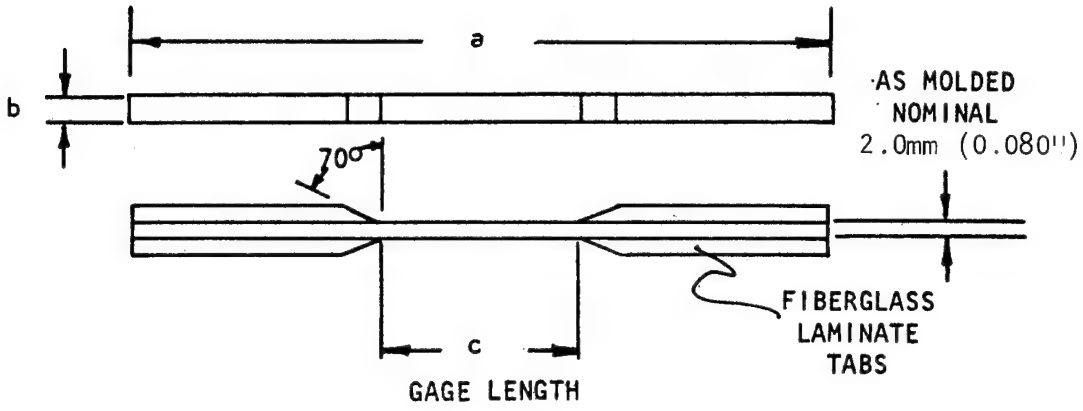

	0°	
	mm	INCHES
a	203.2	8
b	6.3	1/4
c	76.2	3

NOTE: EPOXY/FIBERGLASS CLOTH LAMINATE TABS BONDED WITH ROOM TEMPERATURE CURING EPOXY ADHESIVE.

FIGURE 7 TENSILE STRENGTH SPECIMENS

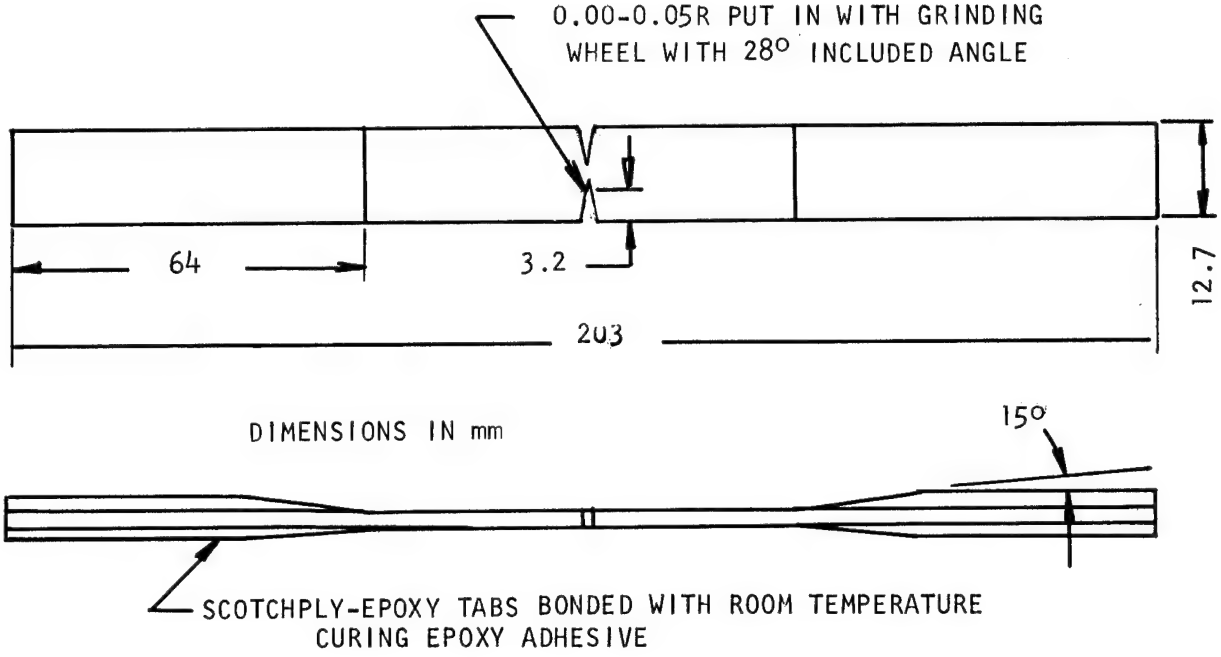

FIGURE 8 FRACTURE TOUGHNESS SPECIMEN

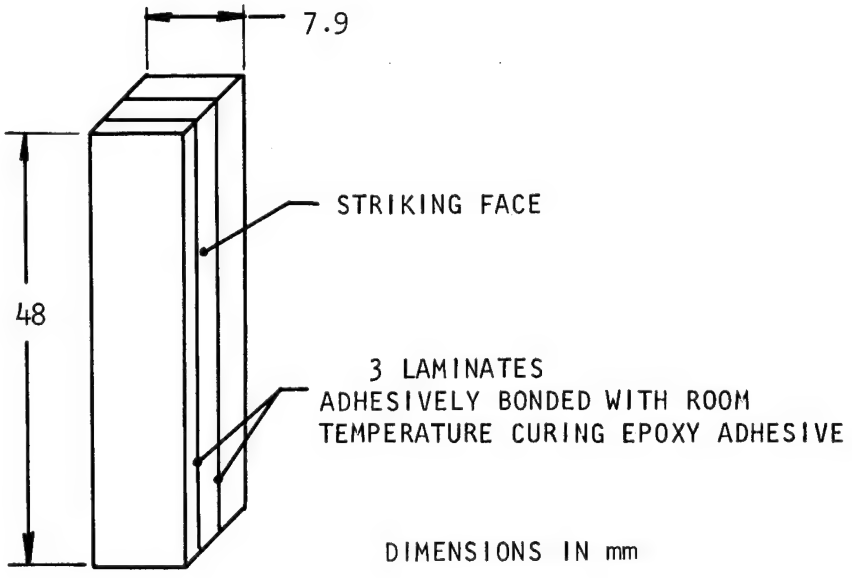

FIGURE 9 MODIFIED IZOD IMPACT STRENGTH SPECIMEN

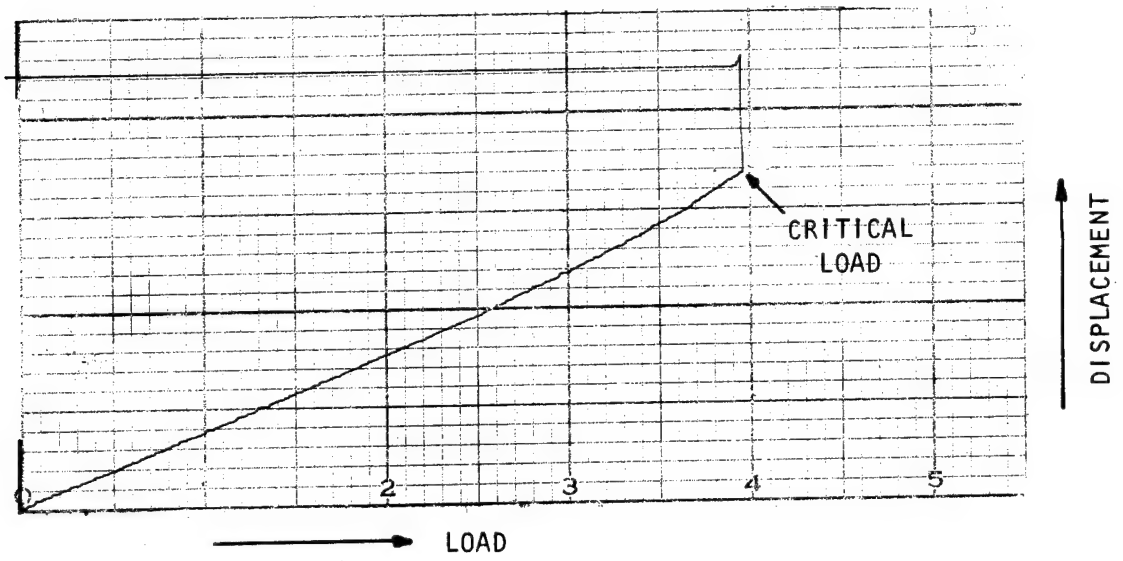

LAM 719-72 SPECIMEN #2 A-U FIBER WITH 0.05 μm K-500 COATING

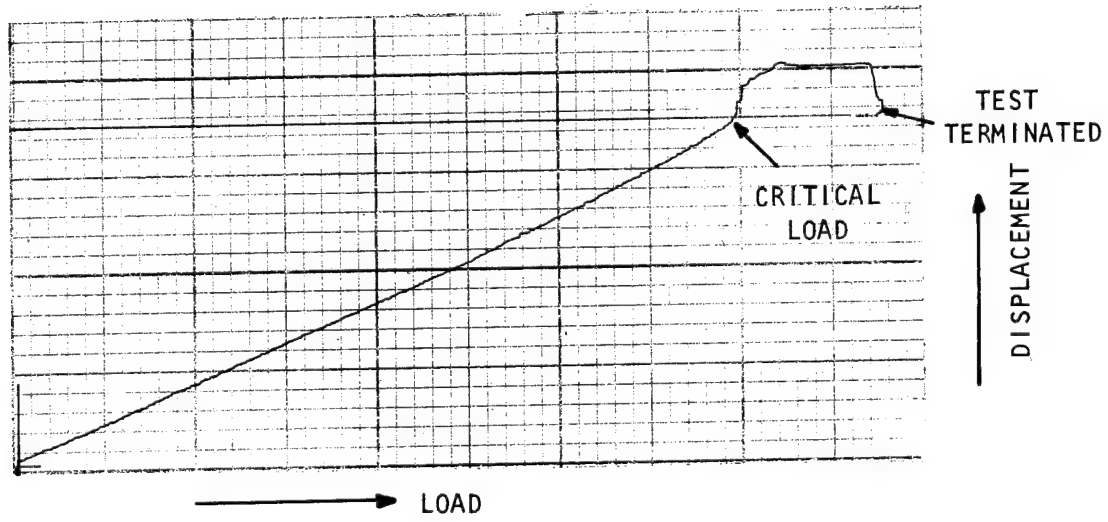

LAM 722-14 SPECIMEN #2 A-U FIBER WITH 0.10μm K-500 COATING

FIGURE 10 TYPICAL FRACTURE TOUGHNESS LOAD-DEFLECTION CURVES FROM INSTRON TENSILE TESTER

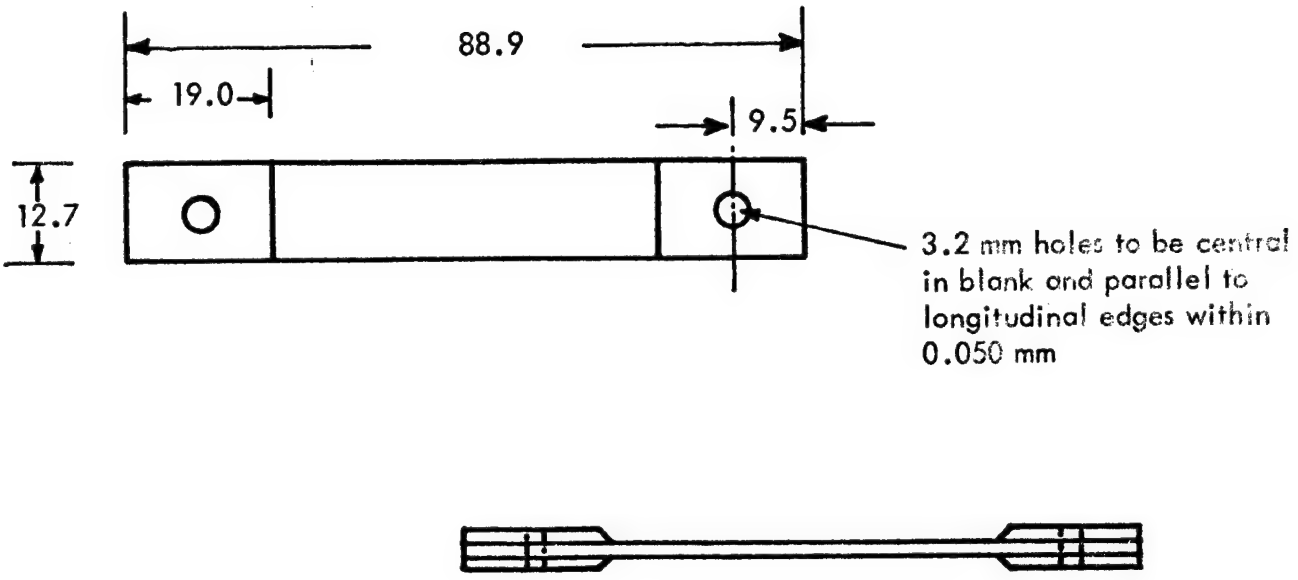

NOTES: (a) Dimensions in millimeters
(b) Laminate thickness as molded, nominal 2.0 mm
(c) Tab material glass cloth polyimide resin laminate
(d) Tabs bonded on with Kerimid 501 polyamide-imide film. The film adhesive was used to limit adhesive flow.

FIGURE 11 TRANSVERSE TENSILE STRENGTH SPECIMEN

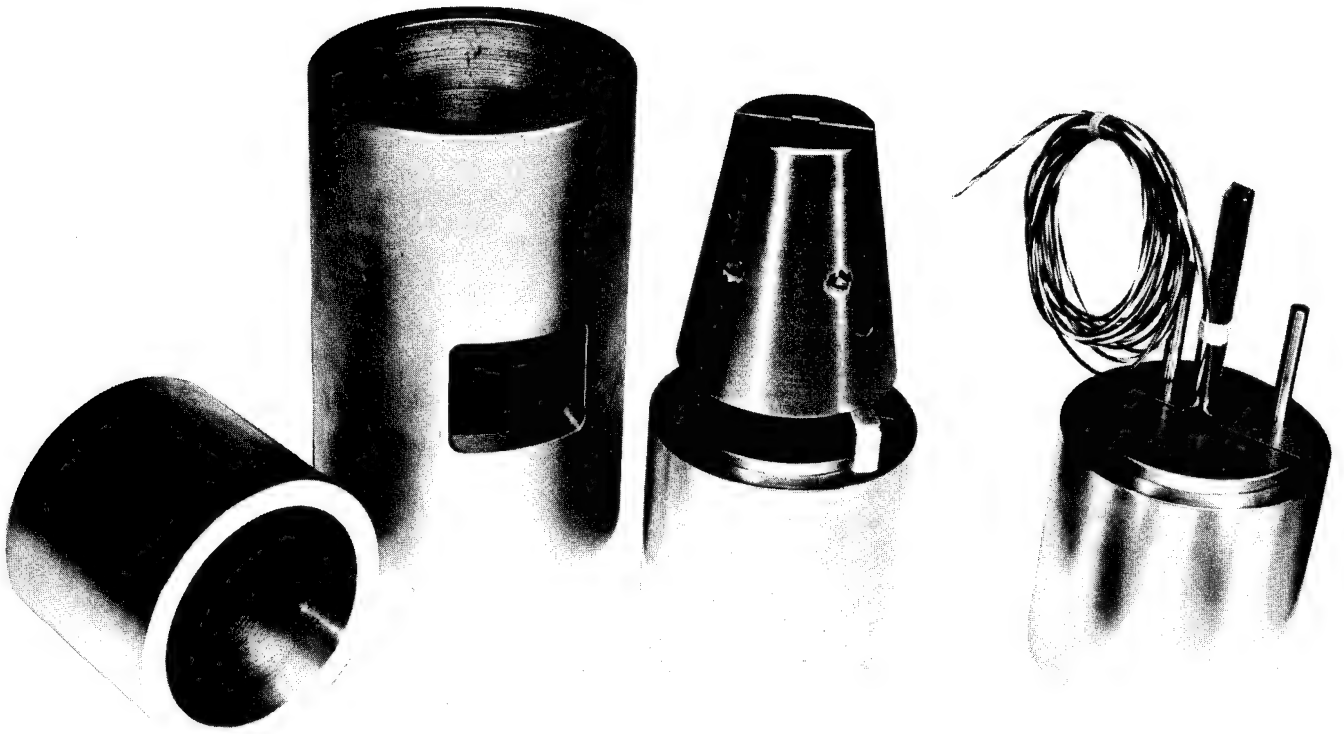

FIGURE 12 COMPRESSION STRENGTH TEST FIXTURE

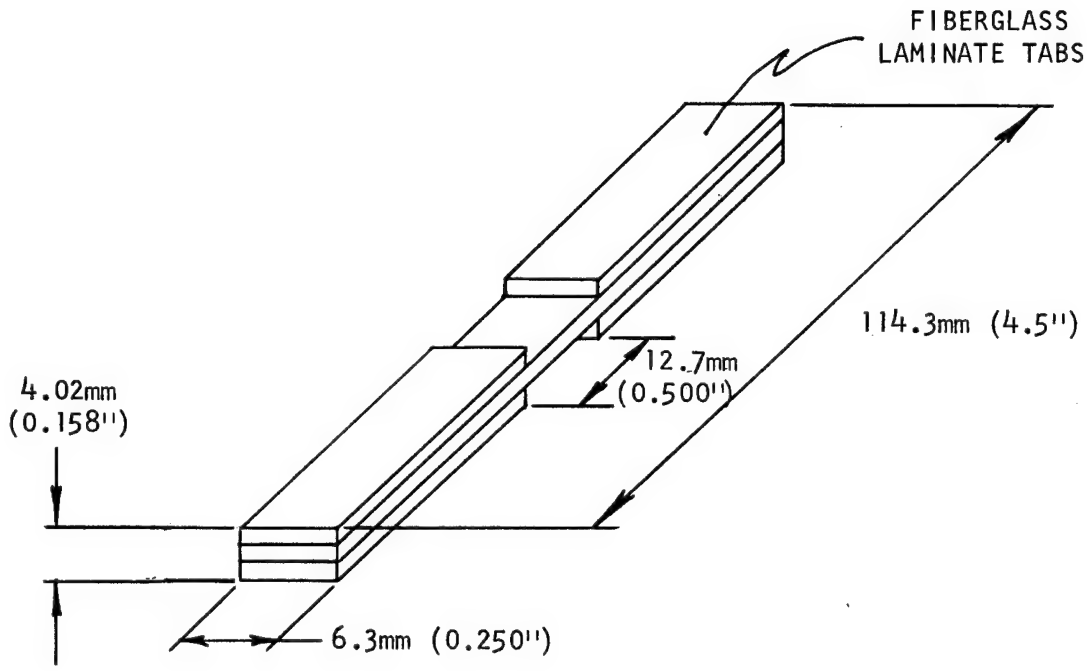

NOTE: EPOXY/FIBERGLASS CLOTH LAMINATE TABS BONDED WITH EPOXY ADHESIVE.

FIGURE 13 CELANESE TYPE COMPRESSION STRENGTH SPECIMEN

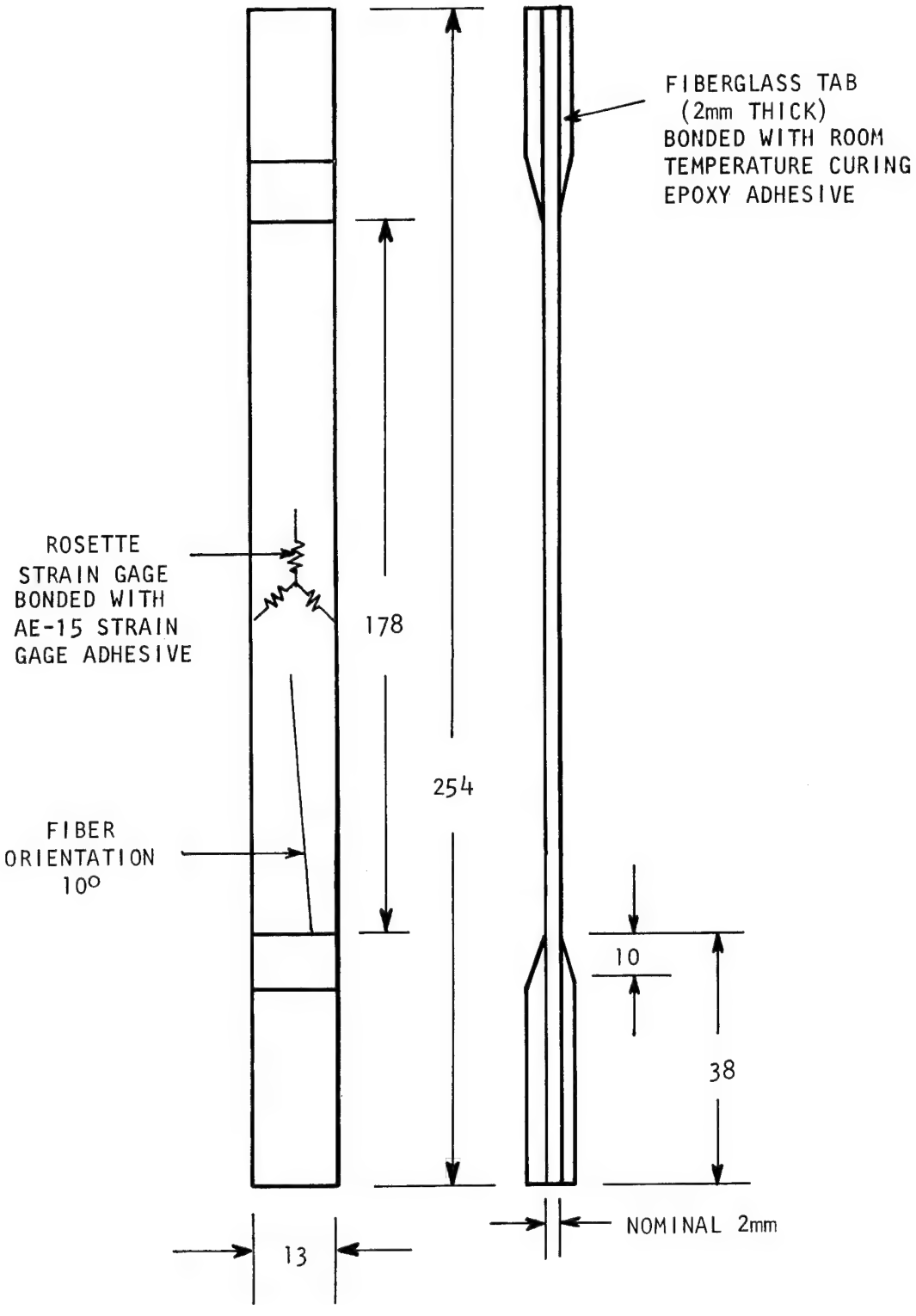

FIGURE 14 INTRALAMINAR SHEAR STRENGTH SPECIMEN

GOVERNING EQUATIONS

$$\sigma_{\ell 12} = \sigma_{cxx} \sin 2\hat{\theta}/2$$

$$\epsilon_{\ell 12} = (\epsilon_{cyy} - \epsilon_{cxx}) \sin 2\theta + \epsilon_{cxy} \cos 2\theta$$

OTHER STRESSES

$$\sigma_{\ell 22} = \sigma_{cxx} \sin^2\theta$$

$$\sigma_{\ell 11} = \sigma_{cxx} \cos^2\theta$$

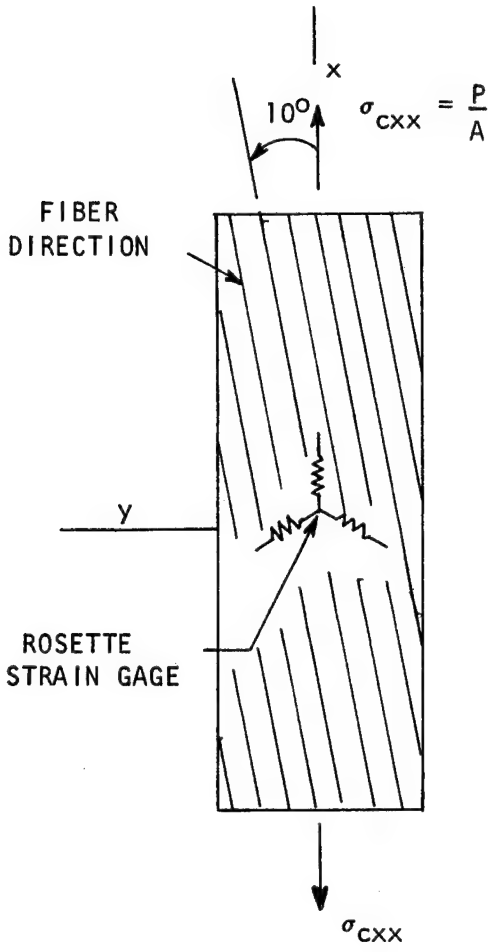

FIGURE 15 EQUATIONS FOR INTRALAMINAR SHEAR STRENGTH TEST

7414-c

$$\begin{Bmatrix} \epsilon_1 \\ \epsilon_2 \\ \epsilon_3 \end{Bmatrix} = \begin{bmatrix} \cos^2\theta_1 & \sin^2\theta_1 & 1/2 \sin 2\theta_1 \\ \cos^2\theta_2 & \sin^2\theta_2 & 1/2 \sin 2\theta_2 \\ \cos^2\theta_3 & \sin^2\theta_3 & 1/2 \sin 2\theta_3 \end{bmatrix} \begin{Bmatrix} \epsilon_{xx} \\ \epsilon_{yy} \\ \epsilon_{xy} \end{Bmatrix} \quad (1)$$

$$\begin{Bmatrix} \epsilon_1 \end{Bmatrix} = \begin{bmatrix} R \end{bmatrix} \begin{Bmatrix} \epsilon_x \end{Bmatrix}$$

$$\begin{Bmatrix} \epsilon_x \end{Bmatrix} = \begin{bmatrix} R \end{bmatrix}^{-1} \begin{Bmatrix} \epsilon_x \end{Bmatrix}$$

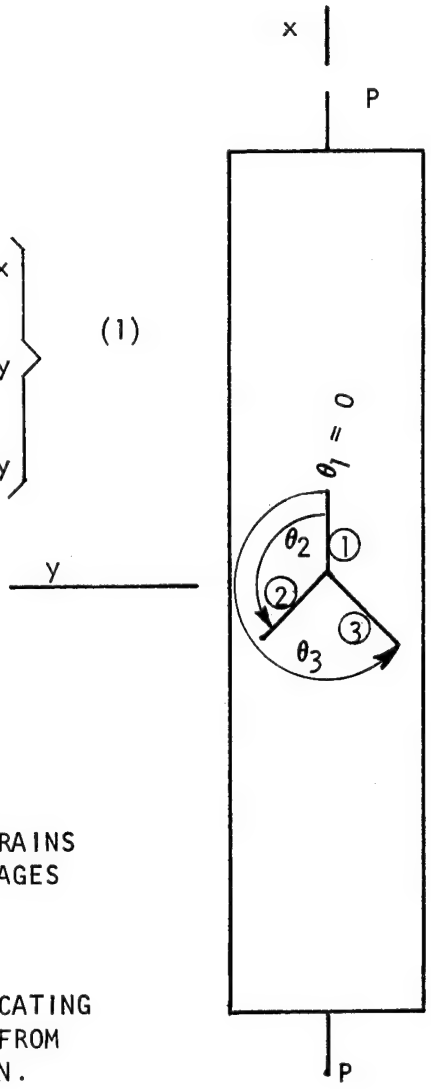

NOTES:

1. ϵ_1, ϵ_2 & ϵ_3 ARE THE ACTUAL STRAINS MEASURED BY THE GAGES IN THE SCHEMATIC.

2. θ_1, θ_2 & θ_3 ARE THE ANGLES LOCATING THE STRAIN GAGES FROM THE LOAD DIRECTION.

3. ϵ_{xx}, ϵ_{yy} & ϵ_{xy} ARE THE STRAINS REQUIRED. THESE ARE OBTAINED FROM EQUATION 1 ABOVE.

FIGURE 16(a) EQUATIONS FOR REDUCING STRAINS FROM INTRALAMINAR SHEAR STRAIN GAGES

STRAINS

$$\begin{bmatrix} \epsilon_1 \\ \epsilon_2 \\ \epsilon_3 \end{bmatrix} = \begin{bmatrix} \cos^2\theta_1 & \sin^2\theta_1 & 1/2\sin 2\theta_1 \\ \cos^2\theta_2 & \sin^2\theta_2 & 1/2\sin 2\theta_2 \\ \cos^2\theta_3 & \sin^2\theta_3 & 1/2\sin 2\theta_3 \end{bmatrix} \begin{bmatrix} \epsilon_{xx} \\ \epsilon_{yy} \\ \epsilon_{xy} \end{bmatrix}$$

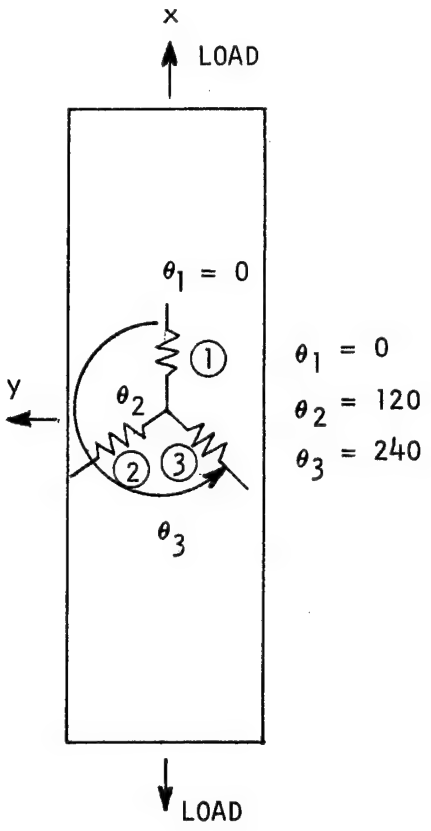

BY SUBSTITUTION:

$$\begin{bmatrix} \epsilon_1 \\ \epsilon_2 \\ \epsilon_3 \end{bmatrix} = \begin{bmatrix} 1 & 0 & 0 \\ .25 & .75 & -.43 \\ .25 & .75 & .43 \end{bmatrix} \begin{bmatrix} \epsilon_{xx} \\ \epsilon_{yy} \\ \epsilon_{xy} \end{bmatrix}$$

BY INVERTING THE MATRIX RELATION:

$$\begin{bmatrix} \epsilon_{xx} \\ \epsilon_{yy} \\ \epsilon_{xy} \end{bmatrix} = \begin{bmatrix} 1 & 0 & 0 \\ -.333 & .667 & .667 \\ 0 & -1.163 & 1.163 \end{bmatrix} \begin{bmatrix} \epsilon_1 \\ \epsilon_2 \\ \epsilon_3 \end{bmatrix}$$

SOLUTION:

$$\epsilon_{xx} = \epsilon_1$$

$$\epsilon_{yy} = .667\,\epsilon_2 + .667\,\epsilon_3 - .333\,\epsilon_1$$

$$\epsilon_{xy} = 1.163\,\epsilon_3 - 1.163\,\epsilon_2$$

FIGURE 16(b) SOLUTION OF INTRALAMINAR SHEAR STRAIN EQUATIONS

7416-C

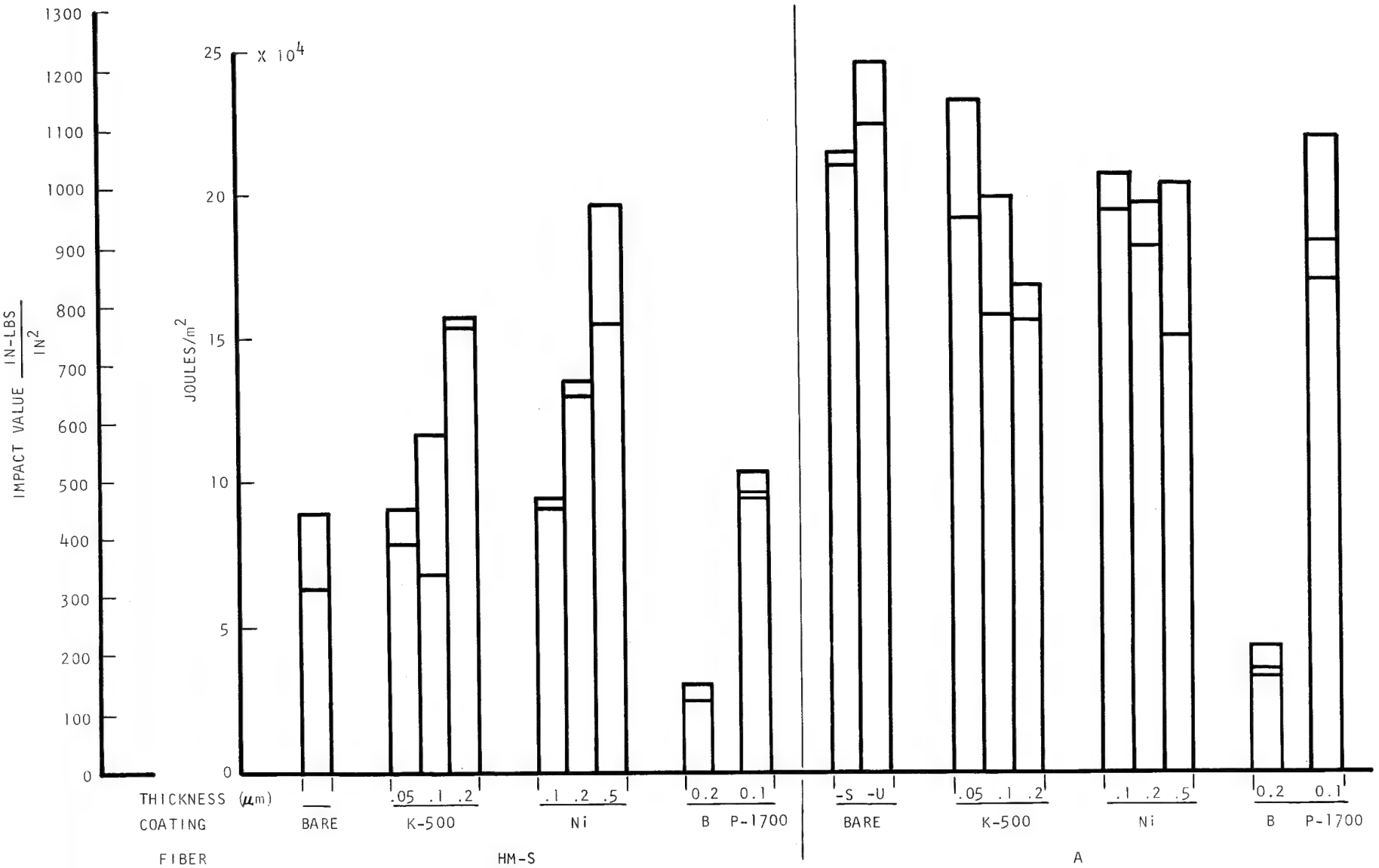

FIGURE 17 TASK I UN-NOTCHED IZOD IMPACT STRENGTH RESULTS
COMPARISON OF IMPACT ENERGY DIVIDED BY CROSS-SECTIONAL AREA

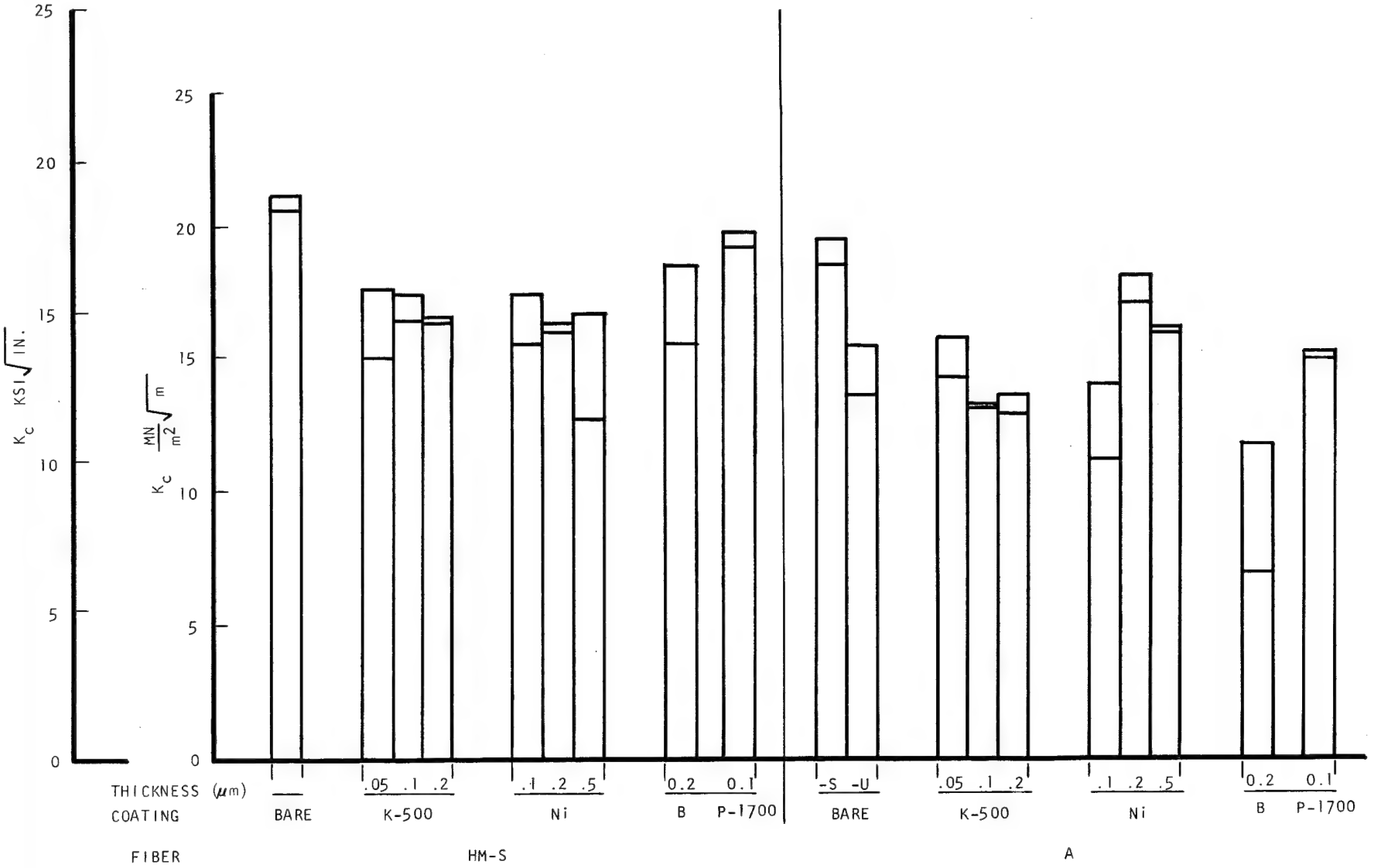

FIGURE 18 TASK I FRACTURE TOUGHESS RESULTS
COMPARISON OF CRITICAL STRESS INTENSITY FACTOR, K_c

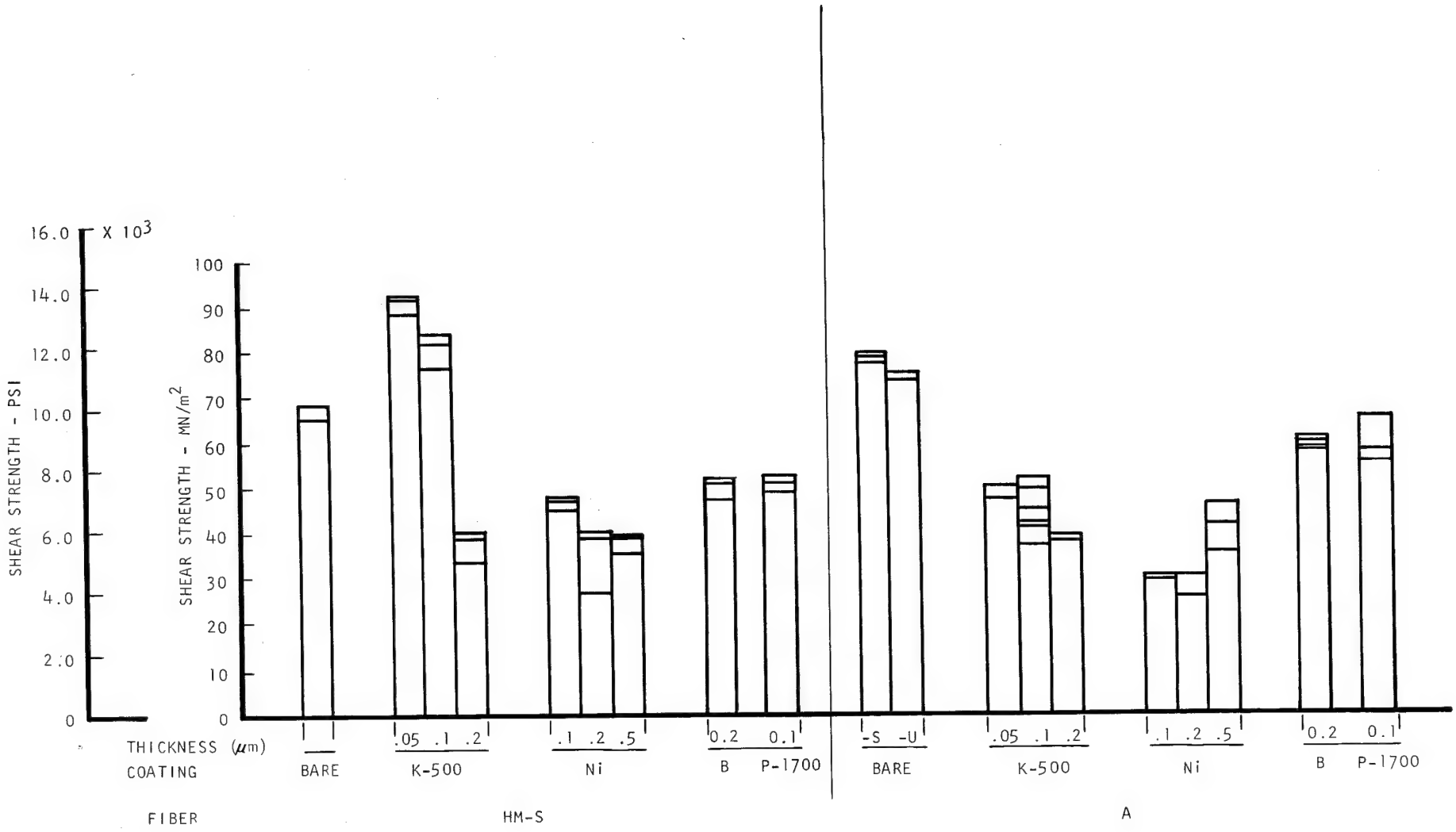

FIGURE 19 TASK I SHORT BEAM SHEAR STRENGTH RESULTS

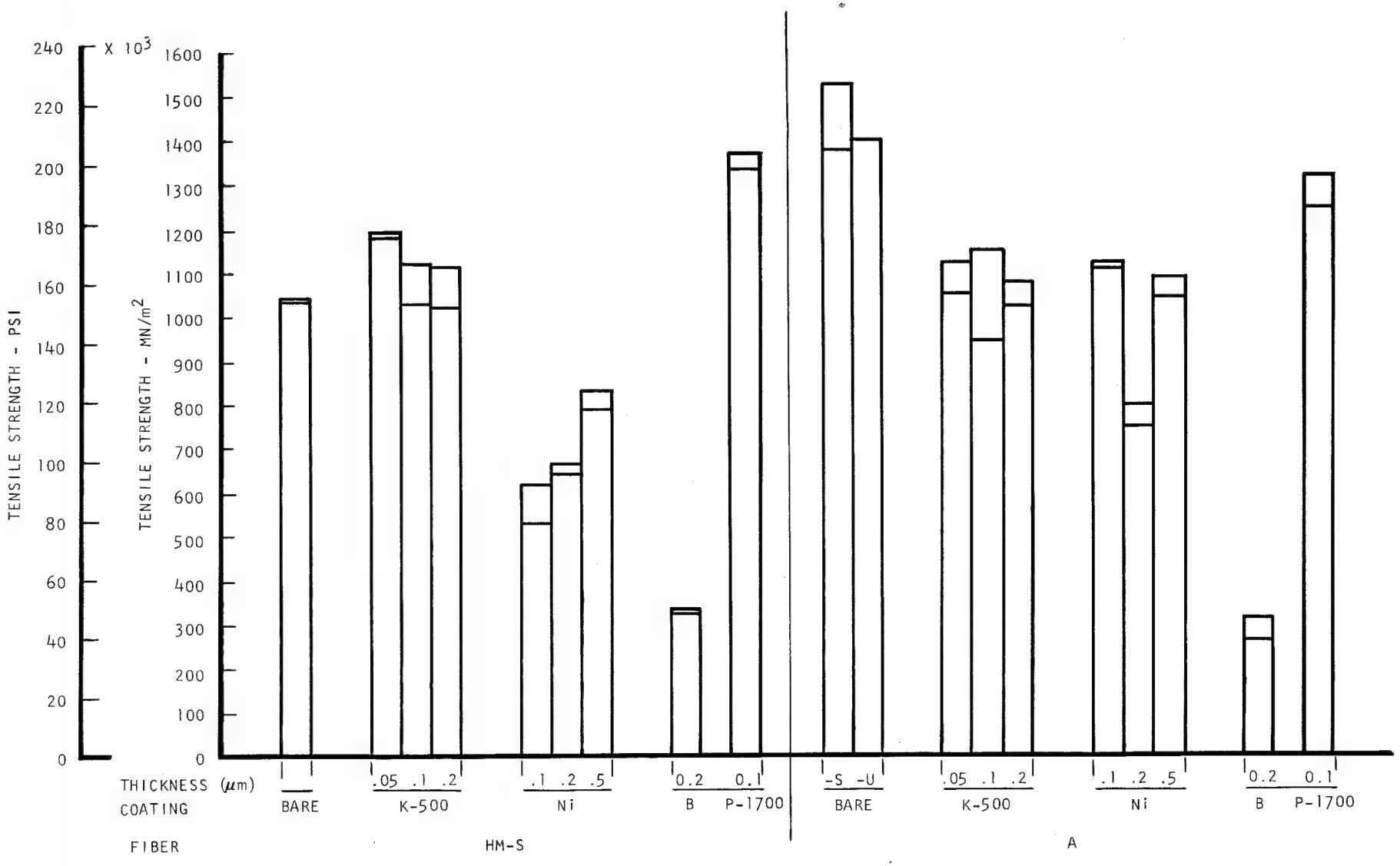

FIGURE 20 TASK I TENSILE STRENGTH RESULTS

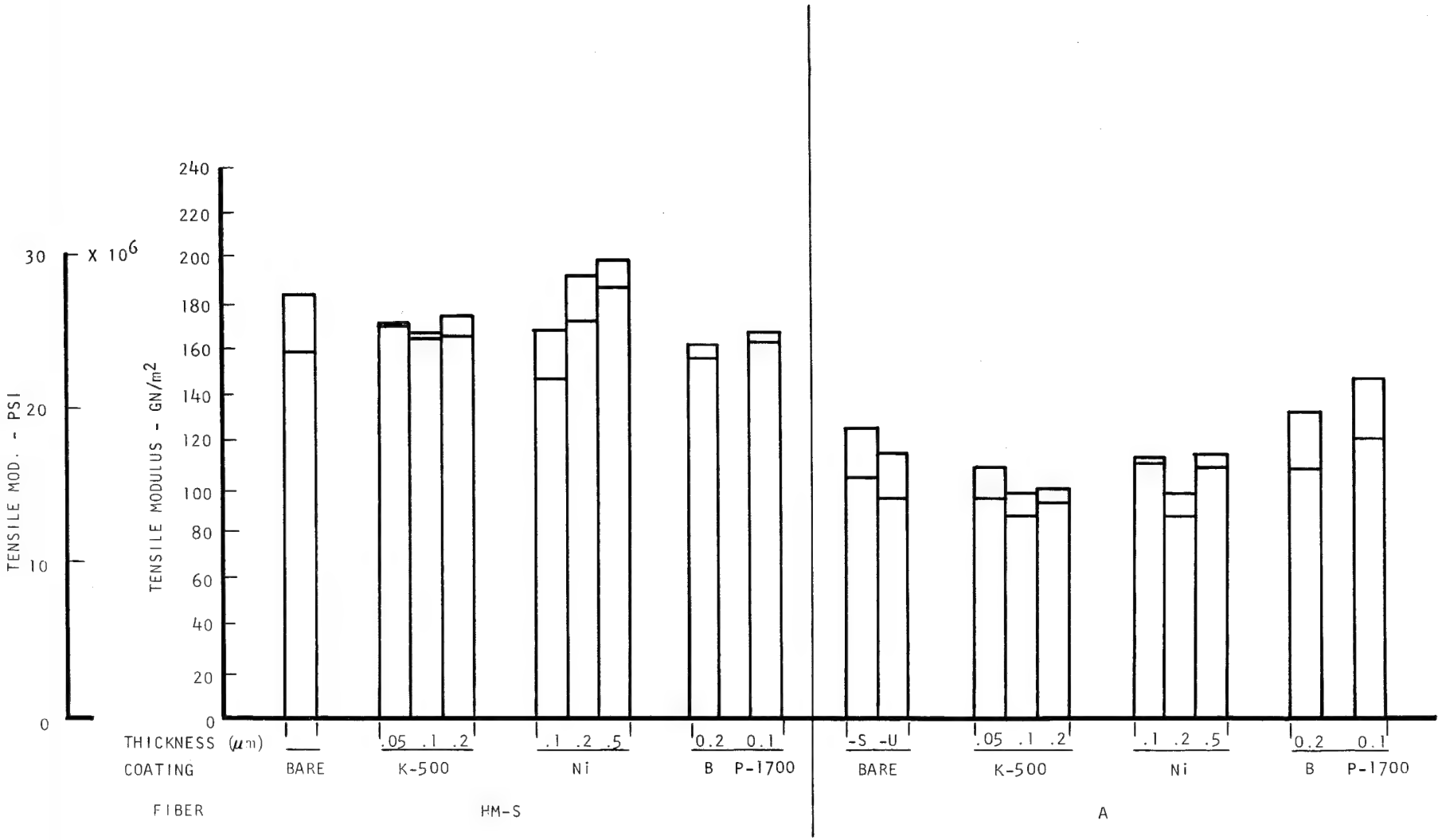

FIGURE 21 TASK I TENSILE MODULUS RESULTS

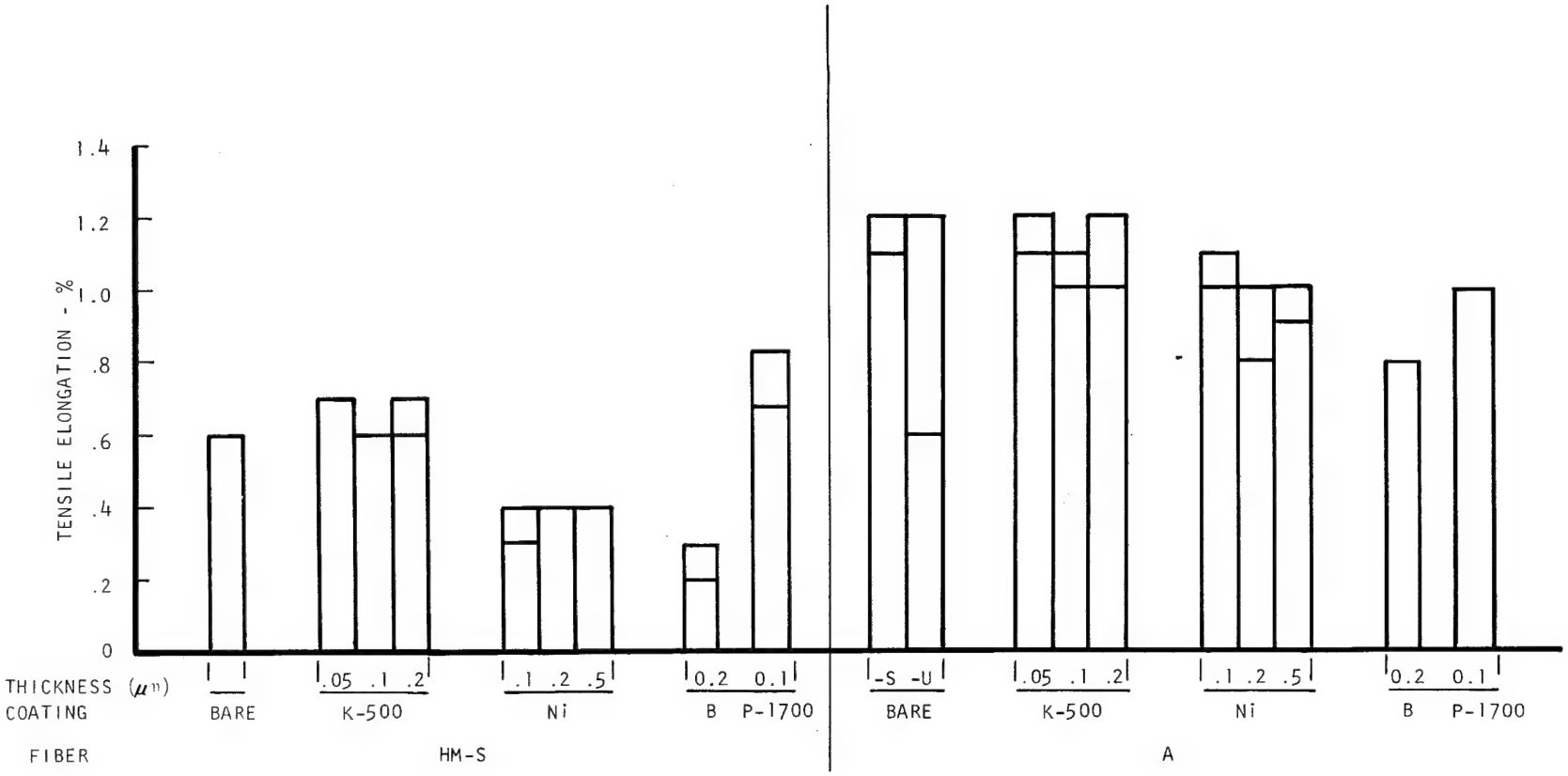

FIGURE 22 TASK I TENSILE ELONGATION RESULTS

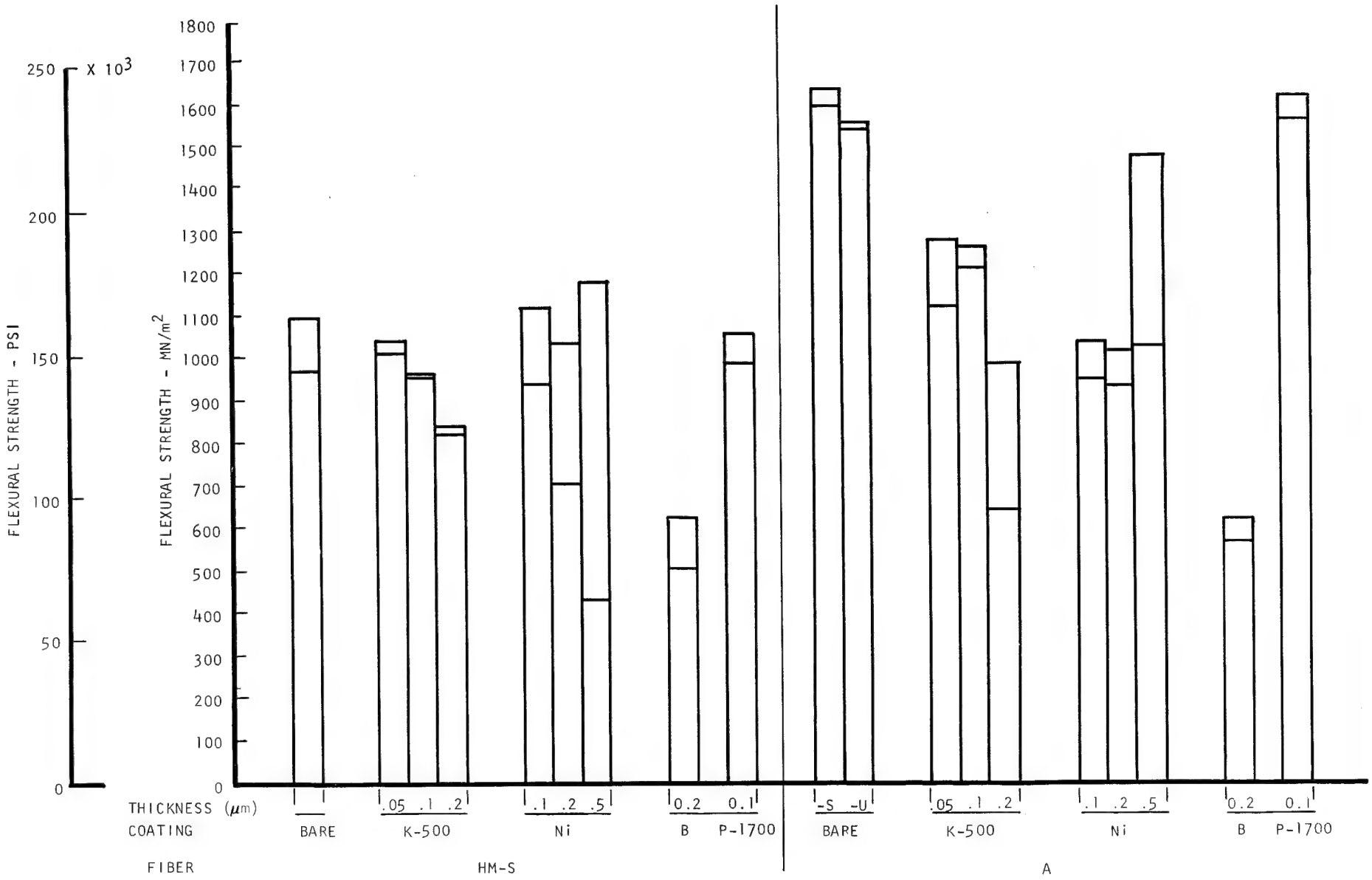

FIGURE 23 TASK I FLEXURAL STRENGTH RESULTS

A-S FIBER

18.1×10^4 J/m^2

A-U FIBER

21.1×10^4 J/m^2 20.0×10^4 J/m^2 13.5×10^4 J/m^2

HM-S FIBER

5.5×10^4 J/m^2 6.8×10^4 J/m^2 13.6×10^4 J/m^2

0.05 m 0.20 m

UNCOATED K-500 COATING

FIGURE 24 FRACTURED IZOD IMPACT STRENGTH SPECIMENS

7417-C

A-U FIBER

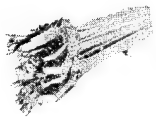

17.8×10^4 J/m^2

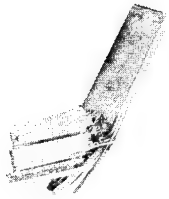

13.0×10^4 J/m^2

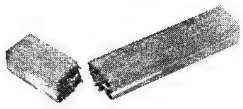

3.8×10^4 J/m^2

HM-S FIBER

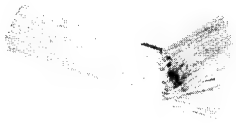

7.9×10^4 J/m^2

0.10 m

NICKEL COATING

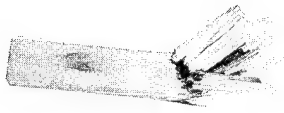

17.0×10^4 J/m^2

0.50 m

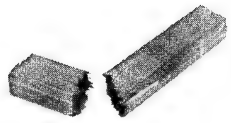

0.20 m

BORON COATING

8.1×10^4 J/m^2

0.10 m

P-1700 COATING

FIGURE 24 (Cont.) FRACTURED IZOD IMPACT STRENGTH SPECIMENS

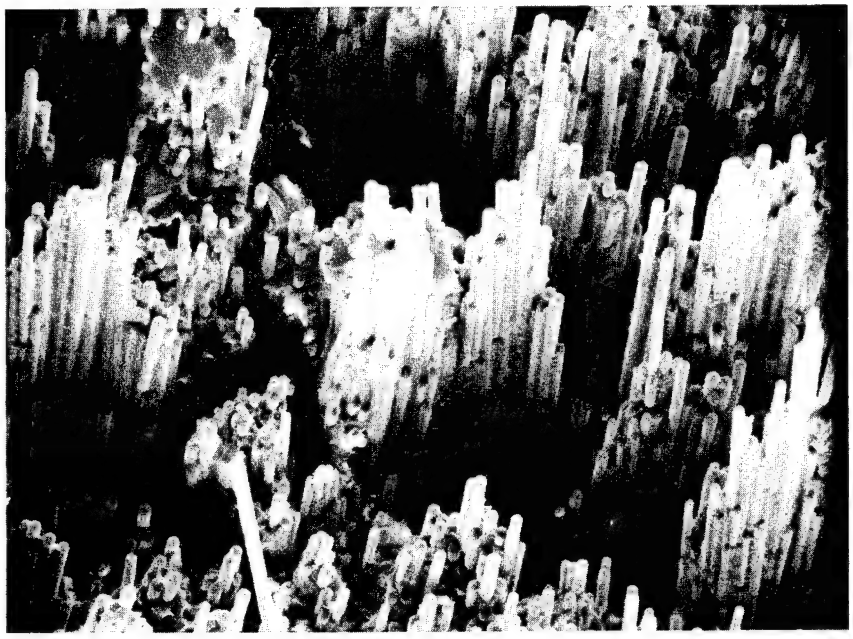

200X

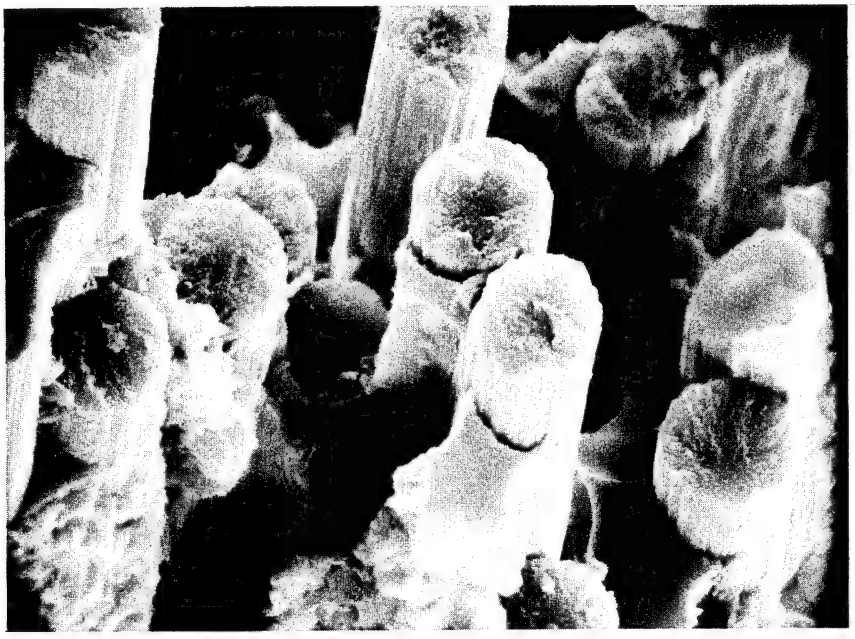

2000X

FIGURE 25 SEM OF FRACTURE SURFACE OF IZOD IMPACT STRENGTH SPECIMEN 719-34/1. BARE A-S FIBER.

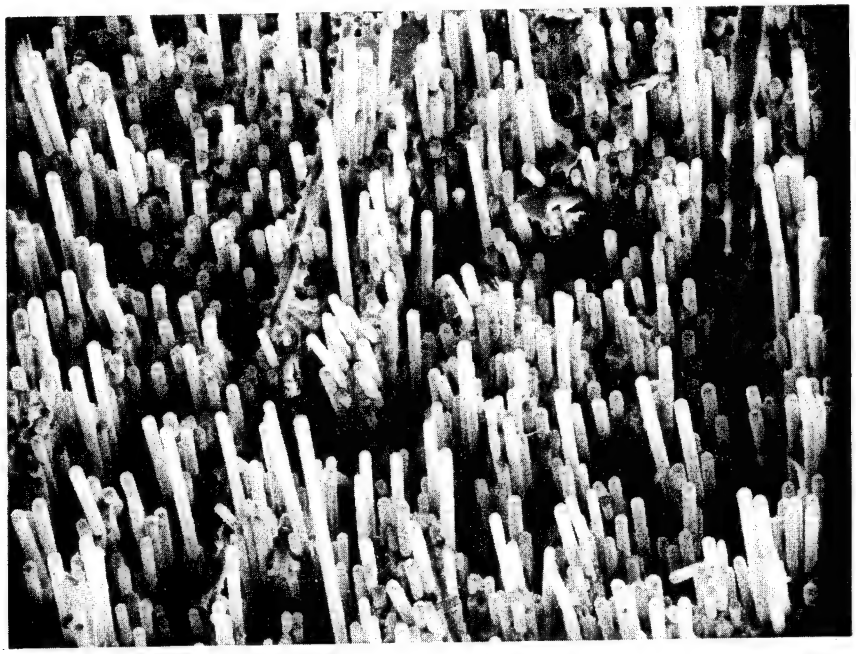

200X

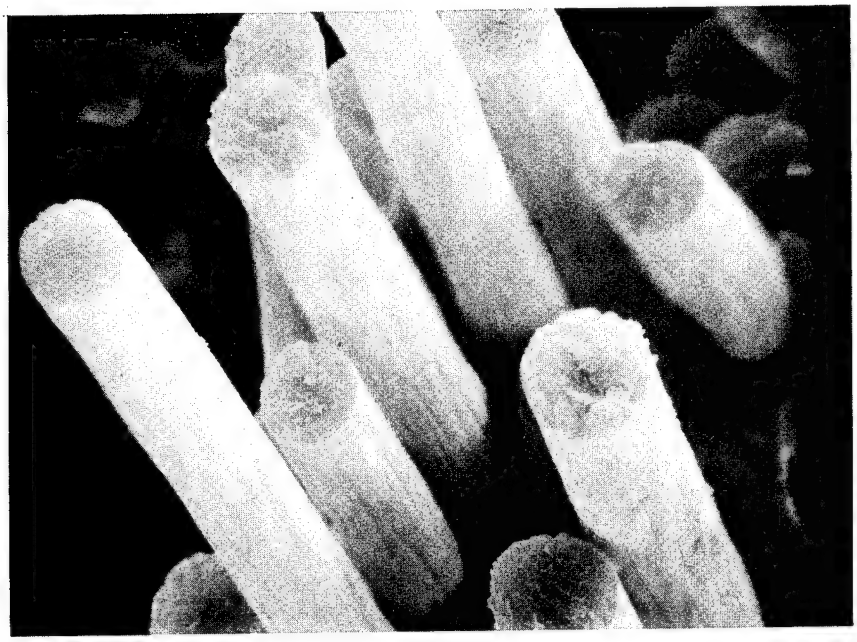

2000X

FIGURE 26 SEM OF FRACTURE SURFACE OF IZOD IMPACT STRENGTH SPECIMEN 719-28/1. BARE A-U FIBER.

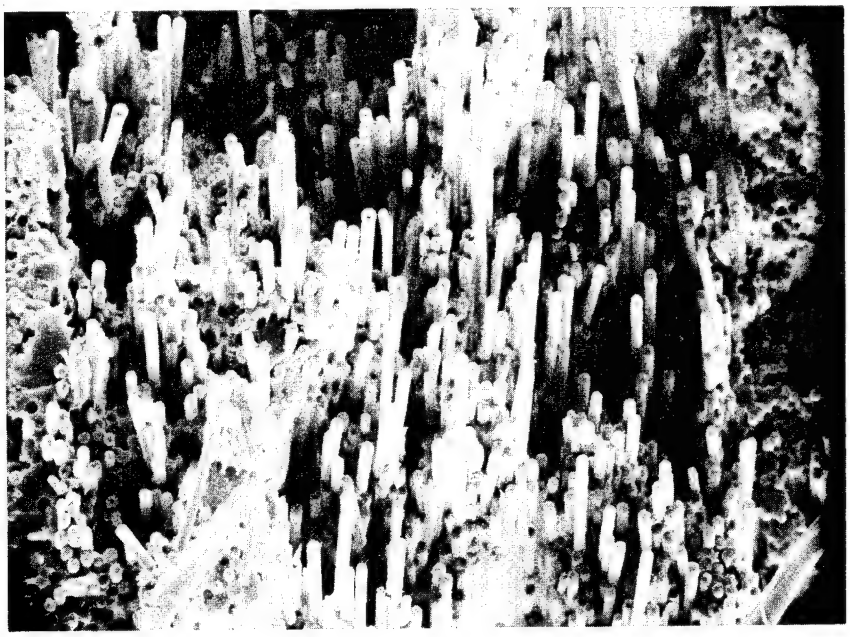

200X

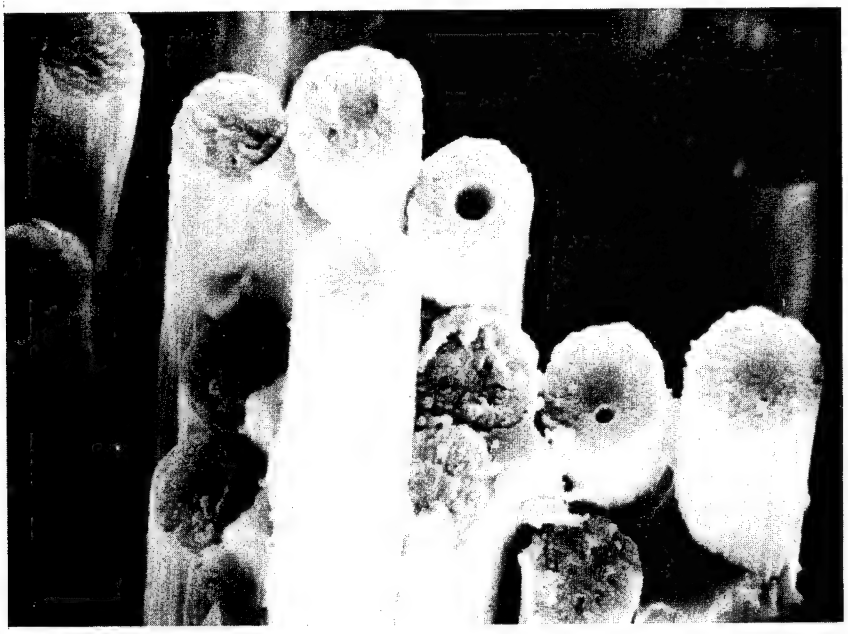

2000X

FIGURE 27 SEM OF FRACTURE SURFACE OF IZOD IMPACT STRENGTH SPECIMEN 719-52/1. BARE HM-S FIBER.

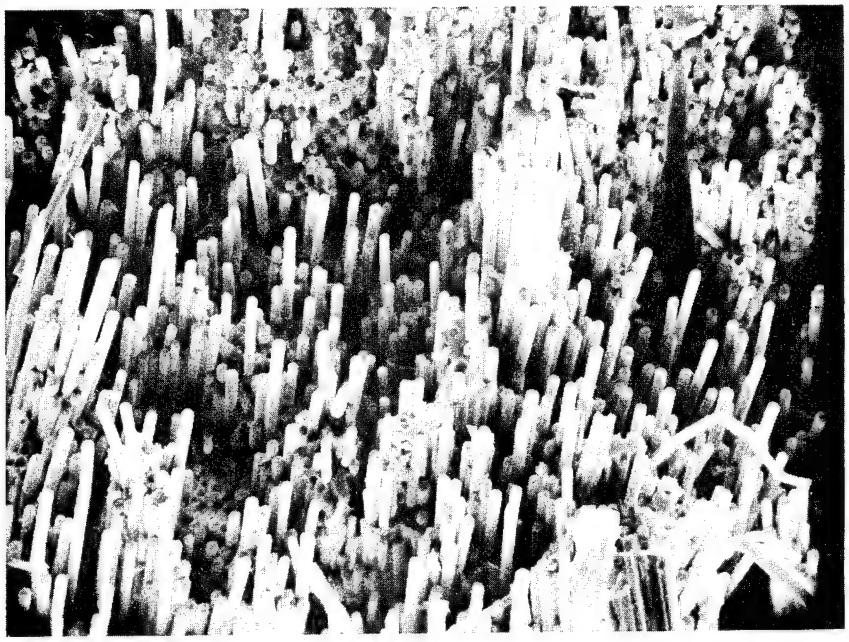

200X

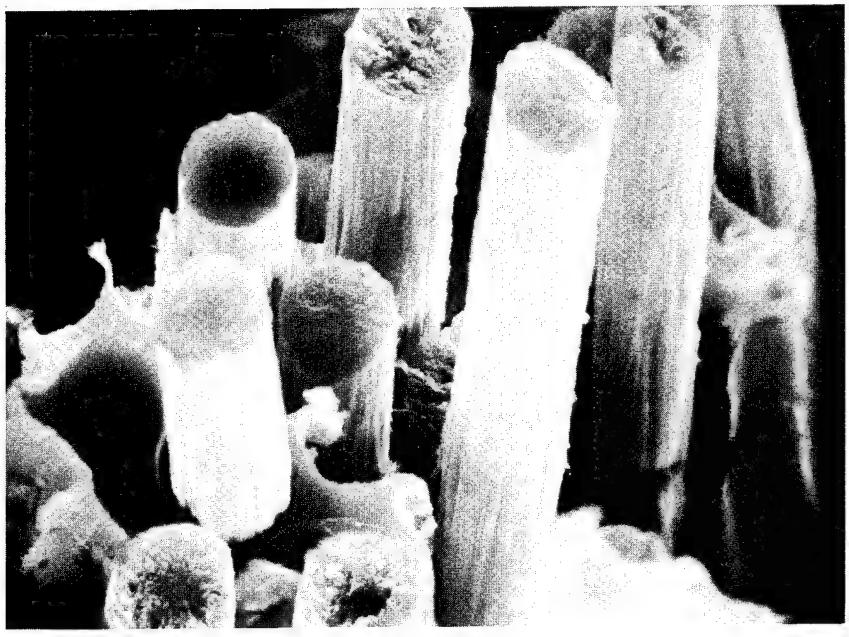

2000X

FIGURE 28 SEM OF FRACTURE SURFACE OF IZOD IMPACT STRENGTH SPECIMEN 719-58/1. K-500 COATED (0.10 μm) HM-S FIBER.

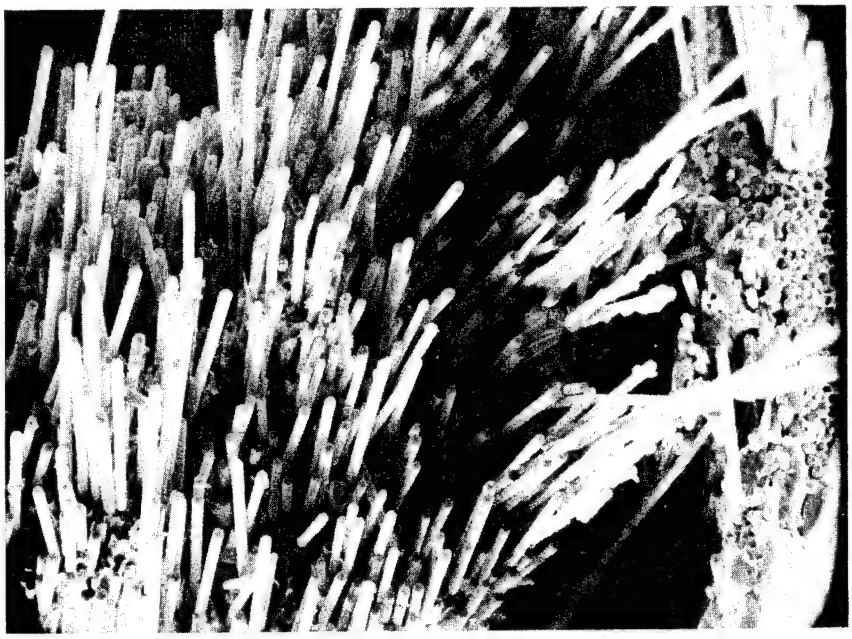

200X

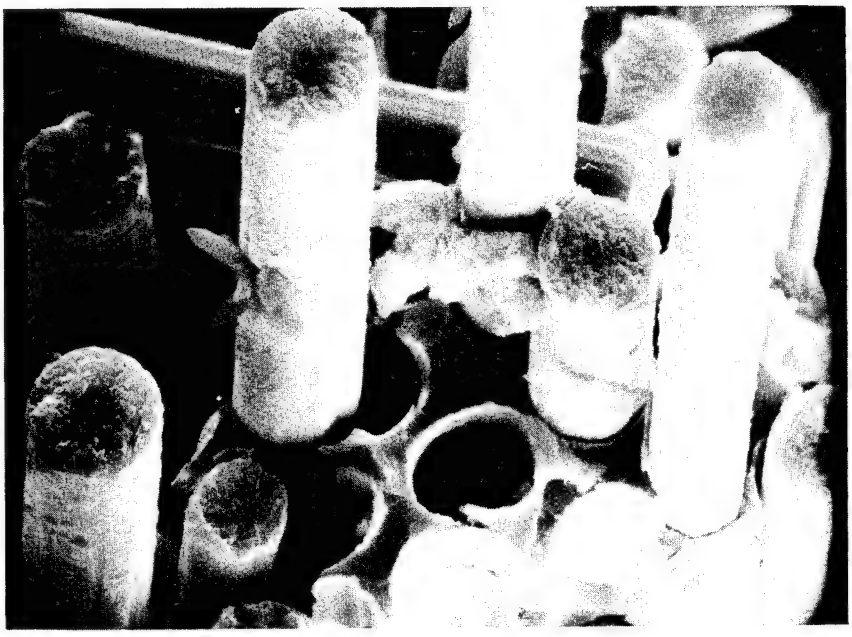

2000X

FIGURE 29 SEM OF FRACTURE SURFACE OF IZOD IMPACT STRENGTH SPECIMEN 719-91/2. NICKEL COATED (0.50 μm) HM-S FIBER.

7423-c

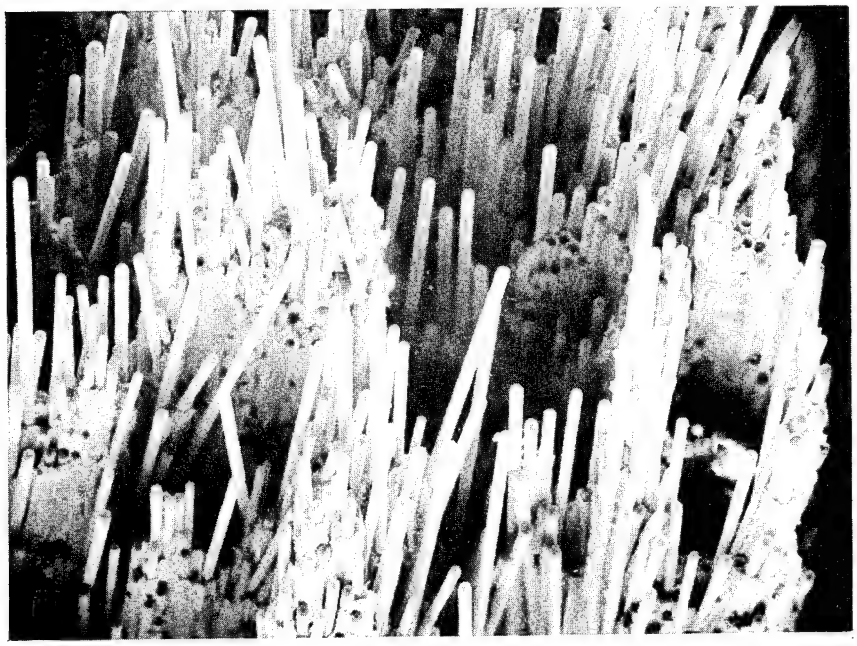

200X

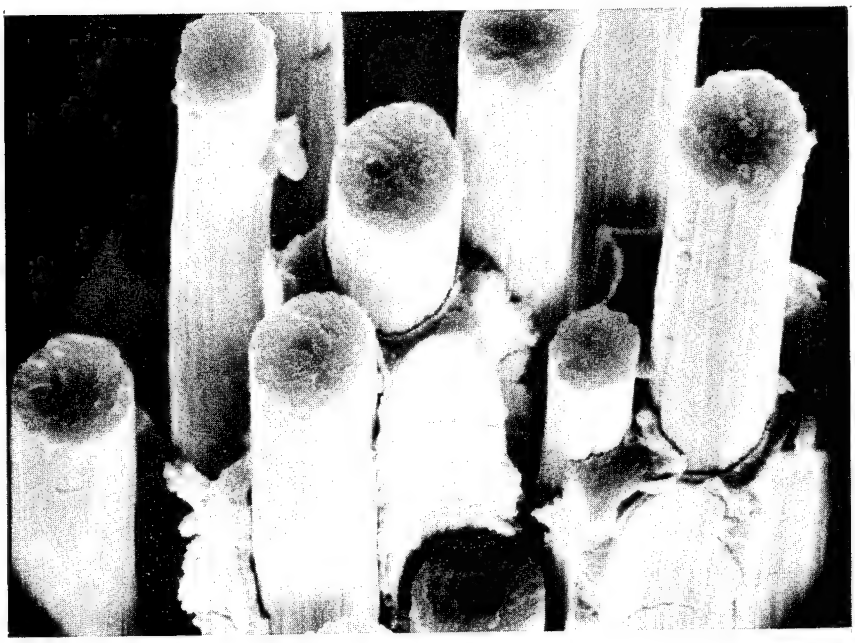

2000X

FIGURE 30 SEM OF FRACTURE SURFACE OF IZOD IMPACT STRENGTH SPECIMEN 719-77/1. NICKEL COATED (0.50 μm) A-U FIBER.

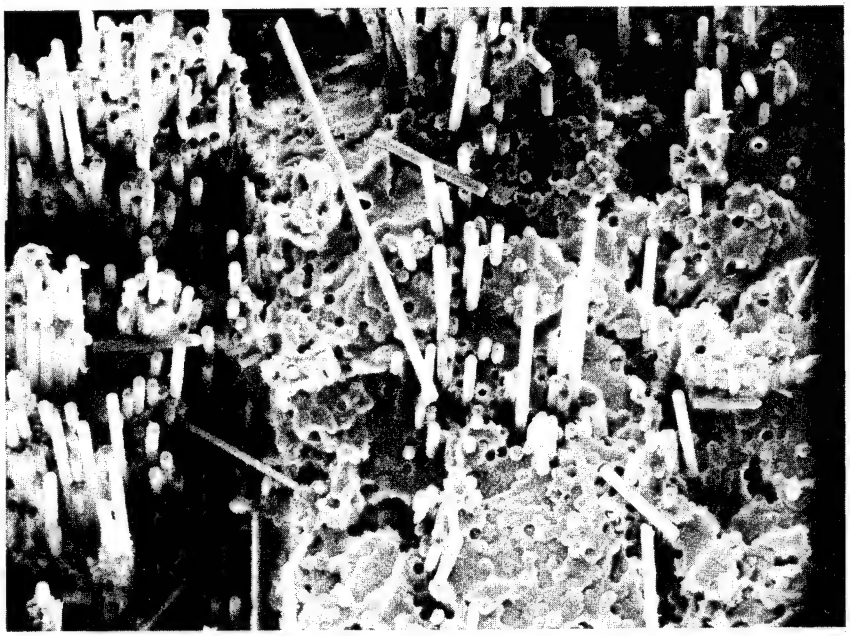

200X

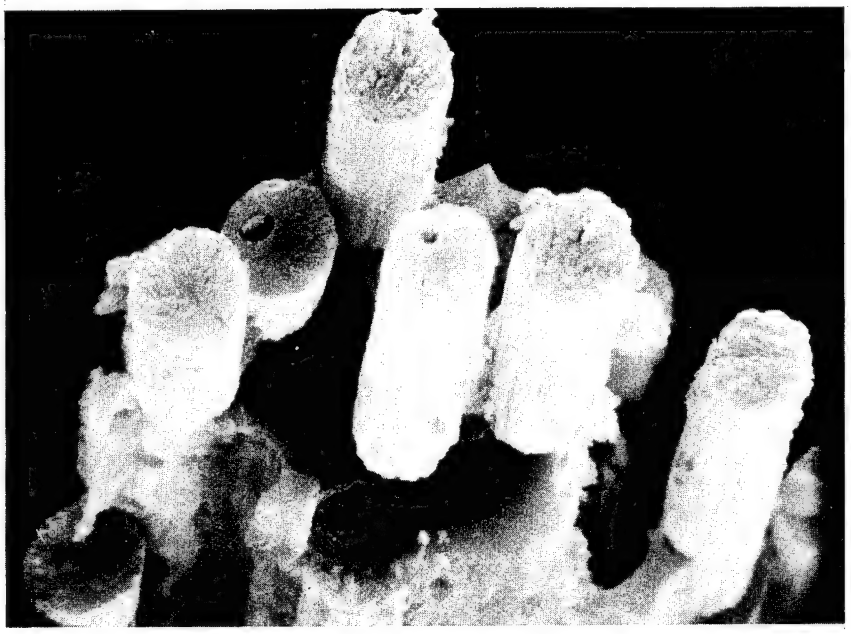

2000X

FIGURE 31 SEM OF FRACTURE SURFACE OF IZOD IMPACT STRENGTH SPECIMEN 722-23/2. BORON COATED (0.20 μm) HM-S FIBER.

7425-C

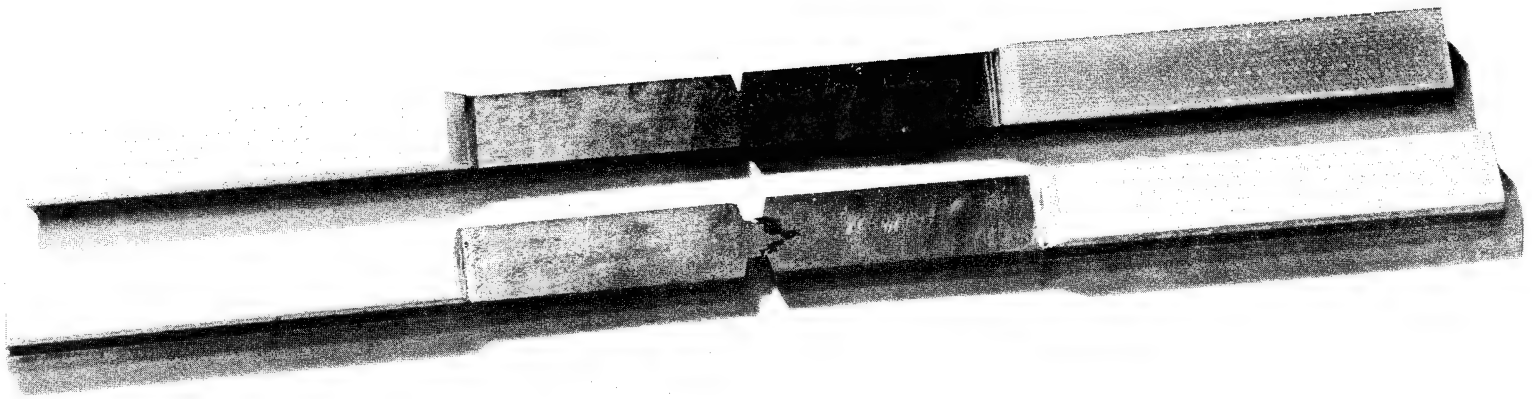

FIGURE 32 FRACTURE TOUGHNESS SPECIMENS SHOWING FAILURE MODE OF BORON COATED A-U SPECIMEN (BELOW) AND P-1700 COATED HM-S (ABOVE)

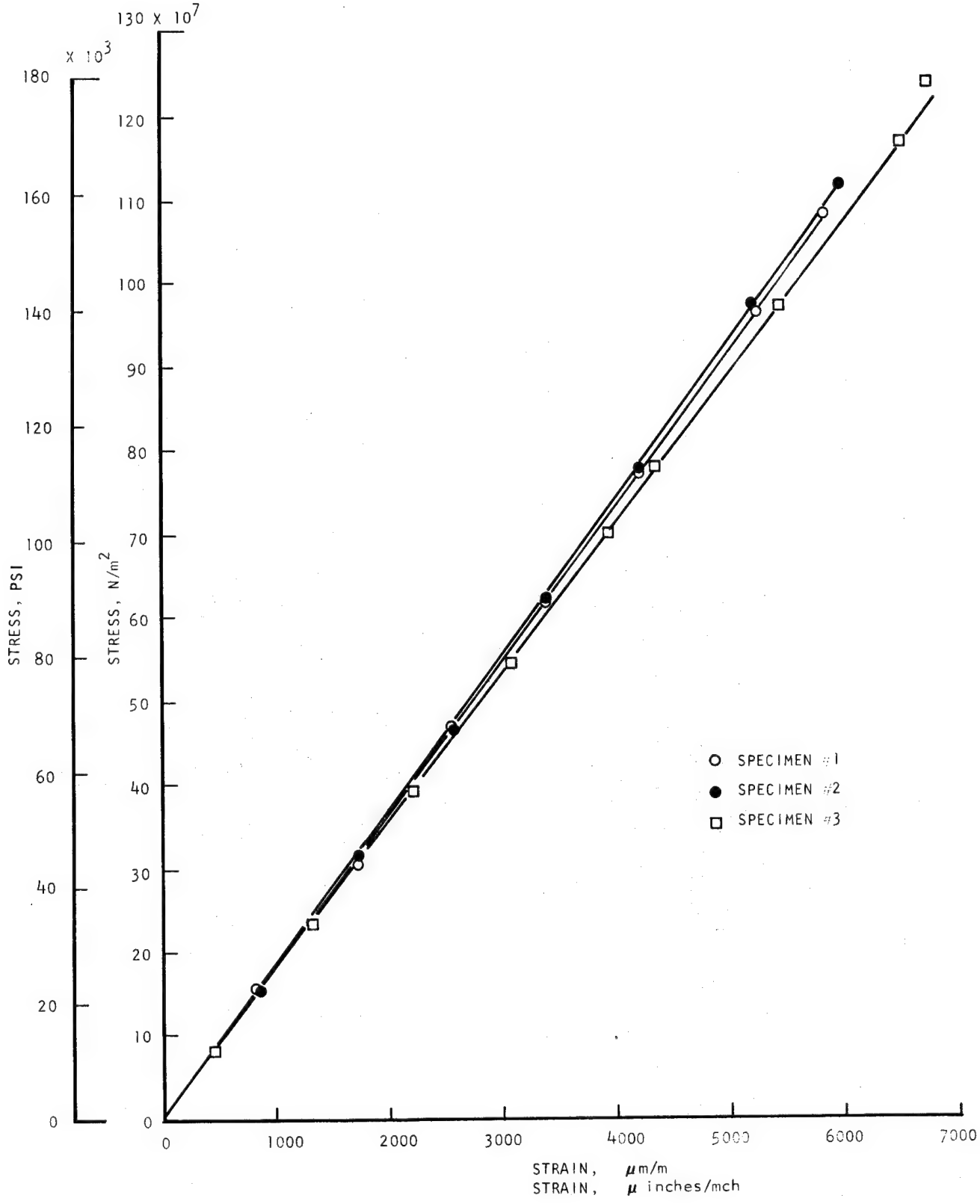

FIGURE 33 LONGITUDINAL TENSILE STRESS/STRAIN CURVES OF K-500 COATED (0.15μm) HM-S COMPOSITE.

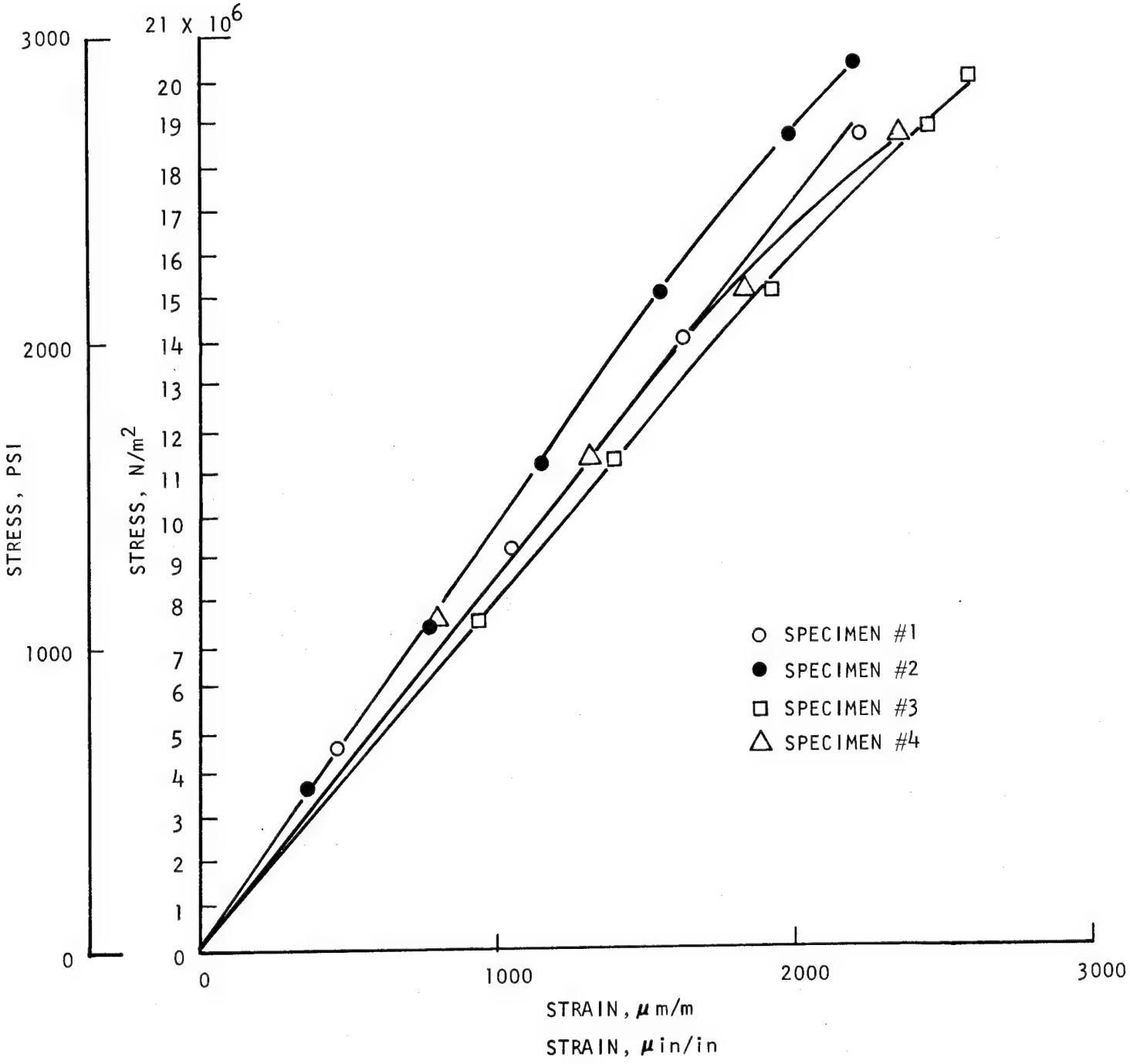

FIGURE 34 TRANSVERSE TENSILE STRESS/STRAIN CURVES OF K-500 COATED (0.15μm) HM-S COMPOSITE

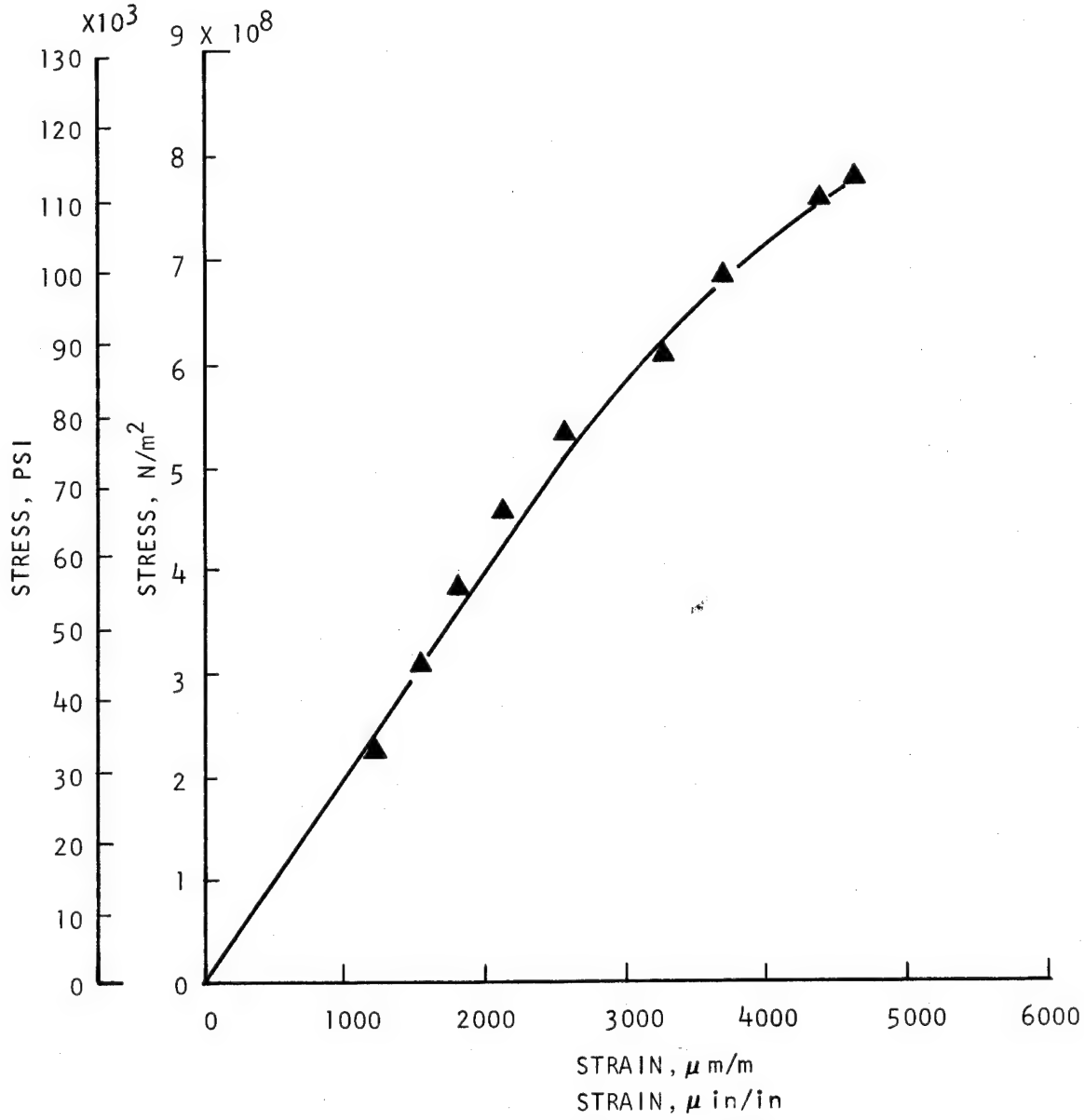

FIGURE 35 TYPICAL LONGITUDINAL COMPRESSION STRESS/STRAIN CURVES OF K-500 COATED (0.15μm) HM-S COMPOSITE

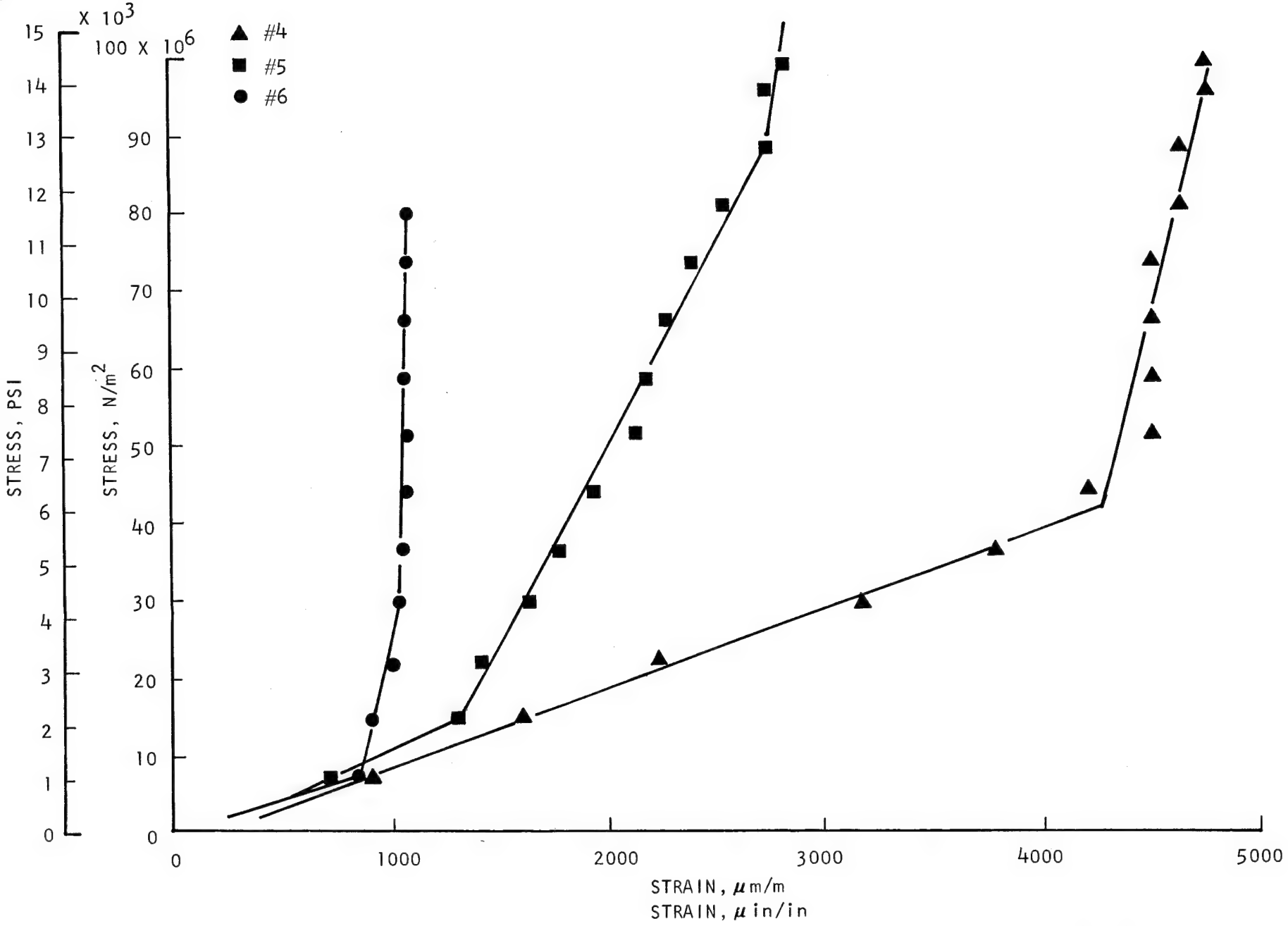

FIGURE 36 TRANSVERSE COMPRESSION STRESS/STRAIN CURVES OF K-500 COATED (0.15μm) HM-S COMPOSITE

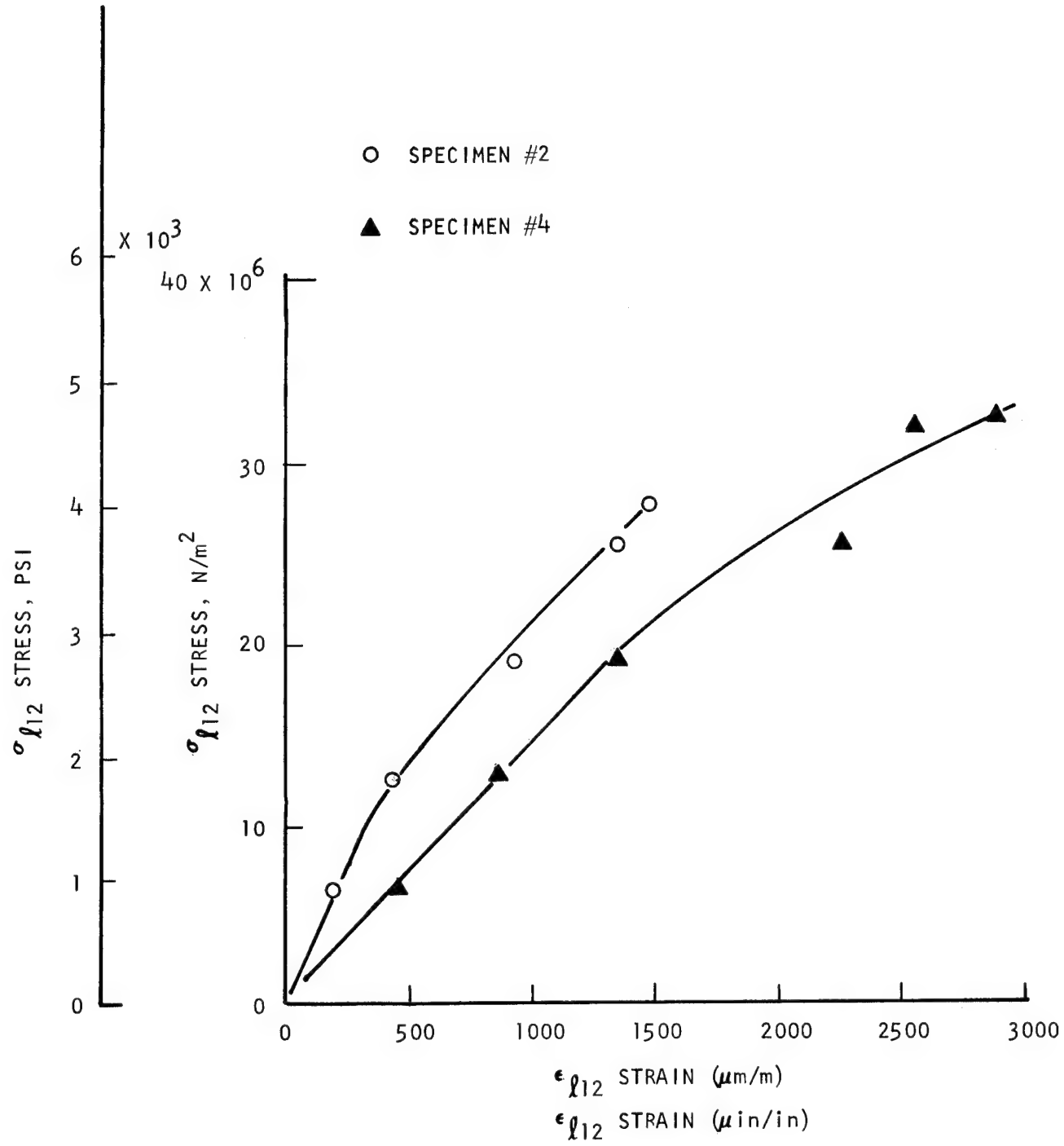

FIGURE 37 INTRALAMINAR SHEAR STRESS/STRAIN CURVES OF K-500 COATED (0.15μm) HM-S COMPOSITE

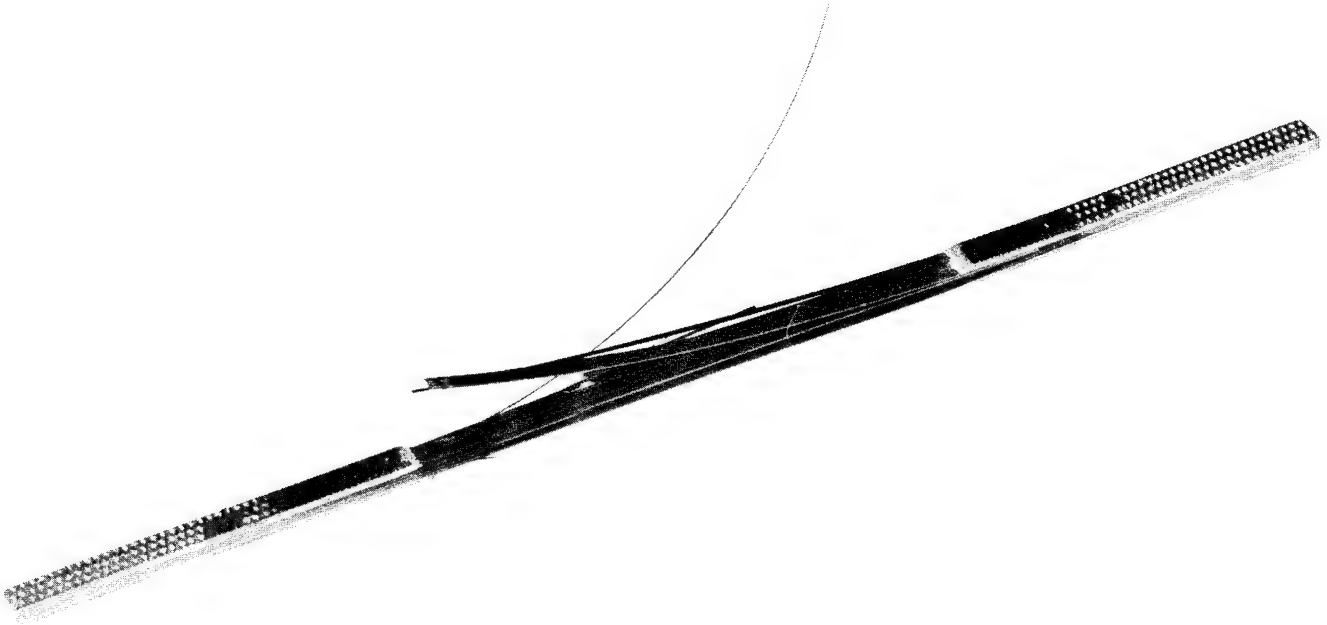

FIGURE 38 LONGITUDINAL TENSILE SPECIMEN SHOWING FAILURE MODE TYPICAL OF K-500 COATED FIBERS

FIGURE 39 LONGITUDINAL COMPRESSION SPECIMEN SHOWING FAILURE MODE

FIGURE 40 TRANSVERSE COMPRESSION SPECIMEN SHOWING FAILURE MODE

FIGURE 41 STRAIN GAGED INTRALAMINAR SHEAR STRENGTH SPECIMENS SHOWING TYPICAL FAILURE MODE

REFERENCES

1. Marston, T., "The Effect of a Controlled Intermittent Interfacial Bond Strength on the Tensile Properties of Boron-Epoxy Composite," 20th Refractory Composites Working Group Meeting, Cleveland, Ohio, October 1972.

2. Chamis, C. C., Hanson, M. P. and Serafini, T. T., "Impact Resistance of Unidirectional Fiber Composites," Composite Materials: Testing and Design (Second Conference), ASTM STP 497 American Society for Testing Materials, 1972, pp. 324-347.

3. Morley, J. G., "The Design of Fibrous Composites Having Improved Mechanical Properties," Proc. Royal Society, London, A319, 117-126 (1970).

4. Morley, J. G., "Advanced Fibrous Composite Materials," Composites Materials Meeting, 1st, Kinstanz, West Germany, October 22, 23, 1970.

5. Morley, J. G., "Fibrous Composites with Multiple and Variable-Shear-Strength Interfaces," Composites, June 1971.

6. Morley, J. G., "The Application of Self-Adjusting Interfaces to the Design of Fibrous Composites," Accepted for Publication in Journal of Material Sciences, 1974.

7. Morley, J. G., "Breakthrough in Tough Composites," The Engineer, July 15, 1971.

8. Pinchin, D. J. and Woodhams, R. T., "Pyrolytic Surface Treatment of Graphite Fibers," Journal of Materials Sciences 9 (1974), pp. 300.

9. Kenyon, A. S. and Duffey, H. J., Polymer Engineering and Science, Vol. I, pp. 189 (1967).

10. Kenyon, A. S., Journal of Colloid and Interface Science, 27, (4), 761 (1968).

11. Lavengood, R. E., et al, to be published.

12. Baer, E., Koutsky, J. A. and Walton, A. G., Polymer Letters, 5, 177 (1967).

13. Kardos, J. L., Cheng, F. S. and Tolbert, T. L., "Tailoring the Interface in Graphite-Reinforced Polycarbonate," HPC 71-145, Feb. 1973.

14. Novak, R. C., "Materials Variables Affecting the Impact Resistance of Graphite and Boron Composites," F33615-73-C-5090, Eighth Quarterly Report, April 30, 1975.

15. Mazzio, V. F., Mehan, R. L. and Mullin, J. V., "Basic Failure Mechanisms in Advanced Composites," NASA CR-134525, 1973.

16. Chamis, C. C., Hanson, M. P. and Serafini, T. T., "Impact Resistance of Unidirectional Fiber Composites."

17. Wright, M. A. and Ianuzzi, F. A., "The Application of the Principles of Linear Elastic Fracture Mechanics to Unidirectional Fiber Reinforced Composite Materials," J. Composite Materials, Vol. 7, October 1973, pp. 430.

18. Mulvaney, W. P., "Fracture Mechanics - Epoxy Resins," ASME Publication 65-WA/RP-6, November 7, 1965.

FINAL REPORT DISTRIBUTION LIST

NASA CR-134887

COMPOSITE IMPACT STRENGTH IMPROVEMENT THROUGH A FIBER/MATRIX INTERPHASE

CONTRACT NAS3-18902

TRW EQUIPMENT
TRW INC.

Advanced Research Projects Agency Washington, DC 20525 Attn: Library	1
Advanced Technology Center, Inc. LTV Aerospace Corp. P.O. Box 6144 Dallas, TX 75222 Attn: D. H. Petersen	1
AFC, Inc. Chatfield, MN 55923 Attn: S. Prosen	1
Air Force Flight Dynamics Laboratory Wright-Patterson Air Force Base, Ohio 45433 Attn: T. Norbut (TBP) L. J. Obery (TBP) G. P. Sendeckyj (FBC)	1 1 1
Air Force Materials Laboratory Wright-Patterson Air Force Base, Ohio 45433 Attn: J. D. Ray (LTN) W. H. Gloor (LNF) H. S. Schwartz (LN) T. J. Reinhart (MBC) G. P. Peterson (LC) E. J. Morrisey (LAE) A. Hopkins (LLN) C. E. Husman (MBC) S. Litvak (LTF) S. Tsai (MBS) A. Olevitch (LAE)	1 1 1 1 1 1 1 1 1 1 1
Air Force Office of Scientific Research Washington, DC 20333 Attn: J. F. Masi, SREP	1

Air Force Office of Scientific Research
1400 Wilson Blvd.
Arlington, VA 22209
Attn: SIGL — 1

Air Force Rocket Propulsion Laboratory
Edwards, CA 93523
Attn: Library — 1

Babcock and Wilcox Co.
Advanced Composites Department
P.O. Box 419
Alliance, OH 44601
Attn: R. C. Young — 1

Bell Helicopter Co.
P.O. Box 482
Ft. Worth, TX 76101
Attn: H. Zinberg — 1

The Boeing Co.
P.O. Box 3999
Seattle, WA 98124
Attn: J. T. Hoggatt, M.S. 88-33 — 1

The Boeing Co.
Vertol Division
Morton, PA 19070
Attn: W. D. Harris — 1
R. Pickney — 1

Brunswick Corp.
Defense Products Division
P.O. Box 4594
43000 Industrial Ave.
Lincoln, NB 68504
Attn: R. Morse — 1

Chemical Propulsion Information Agency
Applied Physics Laboratory
8621 Georgia Avenue
Silver Spring, MD 20910
Attn: Library — 1

Commander
Natick Laboratories
U.S. Army
Natick, MA 01762
Attn: Library — 1

Commander
Naval Air Systems Command
U.S. Navy Department
Washington, DC 20360
Attn: P. Goodwin, AIR-5203 1
C. Bersch, AIR-52032A 1
M. Stander, AIR-42032D 1

Commander
Naval Ordnance Systems Command
U.S. Navy Department
Washington, DC 20360
Attn: B. Drimmer, ORD-033 1
M. Kinna, ORD-033A 1

Composites Horizons
6342 N. Irwindale Ave.
Azusa, CA 91702
Attn: I. Petker 1

Defense Metals Information Center
Battelle Memorial Institute
Columbus Laboratories
505 King Avenue
Columbus, OH 43201 1

Department of the Army
U.S. Army Materiel Command
Washington, DC 20315 1

Department of the Army
U.S. Army Aviation Materials Laboratory
Ft. Eustis, VA 23604
Attn: I. E. Figge, Sr. 1
R. Berrisford 1

Department of the Army
U.S. Army Aviation Systems Command
P.O. Box 209
St. Louis, MO 63166
Attn: R. Vollmer, AMSAV-A-UE 1

Department of the Army
Plastics Technical Evaluation Center
Picatinny Arsenal
Dover, NJ 07801
Attn: H. E. Pebly, Jr. 1

Department of the Army
Watervliet Arsenal
Watervliet, NY 12189
Attn: F. W. Schmiedershoff 1

Department of the Army
Watertown Arsenal
Watertown, MA 02172
Attn: A. Thomas 1
B. M. Halpin, Jr. 1

Department of the Army
Redstone Arsenal
Huntsville, AL 35809
Attn: R. J. Thompson, AMSMI-RSS 1

Department of the Navy
Naval Surface Weapons Center
White Oak, Silver Spring, MD 20910
Attn: R. Simon 1

Department of the Navy
U.S. Naval Ship R&D Laboratory, Annapolis
Annapolis, MD 21402
Attn: C. Hershner, Code 2724 1

Director
Deep Submergence Systems Project
6900 Wisconsin Avenue
Washington, DC 20015
Attn: H. Bernstein, DSSP-221 1

Director
Naval Research Laboratory
Washington, DC 20390
Attn: Code 8430 1
I. Wolock, Code 8433 1

E. I. DuPont DeNemours and Co.
DuPont Experimental Station
Wilmington, DE 19898
Attn: C. Zweben 1
J. W. Moore 1
L. Miner 1

Fiber Science, Inc.
245 East 157th Street
Gardena, CA 90248
Attn: L. J. Ashton 1

General Dynamics
P.O. Box 748
Ft. Worth, TX 76100
Attn: W. S. Hay 1
T. P. Airhart 1

General Dynamics/Convair
P.O. Box 1128
San Diego, CA 92112
Attn: J. L. Christian 1

General Electric Co.
Evendale, OH 45214
Attn: C. Stotler 1

General Electric Co.
Space Sciences Laboratory
Philadelphia, PA 19101
Attn: V. Mazzio 1

General Motors Corporation
Detroit Diesel Allison Division
Indianapolis, IN
Attn: M. Herman 1

Grumman Aerospace Corporation
Bethpage, Long Island, NY 11714
Attn: B. Aleck 1

Hercules, Inc.
Wilmington, DE 19899
Attn: G. Kuebeler 1

Hercules, Inc.
Allegheny Ballistics Laboratory
P.O. Box 210
Cumberland, MD 21052
Attn: W. T. Freeman 1

IIT Research Institute
Technology Center
Chicago, IL 60616
Attn: L. M. Daniel 1

Jet Propulsion Laboratory
4800 Oak Grove Dr.
Pasadena, CA 91103
Attn: W. Jensen 1
Library 1

Lawrence Livermore Laboratory
P.O. Box 808
Livermore, CA 94550
Attn: T. T. Chiao 1
M. Hamstad 1

Lockheed-Georgia Co.
Advanced Composites Information Center
Dept. 72-14, Zone 402
Marietta, GA 30060 1

Lockheed Missiles and Space Co.
P.O. Box 504
Sunnyvale, CA 94087
Attn: R. W. Fenn 1

McDonnell Douglas Aircraft Corp.
P.O. Box 516
Lambert Field, MS 63166
Attn: J. C. Watson 1

McDonnell Douglas Aircraft Corp.
3855 Lakewood Blvd.
Long Beach, CA 90810
Attn: H. C. Schjelderup 1

Massachusetts Institute of Technology
Cambridge, MA 02139
Attn: Prof. F. J. McGarry 1

Materials Sciences Corp.
1777 Walton Rd.
Blue Bell, PA 19422
Attn: B. W. Rosen 1

NASA-Ames Research Center
Moffett Field, CA 94035
Attn: Library 1

NASA-Flight Research Center
P.O. Box 273
Edwards, CA 93523
Attn: Library 1

NASA-George C. Marshall Space Flight Center
Huntsville, AL 35812
Attn: D. D. Thompson, S&E, ASTN-PPA 1
H. M. Walker, S&E-PP-MSX 1
C. E. Cataldo, S&E-ASTN-MX 1
Library 1

NASA-Goddard Space Flight Center
Greenbelt, MD 20771
Attn: Library 1

NASA-Langley Research Center
Hampton, VA 23365
Attn: E. E. Mathauser, MS 188a 1
R. A. Pride, MS 188a 1
Library 1

NASA-Lewis Research Center
21000 Brookpark Road
Cleveland, OH 44135
Attn: Contracting Officer, MS 500-313 1
Tech. Report Control, MS 5-5 1
Technical Utilization, MS 3-19 1
AFSC Liaison, MS 501-3 1
Rel. and Quality Assur., MS 500-211 1
R. A. Signorelli, MS 106-1 1

M. P. Hanson, MS 501-7 1
R. H. Kemp, MS 49-3 1
R. F. Lark, MS 49-3 14
J. R. Faddoul, MS 49-3 1

J. C. Freche, MS 49-1 1
R. H. Johns, MS 49-3 1
N. T. Saunders, MS 105-1 1

C. C. Chamis, MS 49-3 1
T. T. Serafini, MS 49-1 1
Library, MS 60-3 2

NASA-Lyndon B. Johnson Space Center
Houston, TX 77001
Attn: R. L. Johnston, SMD-ES5 1
R. E. Johnson, SMD-ES5 1
S. Glorioso, SMD-ES52 1
D. Kendrick, PPD-EP42 1
R. N. Prince, CSD-EC3 1
Library 1

NASA Scientific & Technical Info. Facility
Attn: Accessioning Department
P.O. Box 8757
Balt/Wash International Airport
MD 21240 10

National Aeronautics & Space Administration
Office of Advanced Research and Technology
Washington, DC 20546
Attn: L. A. Harris, Code RWS 1

National Aeronautics & Space Administration
Office of Technology Utilization
Washington, DC 20546 1

National Technology Information Service
Springfield, VA 22151 6

North American Rockwell Corp.
Space Division
12214 Lakewood Blvd.
Downey, CA 90241
Attn: Max Nabler 1
L. Korb 1

Northrop Space Laboratories
3401 West Broadway
Hawthorne, CA 90250
Attn: D. Stanbarger 1

Cornell University
Dept. Theoretical & Applied Mech.
Ithaca, NY 14853
Attn: F. C. Moon 1

Sikorsky Aircraft Division
United Aircraft Corp.
Stratford, CT 06602
Attn: M. Salkind 1

Southwest Research Institute
8500 Culebra Road
San Antonio, TX 78284
Attn: G. C. Grimes 1

Space and Missile Systems Organization
Air Force Unit Post Office
Los Angeles, CA 90045
Attn: Technical Data Center 1

Structural Composites Industries, Inc.
6344 No. Irwindale Avenue
Azusa, CA 91702
Attn: E. E. Morris 1

Union Carbide Corp.
P.O. Box 6116
Cleveland, OH 44101
Attn: J. C. Bowman 1

U.S. Army Materials and Mechanics
Research Center
Watertown Arsenal
Watertown, MA 02192
Attn: S. Arnold 1

United Technologies Research Center
East Hartford, CT
Attn: R. A. Pike 1
R. C. Novak 1

Pratt & Whitney Aircraft
East Hartford, CT
Attn: A. J. Dennis 1